LIBRARY
OCT - 9 2001
National Oceanic &
Atmospheric Administration
U.S. Dept. of Commerce

ISSN 1000-9620

Marine Science Bulletin

Volume 2 • Number 1 2000

LIBRARY
Pacific Islands Fisheries Science Center
NOAA Fisheries
Honolulu, Hawai'i

ISSN 1000-9620
02>
9 771000 962001

NATIONAL MARINE DATA AND
INFORMATION SERVICE OF CHINA

NOAA
U.S. NATIONAL OCEANIC AND ATMOSPHERIC ADMINISTRATION
DEPARTMENT OF COMMERCE

MARINE SCIENCE BULLETIN

Vol.2 No.1 May 2000

LIBRARY
OCT - 9 2001
National Oceanic &
Atmospheric Administration
U.S. Dept. of Commerce

CONTENTS

Discovery and Comparison of Restriction Patterns of *Porphyra* Total DNAs
..... *Guo Baotai Dai Jixun* et al (1)

Combined Impacts of MSL Rise and the Secular Trend in MLTR on Marine Environment in the Areas Around the Huanghe River Mouth
..... *Zhang Jinwen* and *Wang Ji* (6)

Characteristics of Suspended Sediment Concentrations over the Areas Adjacent to Changjiang River Estuary, the Summer of 1998
..... *Gao Shu Cheng Peng Wang Yaping* and *Cao Qiyuan* (14)

Tentative Ideas on the Development of "Digital Ocean" in China
..... *Hou Wenfeng* (25)

Research on the Distributional Features of and Interrelationships Between the Dissolved Oxygen, Salinity, pH Value and Nutrient Salts in the Honghai Bay Waters
..... *Wang Xiaoping, Jia Xiaoping , Lin Qin* et al. (38)

Study on Basic Hydrologic and Meteorological Parameters in the Ice-covered Bohai Sea
.....*Wang Keguang, Wang Caixin* and *Wu Huiding* (45)

Analysis of the Sedimentary Characteristics and Origin of the "Old Red Sands" in the Coastal Areas of Southeast Fujian
.....*Zeng Congsheng, Chen Jucheng* and *Wu Yougong* (58)

The Verfication of the Resonance Prediction Method or Great Earthquake Motion and its Prediction
.....*Zheng Wenzhen*(68)

A Three-dimensional Forecasting Model for Oil Spill
..... *Sun Yinglan, Wang Lixia* and *Sun Changqing* (75)

Distribution and Sources of Polycyclic Aromatic Hydrocarbons (PAHs) in the Surface Seawater of the Western Xiamen Harbor
..... *Liu Yan, Zhang Zulin* and *Hong Huasheng* (83)

Preliminary Research on the Characteristics and Causes of Formation of Seiches in the Bays
..... *Wu Shaohua, Wang Xinian* and *Dai Mingrui* (88)

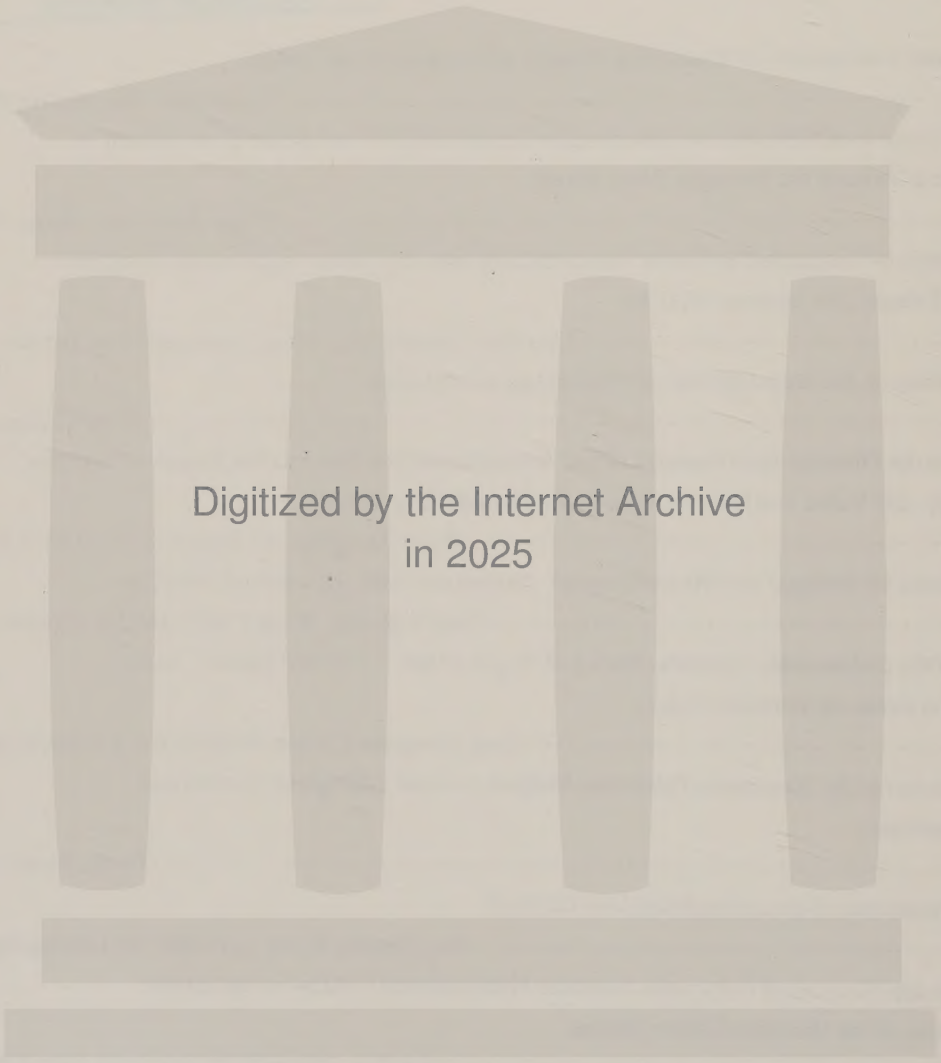

Digitized by the Internet Archive
in 2025

https://archive.org/details/marine-science-bulletin_2000_2_1

Discovery and Comparison of Restriction Patterns of *Porphyra* Total DNAs

Guo Baotai(郭宝太)[1] Dai Jixun（戴继勋）[1] Yang Rui（杨瑞）[1] Bi Yuping（毕玉平）[2]
Li Guangcun（李广存）[2] Lu Yanhui（路艳辉）[2]
(*1 College of Marine Life Sciences, Ocean University of Qingdao, Qingdao 266003*)
(*2 Biotechnology Research Center, Shandong Academy of Agricultural Sciences, Jinan 250100*)

Abstract Total DNA is isolated from *Porphyra* cells which have been prepared from sea snail enzyme digests of *Porphyra* thalli. The crude extracts of total DNA are rapidly purified with Wizard DNA Clean-up resin by using modified washing solution. DNA bands are clearly observed in the restriction endonuclease patterns of *P. yezoensis* and *P. haitanensis* total DNAs. Both *P. yezoensis* and *P. haitanensis*have specific DNA bands in the restriction patterns of EcoRI, PastI and HaeIII. According to the band pattern of total DNA, the discrimination between *P. yezoensis* and *P. haitanensis* is very easy especially in the restriction pattern of HaeIII. The comparative results indicate that the band pattern of total DNA is a new type and reliable DNA marker for identification and classification of *Porphyra* species.

Key words *P. yezoensis*; *P. hainensis*; total DNA ; restriction digestion; DNA band; molecular taxonomy

Introduction

The *Porphyra* (Rhodophyra) species are widely distributed seaweeds in temperate sea waters. More than seventy species have been reported in this genus. Due to the simple morphology of the thalli and little distinct characters for classification, the existent taxonomy of *Porphyra* has some limitations.

DNA analysis technique is efficient to detect the difference between or among genomes, which provides a new way to identify and classify the *Porphyra* species. Stiller et al (1993) found the restriction sites of SSUrDNA were different among different *Porphyra* species and there was no variation in different populations of the same species[1]. So the restriction pattern of SSUrDNA can be used as the marker to identify the species of *Porphyra*. Although the method known as PCR-RFLP has the advantages of both PCR and RFLP, it is only focused on one gene or specific sequence of the genome, not the whole genome. We have found there are evident DNA bands in the agarose gel electrophoresis pattern of the restriction endonuclease digests of high-quality total DNA in *Porphyra*. The band patterns are quite different in different species, which shows the typical data for the whole genome of the species. In this paper, our goal is to compare the restriction patterns of *P. yezoensis* and *P. haitanensis*to evaluate the possibility of the restriction pattern of total DNA as molecular marker for classification of *Porphyra* species.

1 Materials and Methods

1.1 Materials and reagents

The thalli of *P. haitanensis*are kindly provided by Dr. Liu Biqian (Ningbo University, Zhejiang Province). The *P. yezoensis* thalli are collected at Fish Breeding Farm of Rizhao, Shandong Province. Sea snail enzyme is the product of OUQD. The restriction endonucleases and Wizard DNA clean-up purification kit is purchased from Promega Co.

1.2 Extraction and purification of total DNA

1~2g thalli of *Porphyra* are treated with sea snail enzyme as described by Dai[2] to get *Porphyra* cells. The isolated cells are suspended with 10 ml extraction buffer (3%SDS, 150mmol/L Tris-HCl, pH 8.0, 0.2mol/L NaCl, 0.2% β –mercaptoethanol) and Proteinase K is added to a final concentration of 300 μ g/ml. After incubation at 55℃~60℃ for 1hr, the mixture is extracted with equal volume of phenol, phenol/chloroform and chloroform respectively. Total nucleic acids are precipitated from the supernatant with isopropanol and RNA in total nucleic acids is digested with RNaseA as Goff[3]. The extracts of total DNA are treated with Wizard DNA clean-up resin, and the resin is washed with modified washing solution (60% ethanol, 20mmol/L Tris-HCl, pH 8.0, 1mmol/L EDTA and 0.2mol/L NaCl). Finally, high-quality DNA is eluted from the resin with 68℃ double distilled water.

1.3 Restriction digestion and electrophoresis

Total DNA is mixed with restriction endonuclease (10 μ l/ μ g DNA) and the mixture is incubated at 37℃ overnight. The digests of total DNA are analysed by 0.8% agarose gel electrophoresis in TAE buffer at the voltage of 3v/cm.

2 Results

Table 1 Specific DNA bands in the restriction patterns of *P. yezoensis* and *P. haitanensis* total DNAs (Kb)

Materials	Restriction endonucleases		
	EcoR I	Pst I	HaeIII
P. yezoensis	0.91 1.17 1.33 1.78	0.83 0.98 1.15 1.70 1.90 2.29	0.42 5.57 12.02
P. haitanensis	2.75 3.47 4.27 4.57	1.05 1.23 2.19	0.66 0.98 2.00 5.15 8.32 16.60

*Porphyra*total cellular DNA is purified with Wizard resin, and the resulting DNA can be completely digested by restriction endonucleases, which shows that the purified total DNA is of sufficient quality. Unexpectedly, distinct DNA bands are observed in the agarose gel electrophoresis patterns of digests of total DNA. DNA bands are smaller than 5Kb in the restriction patterns of EcoRI and PstI, and the bands more than 5Kb are hardly recognizable (Fig.1), but DNA bands ranged in sizes from 0.42Kb to 16.6Kb are clearly observed in the HaeIII pattern. DNA band patterns are apparently different due to difference of restriction enzymes. Generally, there are no recognizable DNA bands in the restriction patterns of nuclear DNA or total cellular DNA. The exception of DNA bands in the restriction pattern of *Porphyra*total

DNA may be the result of the small size of nuclear genomes in this genus.

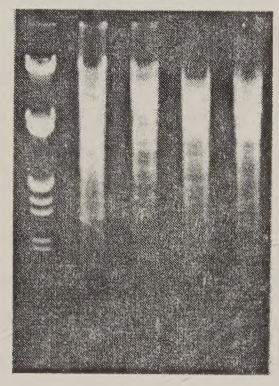

a b c d e

Fig.1 EcoR I and Pst I digestion of *P. yezoensis* and *P. haitanensis* total DNAs

a. λ DNA/EcoR I +HindIII marker

b.EcoR I digestion of *P. yezoensis* total DNA

c.EcoR I digestion of *P. haitanensis* total DNA

d.Pst I digestion of *P. yezoensis* total DNA

e.Pst I digestion of *P. haitanensis* total DNA

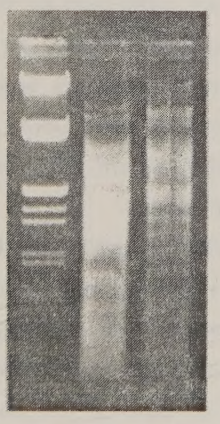

a b c

Fig.2 HaeIII digestion of *P. yezoensis* and *P. haitanensis* total DNAs

a. λ DNA/EcoR I +HindIII marker

b.HaeIII digestion of *P. yezoensis* total DNA

c..HaeIII digestion of *P. haitanensis* total DNA

Restriction patterns are compared between *P. yezoensis* and *P. hainensis*. Great differences of DNA bands exist in two species, and rare similar bands can be found. In the restriction pattern of EcoR I , four distinct DNA bands of size from 2 to 5 Kb are found in *P. haitanensis*, while no corresponding bands found in *P. yezoensis*(Fig.1 b,c; Tab.1). On the other hand, four specific bands from 0.9Kb to

1.8Kb are observed in *P. yezoensis*, and no corresponding bands in *P. haitanensis*. Only two bands of size 1.5Kb and 2.0 Kb coexist in two species (Fig1 b,c). In the restriction pattern of Pst I , there are six specific bands from 0.8Kb to 2.3Kb in *P. yezoensis*, and three specific bands from 1 to 2.2Kb are found in *P. haitanensis* (Fig1 d, e; Table 1). The Pst I patterns of two species are also different. The HaeIII restriction patterns are greatly different between *P. yezoensis* and *P. hainensis*, and the differences are more easily detected in HaeIII pattern than in those of EcoR I and Pst I . Above 5Kb, there are two specific bands of 5.75Kb and 12.2Kb in *P. yezoensis* and three bands of 5.15Kb, 8.22Kb and 16.60Kb in *P. haitanensis* respectively (Fig2 b, c). Below 5Kb, there are two specific bands of 2.0Kb and 0.42Kb in *P. yezoensis*, and there is a DNA ladder which has four clear bands of sizes 0.66Kb, 098Kb, 1.10Kb and 1.23kb in *P. haitanensis*. The two small bands of 0.66Kb and 0.98Kb are only found in *P. haitanensis*.

Generally speaking, the restriction pattern of total DNA has specification in species and can be used as a DNA marker for identification and classification of *Porphyra* species.

3 Discussion

The presence of distinct DNA bands in restriction pattern makes it available to compare total DNA bands between or among *Porphyra* species directly. Without the use of molecular hybridization, we call it direct restriction fragment length polymorphism (RELP) analysis. The species specification in total DNA pattern proves it is a feasible molecular marker for discrimination and identification of *Porphyra* species. Furthermore, the total DNA pattern is not influenced by the habitats and developing stages of the organisms. So the total DNA pattern is stable and reliable. In addition, the total DNA patterns vary with treatments of different enzymes, the more enzymes are used, the more information about genome is revealed. In general, direct RELP analysis of total DNA is an effective method for taxonomy of *Porphyra* species. Whether or not total DNA pattern is available in discrimination within populations of the same *Porphyra* species is under investigation.

Plastic DNA (cpDNA) direct RFLP analysis has been successfully applied in red algae taxonomy [3,4]. Although cpDNA pattern is an effective marker for classification, the obvious difficulty in cpDNA extraction has limited the application of this technique in red algae taxonomy. Direct RFLP of total DNA needs not molecular hybridization and sophisticated apparatus, it has the advantages of both easy extraction of sufficient quantity of pure DNA, and direct occurrence of DNA bands in electrophoresis pattern. Therefore direct RFLP of total DNA is much easier to use than cpDNA direct RFLP in practice.

The comparison of DNA bands provides a new way of gene cloning. Young et al (1978) located and cloned the fused mitochondrial gene associated with male sterility in petunia by the comparison of mitochondrial DNA bands. So it is worthwhile to pay attention to the location and cloning of species-specific gene in *Porphyra* through comparison of total DNA patterns.

Reference

1 Stiller J W and Waaland J R, (1993) Molecular analysis reveals cryptic diversity in *Porphyra*(Rhodophyra). J Phycol, 29:505~517

2 Dai J X, Zhang Q Q and Bao Z M et al, (1990) Studies on the pure line culture, mutagenesis and interspecific fusion of *Porphyra* protoplasts. Oceanol Limnol Sin, 21(3):293~2296

3 Goff L J and Coleman A W, (1988) The use of plastid DNA restriction endonuclease pattern in delineating red algal species and populations. J Phycol, 24:357~368

4 Parson T J, Maggs C A and Douglas S E, (1990) Plastid DNA restriction analysis links the heteromorphic phases of an apomictic red algal life history. J Phycol, 26:495~500

5 Young E G and Hanson M R, (1987) A fused mitochondrial gene associated with cytoplasmic male sterility is developmentally regulated. Cell, 50:41~49

Combined Impacts of MSL Rise and the Secular Trend in MLTR on Marine Environment in the Areas Around the Huanghe River Mouth

Zhang Jinwen(张锦文) Wang Ji(王骥)
(*National Marine Data and Information Service, Tianjin, China, 300171*)

Abstract Mean sea level (MSL) rise and the mean large tidal range (MLTR) becoming larger caused by sediment accumulation and subsidence in the areas around the Huanghe River mouth and the Laizhou Bay are presented in this paper.

The results obtained from the tidal numerical simulation and the statistical observed tide data show that the relative MSL rises and the tidal range becomes larger at a quicker rate, so the marine environment and coastline of the Laizhou Bay are changing rapidly. The engineering design standard along the coasts has to be raised.

Keywords Laizhou bay; sediment; mean sea level; design standard; Huanghe estuary

1. Construction

The amount of sediment is about 1.6 billion tons per year from the upper and middle reaches and deposits on the riverbed of the lower reaches and in the areas around the Huanghe River estuary. It causes the delta lobe of Huanghe River to extend towards the southeast of the Laizhou Bay at a rate of 1.8 to 3.6km/a[3], so the amphidrome of semi-diurnal tide has to be migrated to the Laizhou Bay.

The main semi-diurnal constituent M_2 obtained by numerical simulation in deferent years in the Laizhou Bay and by analyzing observed hourly tide data at the tidal station at Yangjiaogou (west coast of the Laizhou Bay) shows that the amplitude of M_2 (HM_2) becomes larger in the west of the bay and the tidal hours are postponed, while HM_2 gets smaller in the southeast of the bay.

As a result of the environmental change of the bay all tidal characters, such as MLTR, the mean higher high waters (MHHWs) and the mean lower low waters (MLLWs), have become larger.

According to the present rate of sedimentation it is estimated that a delta lobe, about 52 km long and 18 km wide[3], will have been formed around the estuary by the year 2000, and meanwhile, the south and the southwest coastline of the Laizhou Bay will be eroded and salinated severely due to the increase in tidal range and MSL rise.

The engineering design standard in the areas around the mouth has to be altered in the light of the change of the marine environment. It is not suitable to calculate the distribution of extreme water level by using observed yearly highest or lowest water levels .

Up to now MSL is rising and the yearly highest water levels are changing continuously, and the estimated high water levels of 50-year return period maybe change into the 20-year return period quite

soon because MHHWs and MSL have risen more than 35cm and 9cm since the end of the 1950s along the coast in the south and southwest of the Laizhou Bay respectively.

2. The Change of Main Semi-diurnal Tidal Constituents at Laizhou Bay

The ocean environment of the Laizhou Bay has changed since the early century because more than one billion tons of sediment coming from the Yellow River deposits in the areas around its mouth every year. Fang and Yang studied the changes of tidal regime in the Laizhou Bay caused by the Yellow River deposition first in 1985[4]. Some recent results of the numerical simulations of constituent M_2 calculated by Professor Fang Guohong and Associate Professor Cao Deming are given in Figs.1 to 3. Engineer Chen Funian draws the tidal charts in the figures.

Figs.1 to 3 show the change of HM_2 (solid lines) and gM_2 (dashed lines) in 1934, in 1959 and in 1989 respectively.

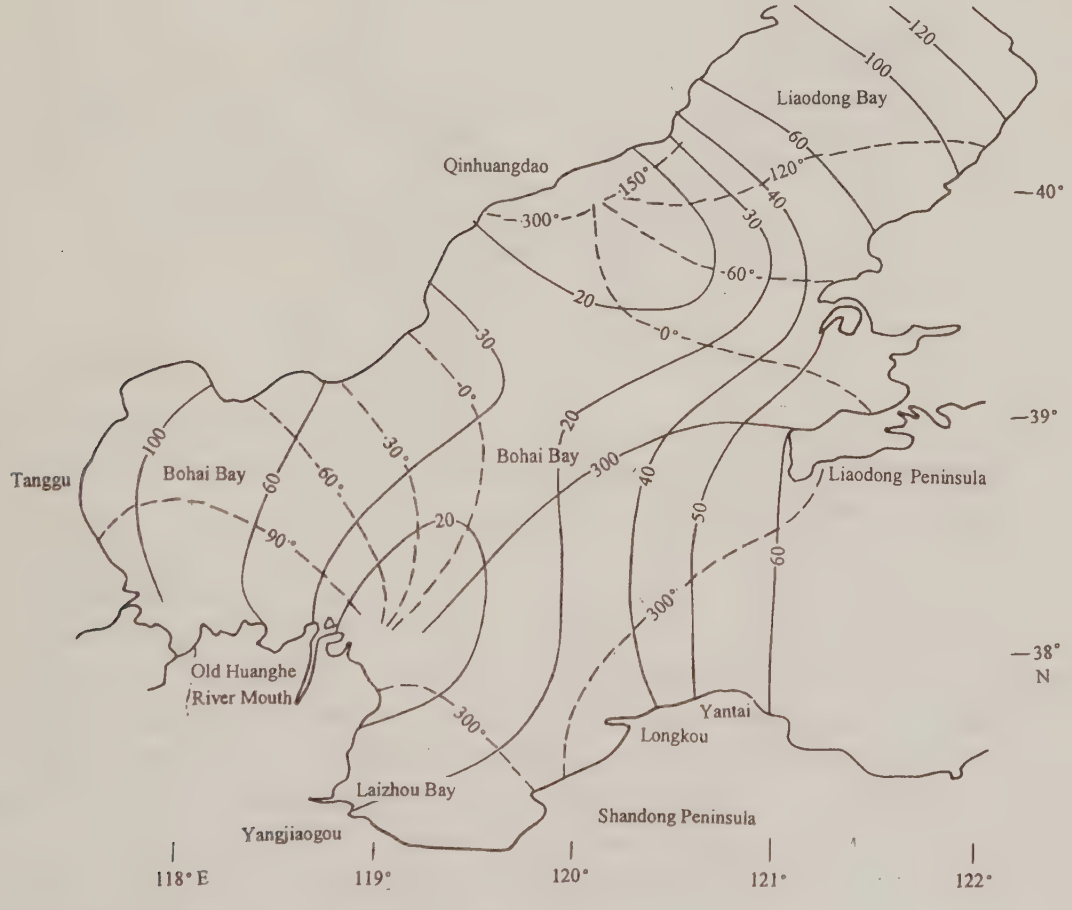

Fig.1 Numerically computed tidal chart of the M2 wave in the Bohai Sea in 1934. The solid line denotes the amplitude (in cm) and the dashed line the phase lags (in degree)(according to Fang Guohong and Cao Deming, 1997)

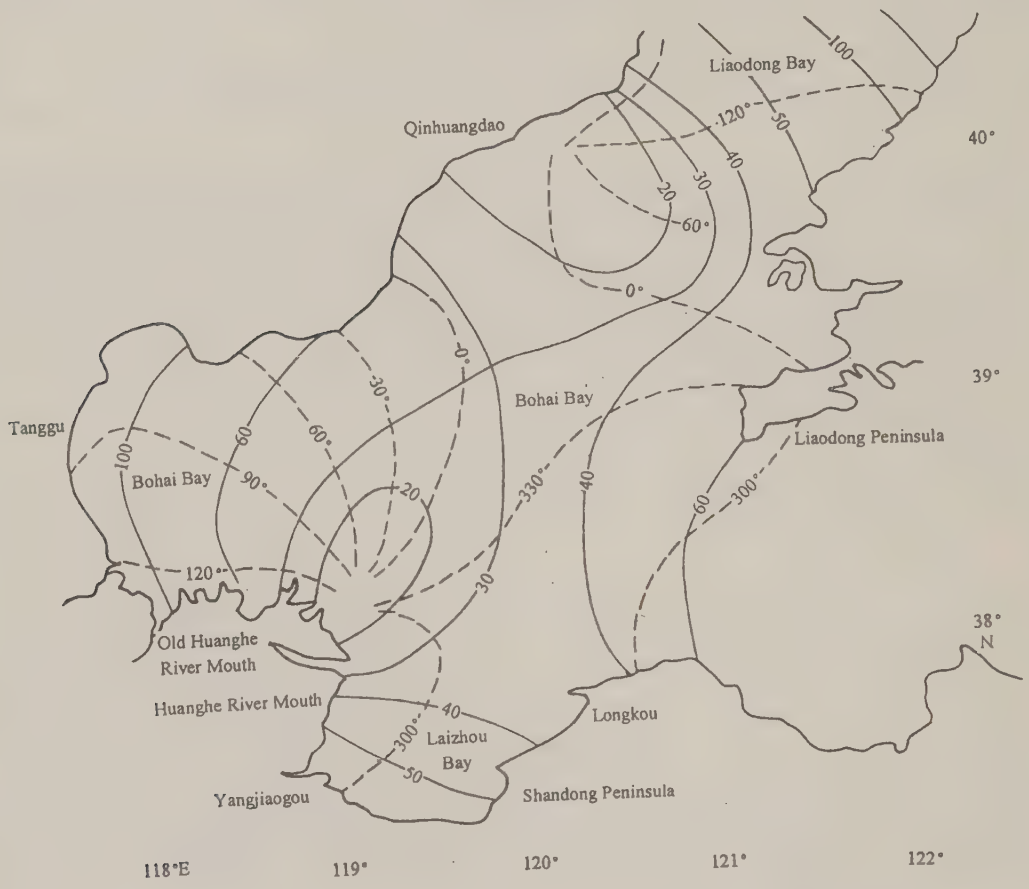

Fig.2 Numerically computed tidal chart of the M_2 wave in the Bohai Sea in 1959. The solid line denotes the amplitudes (in cm) and the dashed line the phase lags (in degree) (according to Fang Guohong and Cao Deming, 1997)

In Fig.1 the Huanghe River mouth is located at 38 ° 05 ′ N , 118 ° 45 ′ E towards the north to the Bohai Bay. And HM_2 is of the order 20 ~ 30cm in the Laizhuo Bay. Along the west coast of the bay HM_2 is less than 25cm. In Fig. 2 the river course was changed to 37 ° 45 ′ N, 118 ° 55 ′ E towards the east to the Laizhou Bay. And HM_2 is of the order 40 ~ 50cm in the Laizhuo Bay. Along the west coast of the Laizhou Bay HM_2 also increases more than 45cm. In Fig. 3 the river mouth migrates at 37 ° 35 ′ N, and 119 ° 15 ′ E towards the southeast to the Laizhou Bay and HM_2 increases to more than 45cm in the Laizhuo Bay, and along the west coast it becomes more than 70cm.

Along the west coast of the bay the phase lag of M_2 , gM_2, is less than 300 ° in 1934, about 315 ° in 1959, and more than 335 ° in 1989. That is to say the semi-diurnal tide hour was postponed 1.3 hours in 1989 compared with that in 1934, which proves that the amphidrome of semi-diurnal tide migrates farther and farther away from the west coast of the Laizhou Bay.

The other main semi-diurnal constituent, HS_2 has been getting larger in the Laizhuo Bay as well since 1934.

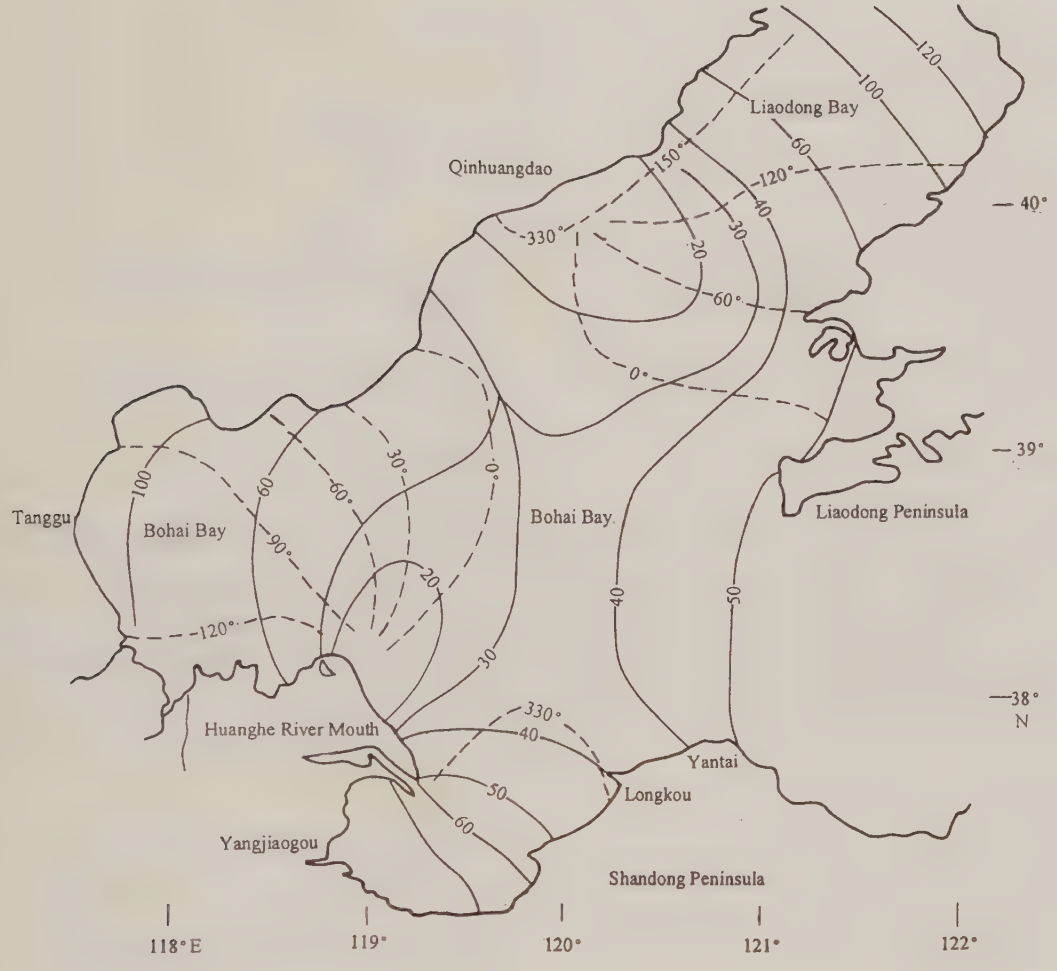

Fig.3 Numerically computed tidal chart of the M2 wave in the Bohai Sea in 1989. The solid line denotes the amplitudes (in cm) and the dashed line the phase lags (in degree) (according to Fang Guohong and Cao Deming, 1997)

The analysis of hourly observed tide data[12] at the tide station at Yangjiaogou also proves the fact that HM_2 increased 30cm from1952 to 1994, while HS_2 also increased 7cm. The correlative analysis between HM_2 and time series and HS_2 and time series, shown in Figs. 4 and 5, indicates that HM_2 and HS_2 increased at a rate of 0.77cm/a and 0.21 cm/a in the period respectively.

On the contrary, at Longkou (southeast coast of the Laizhou bay), opposite Yangjiaogou, HM_2 and HS_2 decreased 9cm and 3cm from 1965 to 1995 respectively.

3. The Change of Tidal Character, MLTR, MHHWs, MLLWs and MSL

The transformation of tide character, MLTR, MHHWs and MLLWs, etc. is response to the change

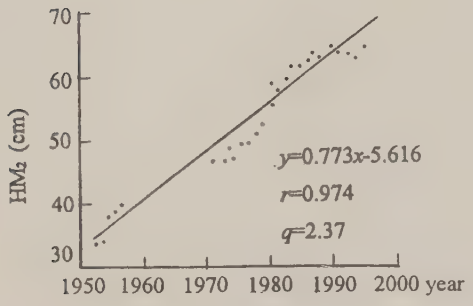

Fig.4 Correlation between HM_2 and time series

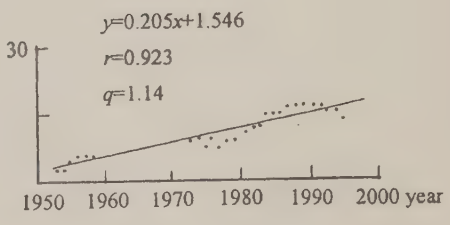

Fig.5 Correlation between HS_2 and time series

of semi-diurnal tide.

Tide character, $(HO_1+HK_1)/HM_2$, was 1.3 in 1952, but 0.69 in 1994 at Yangjiaogou.

Fig. 6 shows the correlation between MLTR and time series. MLTR increased at a rate of 1.6cm/a from 1954 to 1994 in the tide station at Yangjiaogou, which is larger than that around the British Isles and along the adjacent European coastline[1]. "Table 2(a) shows trends in MTR to be small, or even negative, in Scotland (Aberdeen and Lerwick) and in the central and western Irish Sea (Holyhead, Douglas and Dublin), while in most of England they are generally of the order 0.5 ~ 1.0mm/yr^{-1}" [1].

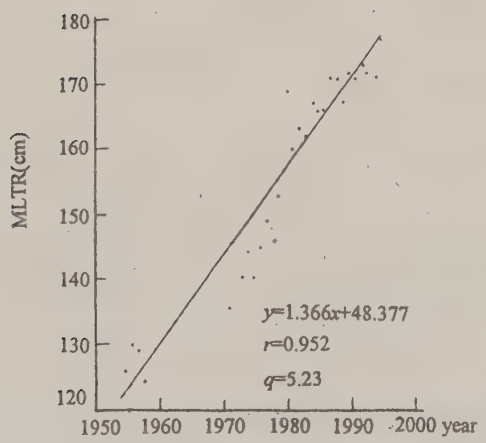

Fig.6 Coorelation between MLTR and time series

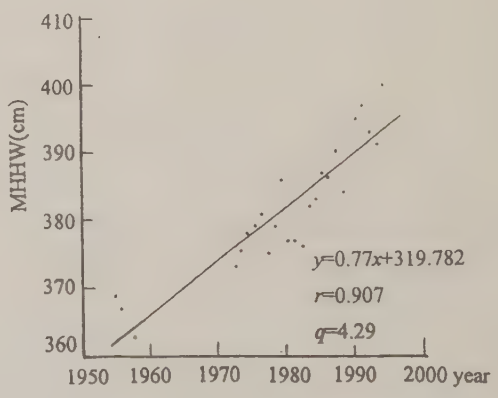

Fig.7 Correlation between MHHW and times series

Figs.7 and 8 show the relationships between MHHWs and time series and between MLLWs and time series at Yangjiaogou. They increased at a rate of 1.0cm/a and 0.6cm/a from 1954 to 1994 espectively. MSL at Yangjiaogou rose at a rate of θ.23cm/a from 1952 to 1994 (sees Fig. 9).

As watercourses become deeper with the change of tidal environment, ships can navigate through the lane safely which they couldn't pass before during the neap tidal hours. And the change also causes the south and the west coast of the Laizhou Bay to be eroded and salinated.

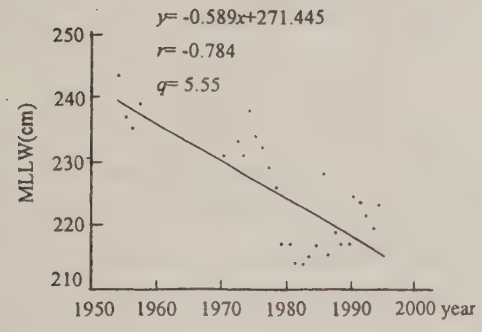

Fig.8 Correlation between MLLW and times series

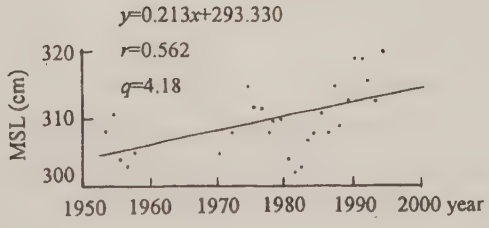

Fig.9 Correlation between MSL and times series

4. The Distribution of Yearly Highest Waters at Yangjiaogou

The distribution of yearly highest waters observed from 1972 to 1994 is shown in Fig.10 (see Appendix III). We suppose that the yearly highest waters would increase at a rate of 1cm/a only owing to the increase of the semi-diurnal tide. The distribution of them is shown in Fig.11 (see Appendix III). It is clear that the height of 50 year return period is 20cm more calculated by using supposed data than by observed data, and the height of 100 year return period 23cm more calculated by using supposed data than by observed data. If MSL rise and other effects are considered, they will be higher than the above.

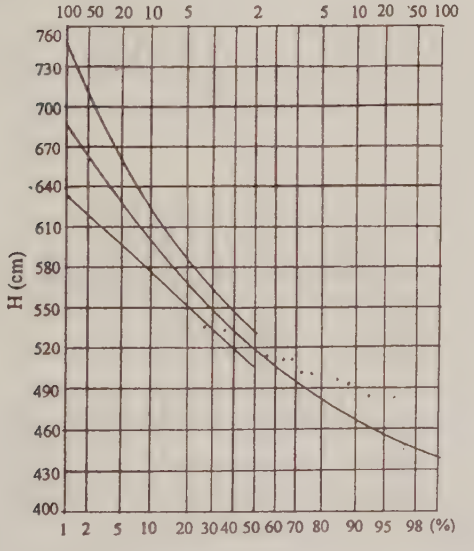

Fig.10 Distribution of yearly highest waters (from 1972 to 1994) at Yangyiaogou

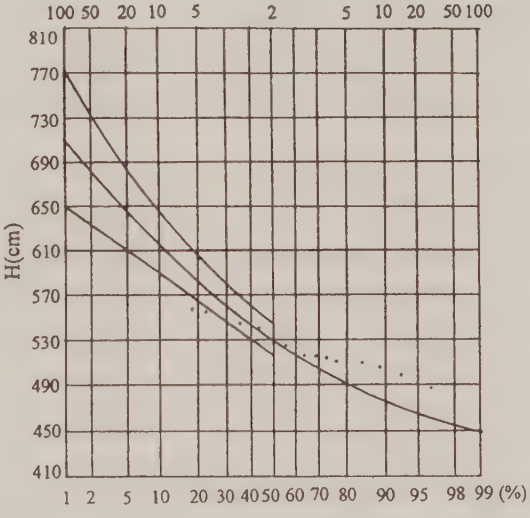

Fig.11 Distribution of yearly highest waters supposed (from 1972 to 1994) at Yangjiaogou

The situation of the marine environment change, such as sediment at the estuary and MSL rise and tidal range increase, has to be studied thoroughly today and tomorrow. The low design standards often cause severe disasters as time goes on. The tropical storms, No. 16 in 1992 and No.11 in 1997, based on

MSL rise and MHHWs increase caused so severe destruction that a lot of sea farms and dams along the west and south coast of the Laizhou Bay were ruined when the bay was effected by them.

5. Discussion

(1) The relationships among sediment, MSL rise, the change of tides, flood and tide currents

The whole environment of the Laizhou Bay has been altered because accumulation sediment coming from the river forms land or muddy coasts that change continuously the original coastlines. Tidal currents change in different directions and at different speeds. Where the mud of the bottoms is moved away by currents, the sea water gets deeper and deeper, tidal ranges get larger and larger, current speeds become faster and faster, the transportation of soil at the bottom becomes more and more quickly and erosion and salinization of the coasts become more and more severely. Especially during storm surges and cold air outbreaks, huge waves and strong storm-forced currents wash and erode the coasts and tide flats overwhelmingly, and new deposited areas are formed here or there. The interactions among the atmosphere, ocean and land are complex processes. From knowledge of the shallow water tides, MTR changes might be expected to depend on change in MSL, or water depth[1].

(2) Research on the whole environment including the river, the bay and the sediment

To try to keep the river mouth under control is related not only to the river mouth itself, but also to the interaction between the land and the marine environment. That is to say every part of the environment of the bay has to be considered. It is necessary to work out adaptable measures to keep the river estuary, the sediment and the marine environment under integrated control instead of only an aspect because the relation to the interaction among all parts is easily destroyed by the water course altered or floods or storm surges and the change of tides.

(3) MSL rise and the change of tides, either of which has taken place up to now or will take place in the future, have to be considered in the engineering design, aquaculture and coast protection standards.

APPENDIX I. REFERENCES

1 P. L. Woodwort, S .M. Shaw and D. L. Blackman, 1991. Secular trends in mean tidal range around the British Isles and along the adjacent European coastline. Geoghys, j, int. 104,593-609

2 Fang Guohong, Zheng Wenzhen, Chen Zongyong and Wang Ji, 1986.*The analysis and prediction of tides ana tidal currents*, China Ocean Press

3 Fan Zhaomu, Guo Yongsheng, 1992.*Analysis charts of remote sensing trends along the Yellow River delta*, China Ocean press

4 Fang Guohong and Yang Jingfei, 1985, A two-dimensional numerical model of the tidal motions in the Bohai Sea. Chinese Journal of Oceanology and Limnology, 3(2), 135-152

5 Fang Guohong and Cao Deming, 1997. Tides in the Bohai Sea - past, present and future (manuscript)

APPENDIX II. NOTATION

The following symbols are used in the paper:

r = coefficient of correlation;

q = residual variance

APPENDIX III.

The distribution of yearly highest water at Yangjiaogou is as follows:

frequency (%)	real data	confidence limit	supposed data	confidence limit	return period years
0.5	709	67	734	73	200
1	685	55	708	59	100
2	660	43	680	46	50
3	641	37	659	40	33
5	524	30	641	32	20
10	596	22	611	23	10

Characteristics of Suspended Sediment Concentrations over the Areas Adjacent to Changjiang River Estuary, the Summer of 1998

Gao Shu(高抒) Cheng Peng（程鹏） Wang Yaping（汪亚平） Cao Qiyuan（曹奇源）
(*Institute of Oceanology, Chinese Academy of Sciences, Qingdao 266071*)

Abstract A major flood event occurred within the drainage basin of the Changjiang River in June-August, 1998. Survey over the East China Sea adjacent to the Changjiang River estuary shows that during the flood the turbid water (with a suspended sediment concentration of higher than 10 mg l^{-1}) reached 123° E. Stratification of the concentration layers was present near 122° 15′ E, with the concentration in the bottom layer being 3 times that in the upper layer, in response to sediment settling processes. The concentration is the lowest in the area of 126° E~ 127° E, representing a characteristic of the Kuroshio water. Although there was some expansion of the turbid water extension compared with the winter situations with low freshwater discharges, the suspended sediment does not appear to disperse towards the northeast from the Changjiang River. Further, several secondary high suspended sediment concentration centers were present on the East China Sea continental shelf, which may result from resuspension of the seabed sediment or advection of seawater containing suspended matter. In order to understand the processes of fine-grained sediment transport/deposition and their impact on the flux of chemical constituents on the shelf, further studies on the hydrodynamics, temperature, salinity and nutrient characteristics are required.

Keywords: Suspended sediments; Concentration, Material flux, Changjiang estuary, East China Sea

1. Introduction

Suspended matter from the Changjing River represents an important source for the sedimentation on the East China Sea continental shelf. The sediment discharge of the river is around 5×10^8 t a^{-1}; one part of the sediment accumulates in the Changjiang River estuary, while the other enters the East China Sea and disperses towards the southeast and the south (Qin and Zheng, 1982). Generally, the turbid water of the Changjiang River cannot reach the areas beyond 122° 30′ E; within the turbid water body, the suspended sediment concentration (SSC) in the bottom layer is higher than that in the upper layer (Yun, 1981; Milliman et al., 1985a; Qin et al., 1989). However, the turbid water may extend to a larger area during a summer flood in the Changjiang River basin. A flood event occurred in the Changjiang River in the summer of 1998, which represents the largest since 1954. Intensive monsoon rainfall had continued for a long time since the beginning of the flood season in middle June. The water level exceeded local warning levels in many places downstream of the Yichang Gauging Station. In addition, heavy rain hit the region

in the south of the lower reaches of the Changjiang River, causing a rapid water level rise. In particular, the flood flux reached a maximum in middle July and the water level exceeded the local historical records in many river sections. For example, the flux at the flood peaks was over 5×10^4 m^3 s^{-1} at the Yicang Gauging Station on a number of occasions (e.g., 5.35×10^4 m^3 s^{-1} on 2nd July; 5.64×10^4 m^3 s^{-1} on 8th July and 5.20×10^4 m^3 s^{-1} on 24th July). The daily water discharge reached 1027×10^8 m^3 in the lower reaches of the river on 30th July (Xie and Zhong, 1999). In response to such a flood event, the water discharge into the sea greatly increased, resulting in a rapid increase in the SSC; the turbid water (with the SSC > 10 mg l^{-1}) reached 123° E.

A cruise to the East China Sea adjacent to the Changjiang River estuary during the flood event was organized by the Institute of Oceanology, the Chinese Academy of Sciences, on board the *R/V Science I*, for the "Land-Ocean Interaction in China Seas" project. In the cruise the seawater temperature, salinity, current velocities and nutrient contents were measured and some water and seabed sediment samples were collected (for the sampling sites, see Figure 1). In the present paper, preliminary results concerned with the analysis of the SSC data are reported (the other data sets are subjected to further analyses and studies). In addition, on the basis of the data obtained, in conjunction with some historical data, the general patterns of the SSC distribution are described.

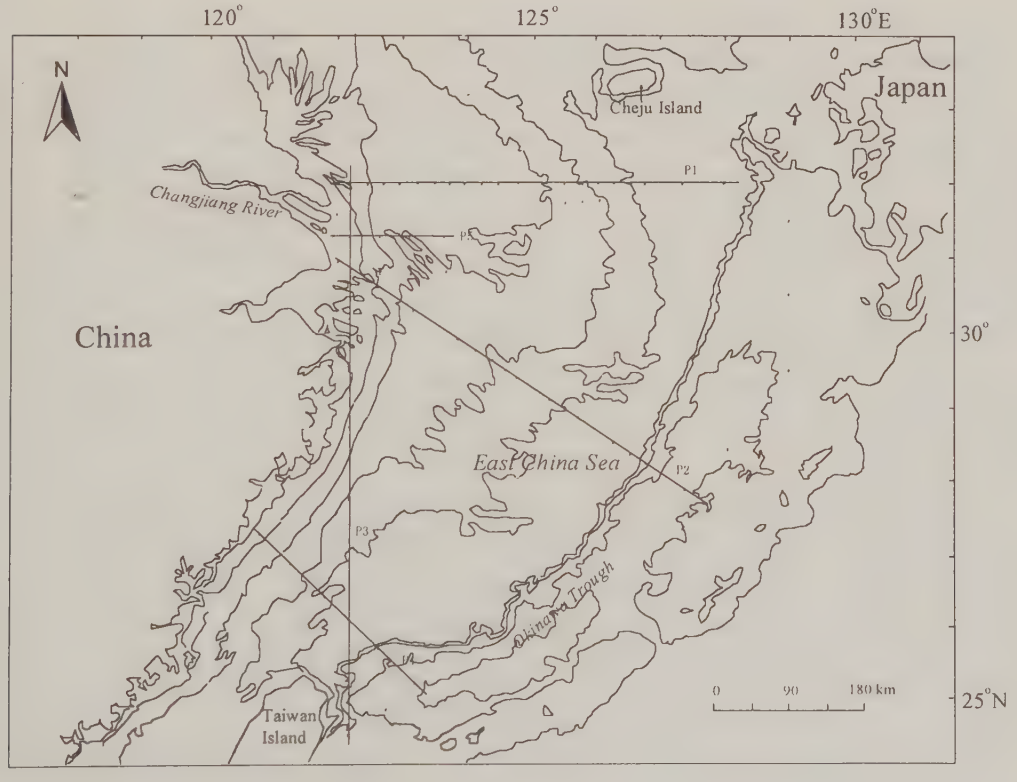

Fig. 1 Location of the study area and SSC sampling stations (on the basis of 1986 Chart)

2. Observations and Data Analysis

During the summer cruise on board the *R/V Science I*, which took place between 1st and 21st July 1998, 302 water samples were collected at 64 stations (Figure 1). The position was fixed using a differential GPS system. It was clear and calm without large waves during the survey.

The water samples were collected using NISKIN sampling bottles from the various layers within the water column (i.e. 0, 10, 20, 30, 50, 75, 100, 150 m etc.), according to the standard described in *Regulations of Marine Surveys* (in Chinese, issued by the State Oceanic Administration). At some stations, the collection of water samples below 150 m from the water surface was not successful because of the equipment malfunctioning at that depth. The SSC was determined using the filtering method in the laboratory. Around 2 L of seawater were filtered for each of the water samples, through a 0.45 μ m filter (a product of the Second Institute of Oceanography, the State Oceanic Administration). The filter with sedimentary material was dried by placing it under an infrared lamp with a temperature of around 40° C. Finally, the SSC was calculated with a method described by Gao et al. (1997).

3. Results

3.1 Horizontal SSC distribution patterns

Horizontal distribution patterns of the SSC (represented by the weighted mean value over the water column) over the East China Sea in the summer of 1998 are shown in Figure 2. The SSC decreases from the Changjiang River estuary towards the east and the south, with a high value of more than 100 mg L^{-1} to the west of 122° E and a low value of only 5 mg L^{-1} at 123° E. Moreover, the 5 mg L^{-1} SSC line protrudes towards the southeast, until beyond 124° E. The turbid water from the Changjiang River with an SSC in excess of 10 mg l^{-1} reaches 122° 30′ E and 123° E along the P1 and P2 profiles, respectively. Thus, the material from the Changjiang River is transported eastward and southeastward in the East China Sea.

Further, relatively high SSC values of 5~10 mg L^{-1} are observed at 32° N, 126° E (i.e. mud deposit area to the south of Cheju Island) and 32° N, 124° E (Figure 2). The SSC is generally less than 5 mg L^{-1} at other stations near these two locations. Such a phenomenon may be related to localized resuspension of the seabed mud.

It is worth noting that the SSC values obtained in this study are significantly higher than those reported elsewhere (Yang et al., 1992). The big flood in the Changjiang River is a major reason for this phenomenon since the rapidly increasing water discharge resulted in a rapid increase in SSCs. A large amount of suspended sediment is dispersed into the sea by the Changjiang River flood water with high SSCs. Hence, the area for SSC dispersal is extended in the flood season than in a low water discharge season. In the winter the turbid water only reaches the west of 122° 30′ E. On the other hand, the dispersal direction towards the northeast, which has been thought as a general pattern in the summer, is not significant in this particular data set.

3.2 Vertical SSC distribution patterns

Vertical SSC distribution patterns in the East China Sea are shown in Figure 3 for Profiles P1, P2 and P3. For Profile P1, the turbid water is confined to the west of 123° E along the latitude of 32° N.

An SSC maximum is present near the Changjiang River estuary, with the values of 10 and 150 mg L^{-1} in surface and bottom water layers, respectively (Figure 3a). The SSC decreases rapidly towards the east

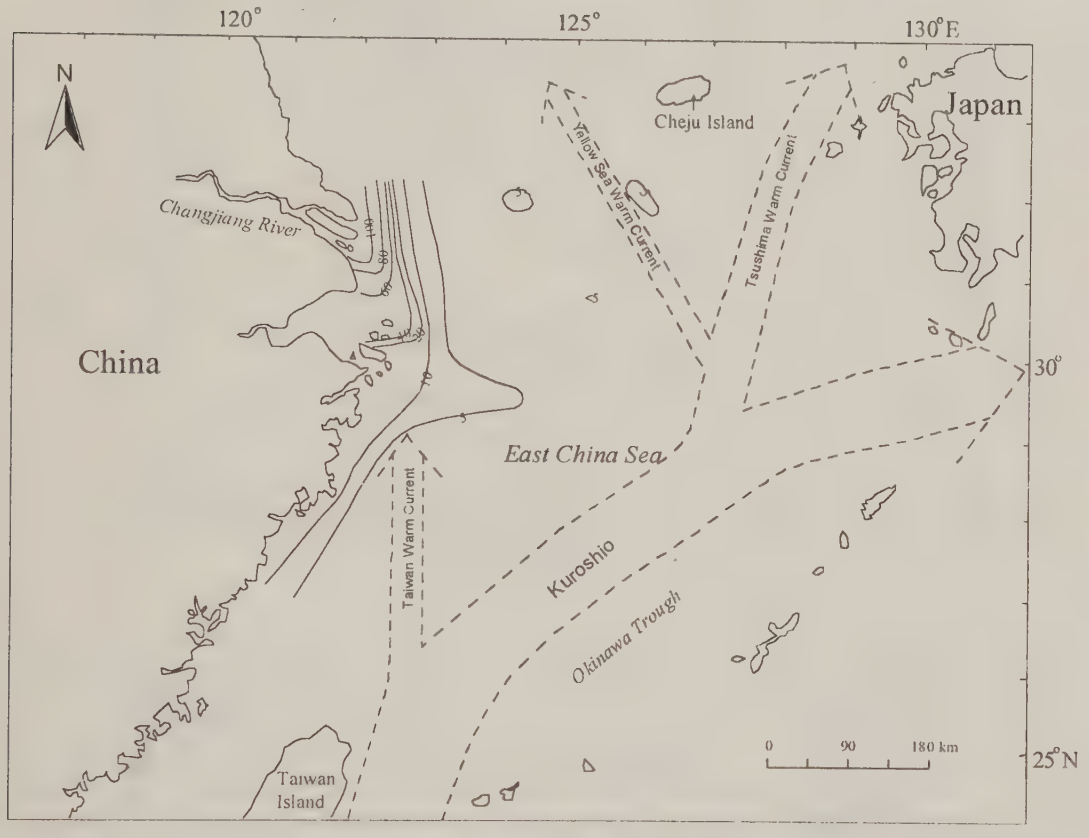

Fig. 2 Horizontal distribution patterns of the suspended sediment concentration (mg L^{-1}) in the East China Sea

and becomes lower than 2 and 10 mg L^{-1} in surface and bottom layers, respectively, in a distance of 100 km from the river mouth. Furthermore, a secondary high SSC center, characterized by an SSC of over 30 mg L^{-1}, is present where the water depth is 50~70 m (125° 30′ E~126° E). The relatively high SSC water extends from 4 m to 20 m above the seafloor, inclined towards the sea, and is separated from the eastern water by a clear water body with an SSC of less than 2 mg L^{-1} and a width of 100 km. Since the water bodies adjacent to the center are associated with very low SSCs, and the high SSC is only found in the water layer near the seabed (Figure 3a), the secondary SSC center may be related to the resuspension of the seabed sediment. However, the high SSCs observed at some sampling stations are probably related to biological activities near the sea surface. The water bodies with low SSCs (< 2 mg L^{-1}) between 125° 30′ E and 127° 30′ E along Profile P1 may represent the characteristics of the Yellow Sea Warm Current and Tsushima Warm Current.

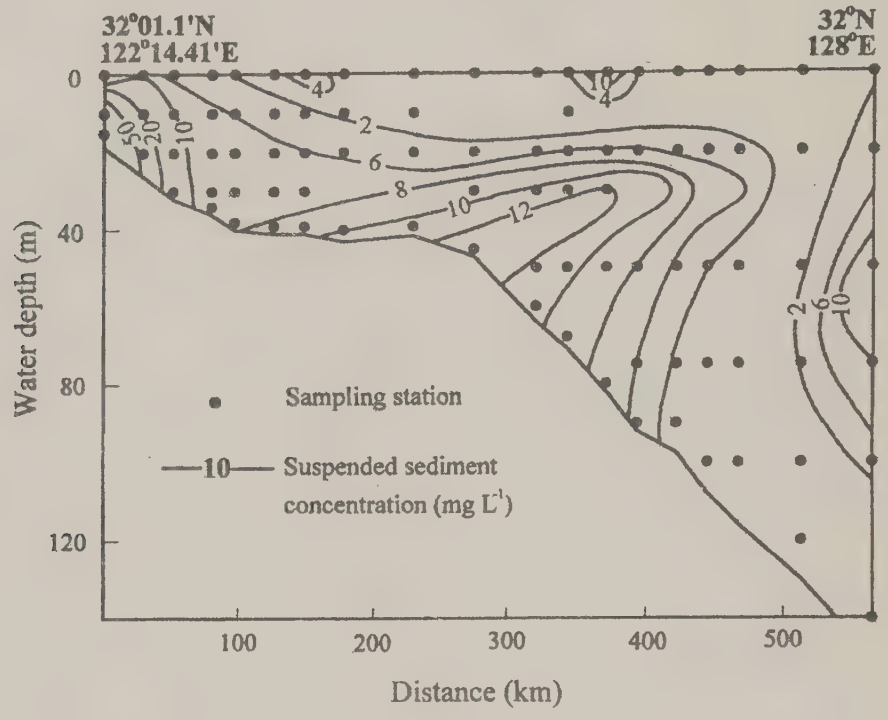
32°01.1'N
122°14.41'E
32°N
128°E
Water depth (m)
0
40
80
120
100
200
300
400
500
Distance (km)
Sampling station
10 Suspended sediment concentration (mg L-1)

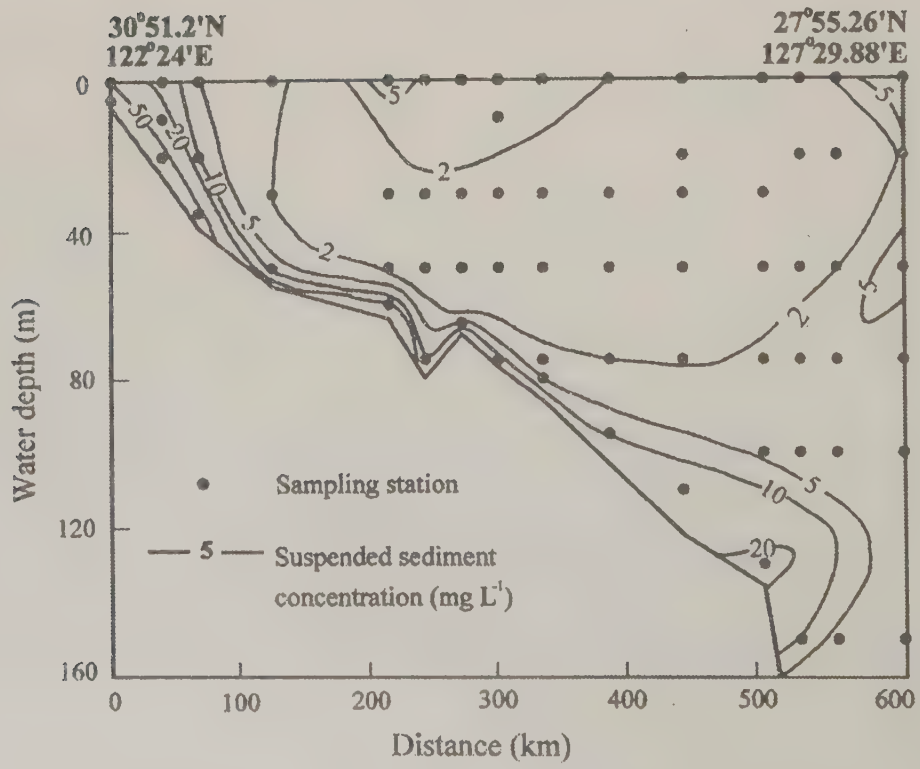
30°51.2'N
122°24'E
27°55.26'N
127°29.88'E
Water depth (m)
0
40
80
120
160
0
100
200
300
400
500
600
Distance (km)
Sampling station
5 Suspended sediment concentration (mg L-1)

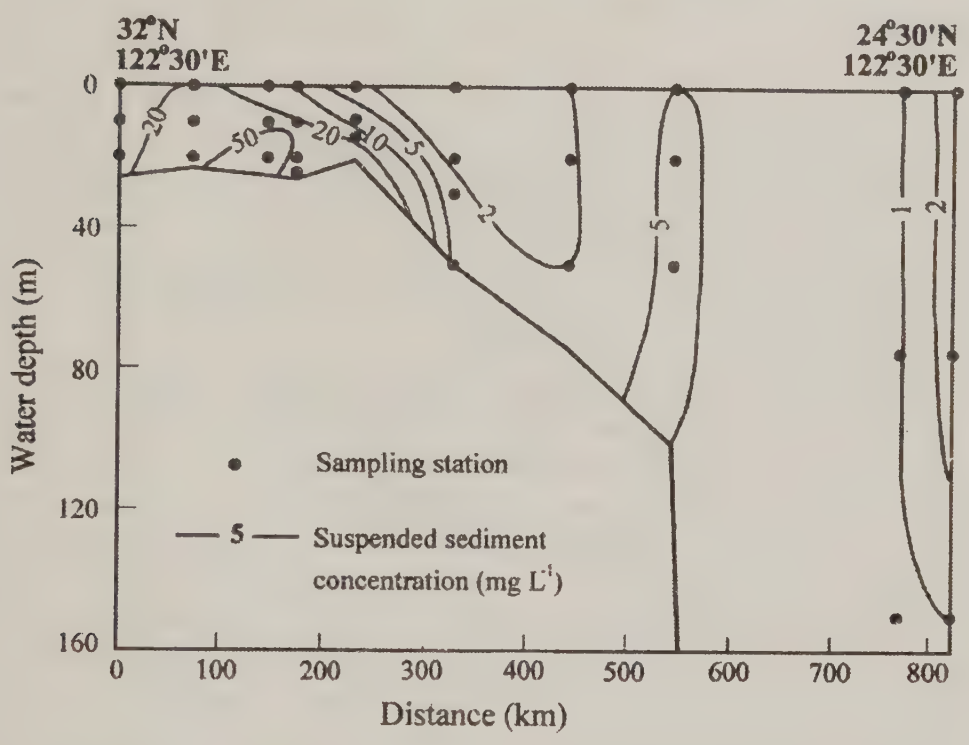

Fig. 3 Vertical distributions of suspended sediment concentration (mg L^{-1}) in the East China Sea along (a) Section P1; (b) Section P2; and (c) Section P3

Along the P2 profile, the turbid water from the Changjiang River reaches 123° E (Figure 3b). Further to the east, the SSC is generally less than 10 mg L^{-1}; such a pattern may result from the settling of the suspended material. A turbid layer with SSCs of larger than 10 mg L^{-1} is present below 10 m above the seabed, extending from the estuary to the shelf edge with a water depth of 150 m. Because the salinity here is high (Wang Fan, personal communication), the turbid layer should represent the effect of material settling rather than the density current. Moreover, the SSC decreases to 2~5mg L^{-1} between 127° E and 128° E. A clear water body with a thickness of 40 m and an SSC of lower than 2 mg L^{-1}, which is connected with the eastern low SSC water, is observed in the middle and upper layers between 124° E and 127° E. A secondary high SSC center (with a maximum value of 22 mg L^{-1}) is also present at the shelf edge with a water depth of 100~150 m. The water column near 126° E-127° E along Profile P2 shows the characteristics of Kuroshio waters (i.e. with high salinity, low temperature and low SSC).

A turbid layer with SSCs in excess of 10 mg L^{-1} extends towards the south of 31° N along Profile P3 (Figure 3c), which results from the Changjiang suspended sediment transported towards the south. Stratification in terms of the SSC is present, with the concentration in the upper layer being 1/3 of that in the lower layer. The SSC is below 2 mg L^{-1} in the seawater between 25° N and 27° N (with an extension of around 200 km). The water column is characterized by SSCs of higher than 5 mg L^{-1} at the shelf edge (water depth of 80~100 m); once again, this may be associated with the resuspension processes.

4. Discussion

The turbid water from the Changjiang River reached 123° E along Profile P2 (Figure 3b). After leaving the Changjiang River, most of the sediment accumulates on the continental shelf due to the reduced current velocity; the remaining part of the material is dispersed towards the deep sea by the ocean currents. However, the fine-grained sediment on the continental shelf is subjected to resuspension and transport by the currents, or dispersion from an area with high SSC to a low SSC area. The intensity and range of the transport and dispersal of suspended sediment on the East China Sea continental shelf is controlled mainly by three factors, as described below.

(1) **Monsoon-induced circulation patterns** During the winter, northerly winds are strong over the eastern China seas. As a result, a lateral circulation pattern, with the surface layer moving landward and the bottom layer directed seaward, is formed due to the winter winds and the Coriolis effect (Figure 4a). Moreover, the seawater with high SSCs is usually located in the bottom layer. Thus, the monsoon-induced circulation favours the dispersal of suspended sediment towards deep seas (e.g. the Okinawa Trough). During the summer, southerly winds dominate over the region and a circulation pattern with a seaward-moving surface layer and a landward-moving bottom layer exists (Figure 4b). This prevents, to some extent, the escape of suspended sediment towards the deep waters. Some experiments with sediment trap deployments in the Okinawa Trough show that the deposition rate is small in summer but large in winter; this observation has been considered as evidence of the monsoon effect on the sediment transport (Iseki, 1994; Hu, 1995). However, because there is a lack of understanding of the combined effect of the monsoon circulation (with a low frequency) and the tidal currents (with relatively high frequencies) on suspended sediment transport, and little is known about sediment transport and settling within the Okinawa Trough, further study is required to delineate the influences of the monsoon on the seasonality of sedimentation in the Okinawa Trough.

(2) **Main route of the movement of the diluted water from the Changjiang River** The diluted water movement has an important influence on the sediment transport patterns. Generally, the diluted water from the Changjiang River flows towards the southeast in winter, but it flows towards the east or northeast in summer when other controlling factors (e.g. the flood in the Changjiang River) prevail (for a thorough review, see Zhu and Shen, 1997). According to the dispersal pattern of the Changjiang sediment shown in Figure 2, the diluted water flows towards the southeast during the summer flood period of 1998; it did not turn towards the east until the flow reached the area to the south of 30° N. The main route of the diluted water changes with seasons and this has an impact on the dispersal direction of suspended sediment. In the future more studies are needed on the mechanism controlling the route of the Changjiang diluted water.

(3) **Kuroshio Current system** Figure 2 shows that the Kuroshio Current enters the East China Sea through the southwest part of the Okinawa Trough near Taiwan Island; afterwards it is separated into three branches with the main branch re-entering the Pacific Ocean off the southern coast of Japan. The other two branches, the Yellow Sea Warm Current and the Tsushima Warm Current, split to the south of Cheju Island and flow towards the northwest and the northeast, respectively. The Kuroshio Current, with low SSCs between 126° E and 127° E, is intensified in summer and impedes the dispersal of the shelf

water into the deep sea. During winter, the Kuroshio Current is weakened, which favours the transport of suspended sediment derived from the Changjiang River or resuspension on the continental shelf towards the deep sea (Yang et al., 1992).

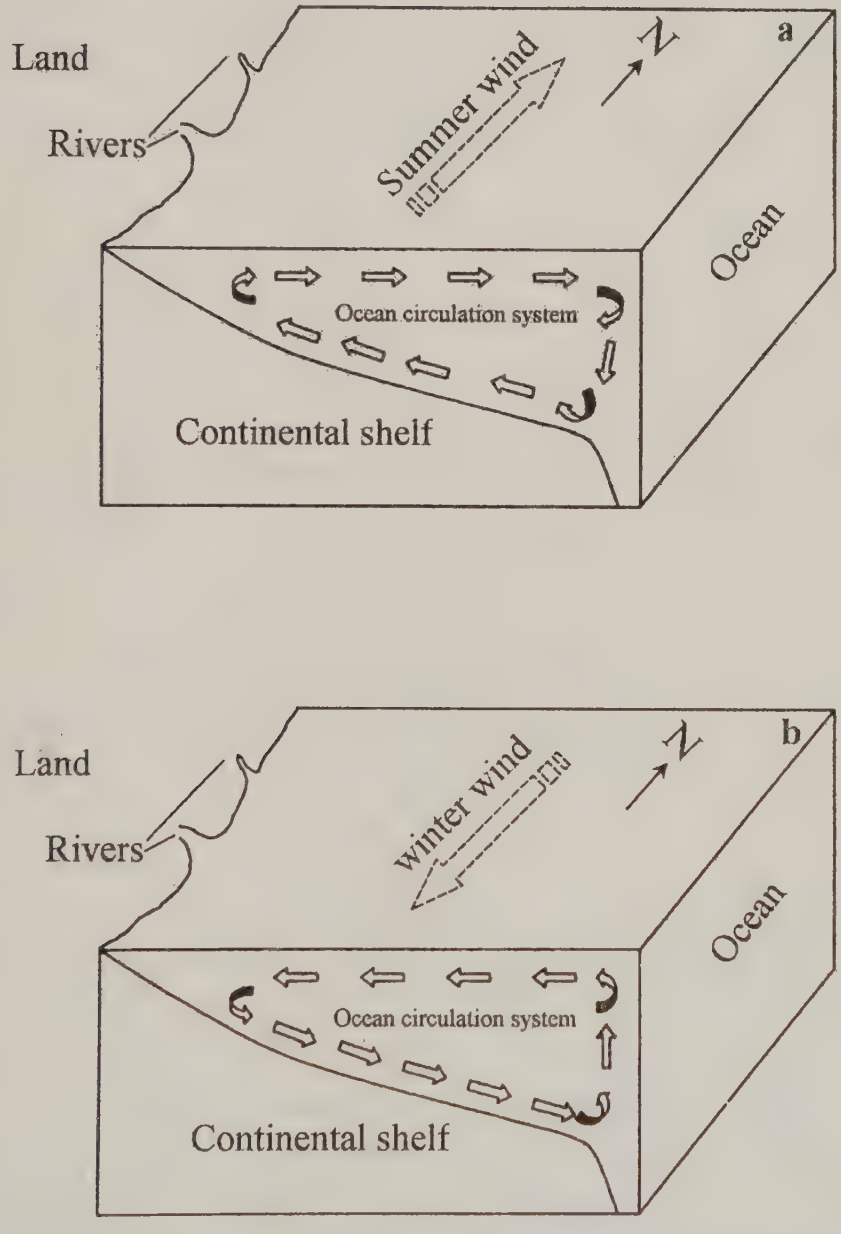

Fig.4 Schematic diagram showing the monsoon-induced circulation patterns on the continental shelf during (a) winter and (b) summer

The secondary high SSC centers identified in the present study are worth discussing. Two of such centers are present to the south of Cheju Island, along Profile P1 (Figure 2), which may result from the

resuspension of seabed mud. The result of grain size analysis using a Cilas 940L Laser Particle Analyzer (produced in France) indicates that the seabed mud of the center (at 32° N, 126° E) is characterized by a mean diameter of 7.7 ϕ ; the material is well-sorted and positively skewed, containing 40% clay and 60% silt (Figure 5). Such material, deposited in a water depth of 50 m, may be resuspended easily by the combined action of waves and currents (Qin et al., 1989; Milliman et al., 1985b). Nevertheless, the current along the northern Jiangsu coast and the seawater with high SSC's in the southern Yellow Sea, which flows towards the south, may also be responsible for the formation of the secondary high SSC centers. Therefore, in order to understand the mechanisms for the formation of the centers, the regional hydrodynamics and the current system in the southern Yellow Sea must be known.

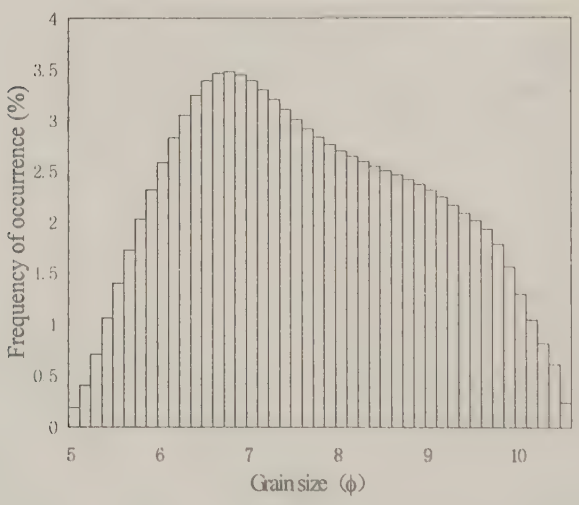

Fig.5 Grain size distribution patterns of a seabed sediment sample collected from the area of one of the secondary high SSC centers (i.e. 32° N, 126° E) on Profile P1

The secondary high SSC centers are formed at the shelf edge along Profiles P2 and P3 (Figure 3b and 3c), which also represent localized high nutrient content centers according to the observations during the same cruise (Zhao Weihong, personal communication). Hence, the vertical distribution pattern of suspended sediment is highly correlated with that of nutrients. It is noticeable that the shelf edge is located exactly on the route of the main Kuroshio Current which may cause resuspension from seabed and within the water column, resulting in high SSCs here. This interpretation appears to be appropriate for the observed relationship between SSCs and nutrient contents. However, we need to undertake further analysis of the current, salinity and temperature data, in order to confirm the resuspension mechanism.

5. Conclusion

Data obtained from a cruise to the East China Sea adjacent to the Changjiang River estuary show that the suspended sediment from the Changjiang River is dispersed over a larger area during the flood period in the summer of 1998. The turbid water (with suspended sediment concentrations of higher than 10 mg l^{-1}) reaches 123° E, directed towards the southeast and the east, without a clear pattern of dispersal towards the northeast.

The dispersal of the sedimentary material, including the fine-grained sediment from the Changjiang River and resuspension on the continental shelf, is influenced by the monsoon-induced circulation patterns, the route of the Changjiang diluted water and the Kuroshio Current system. In order to understand these processes and their influence on the sedimentation in the Okinawa Trough, studies on sediment settling and transport in the Trough should be undertaken.

Several secondary centers with relatively high suspended sediment concentrations are observed at the shelf edge and in the area covered with muddy sediment over the region. The formation of these centers may be related to the resuspension of the seabed sediment or advection of seawater containing suspended matter, but further analysis of the hydrodynamics, temperature, salinity and nutrient conditions as required to confirm this hypothesis.

References

Gao S, Park Y A, Zhao Y Y and Qin Y S, (1997) Transport and resuspension of fine-grained sediments over the southeastern Yellow Sea.*Proceedings of the Korea-China International Seminar on Holocene and Later Pleistocene Environments in the Yellow Sea Basin.* Seoul, Korea, 83-96

Hu D, (1995) The role of vertical circulation in sediment dynamics. In: Ye, D., Lin, H. et al. (editors).*China Contribution to Global Change Studies*, Science Press, Being, 168-170

Iseki K, Okamura K and Tsuchiya Y, (1994) Seasonal variability in particle distribution and fluxes in the East China Sea. In:*Proceedings of the Sapporo IGBP Symposium* (14-17 November 1994, Sapporo, Hokkaido, Japan), 189 -197

Milliman J D, Beardsley R C, Yang Z and Limeburner R, (1985b) Modern Huanghe-derived muds on the outer shelf of the East China Sea: identification and potential transport mechanisms.*Continental Shef Research*, 4 (1/ 2) 175-188

Milliman J D, Shen H, Yang Z and Meade R H, (1985a) Transport and deposition of river sediment in the Changjiang estuary and adjacent continental shelf.*Continental Shelf Research*, 4 (1/2) 37-45

Qin Y S, Li F, Xu S M, Milliman J and Limeburner R, (1989) Suspended matter in the south Yellow Sea.*Oceanolog ia et Limnologia Sinica*, 20 (2) 101-111 (in Chinese, with English abstract)

Qin Y S and Zhen T M, (1982) A study of distribution pattern of sediments on the continental shelf of the East China Sea. *The Geology of the Yellow Sea and the East China Sea.* Beijing: Science Press. 39-51 (in Chinese)

Xie Z X and Zhong X Z, (1999) Three flood in Changjiang River.*Chinese Science*, 51 (2) 27-31 (in Chinese)

Yun C X, Cai M Y and Wang B Q, (1981) An analysis of the diffusion of suspended sediment discharged from the Changjiang River based on the satellite images.*Oceanologia et Limnologia Sinica*, 12 (5) 391-401 (in Chinese, with English abstract)

Zhu J R and Shen H T. (1997)*Mechanism of dilution water of Changjiang River*. Shanghai: East China Normal University Press. (in Chinese)

Yang Z S, Guo Z G, Wang Z X, Xu J P and Gao W B. (1992) Basic pattern of transportation of suspended mater from the Yellow Sea and East China Sea to the east deep seas.*Acta Oceanologica Sinica*. 14 (2) 81-90 (in Chinese, with English abstract)

Tentative Ideas on the Development of "Digital Ocean" in China

Hou Wenfeng (侯文峰)
(*National Marine Data and Information Service, Tianjin, 300171, China*)

Abstract To greet the ocean age of the 21 century, proceeding from the development strategy of the country, China has included the project on the development of the "digital ocean" in the National Marine Science and Technology Development Plan for the period of Tenth Five-year -Plan and the long-term tentative plan for the year 2015. The goal of the project is collect information on 3-D ocean monitoring, complete the digitizing project of marine information and the establishment of the marine spatial data infrastructure and to realize sharing of the marine information and establishment of the basic project of "digital ocean".

Research and development of the project "221" for "digital ocean" will be carried out in the period. That means two key technologies: technology for spatial data infrastructure and technology for "digital ocean" support; two platforms: research and development on dynamic 4-D marine geographical information system and demonstration for application.

Keywords digital earth; digital ocean; development strategy; GIS; China

As soon as the concept of "Digital Earth" comes out, great repercussion has been evoked in the scientific community of China. As a core of the "Digital Earth", the space-to-earth observation system, the information highway, and the National Spatial Data Infrastructure have become hot topics of study in China. The relevant concepts such as "Digital China" and "Digital Land" have been raised one after another. Making full use of this opportunity, the marine science community of China has also gone into action to discuss the relations between the ocean and the "Digital Earth". After a heated discussion, the tentative ideas on the development of "Digital Ocean" in China have been raised. That is to use the digital means to handle and display the ocean processes, help the mankind to understand the ocean and utilize effectively the ocean information resources in full scale.

I The Composition and Development Strategy of Digital Ocean

1. The Composition of "Digital Ocean"

The "Digital Ocean" will be a huge and complicated system, taking the marine objective phenomenon as an object of study and based on marine spatial data infrastructure, relying on the national information infrastructure and information highway, as well as the latest information technologies. There will be three components for "Digital Ocean": data (spatial and non-spatial), operational platform and application model.

The data for the "Digital Ocean" will include large-medium and small-scale marine spatial data, various types of multi-spectrum, multi-time phase, and high resolution marine satellite remote-sensing images, aerial remote-sensing images, special-subject maps of different scales, different types of survey,

observation and statistical data on marine environment, resources, economy, population, marine industry, and marine disasters. Operational platform is a Web-based, dynamic and 4-D (x,y,z,t) marine geographic information system. This system can be used for the handling of marine data matching the spatial position which changes with the marine phenomenon. This will meet the unique requirements of dynamic marine data management, display and development. Application models include different types of research model for marine environment, resources, economy and disasters.

2. Basic Ideas on the" Digital Ocean" Development

Proceeding from the fundamental interests of the Nation, and based on marine information resources, national information infrastructure and future trends of the development of international information technologies, the "Digital Ocean" could be constructed to safeguard marine rights and interests, national security, protect marine ecology and environment, enhance the capability for the development of marine resources, and promote the marine economic development. Research and development project "221" for "Digital Ocean" will be carried out. That means two key technologies: technology for spatial data infrastructure and technology for "Digital Ocean support"; two platforms: research and development on the dynamic 4-D marine geographical information system and spatial data platform; one prototype: construction of "Digital Ocean" prototype system and demonstration for application; making contribution to the development of Chinas marine information course.

3. Development Strategy of "Digital Ocean"

"Digital Ocean" is a strategic information project, which is important to the development of the Nations economy, science and technology and national defense. To study and construct the "Digital Ocean " should have a relevant national strategy and its objectives:

(1) Proceeding from the Nations interests and the long-term development, overall plan and development strategy will be made to provide guiding ideas for scientific research and specific implementation of "Digital Ocean" project;

(2) Overall framework for "Digital Ocean" data, technology and application will be constructed in the light of national economic and scientific and technological development objectives;

(3) Analyzing national and international basis objectively and facing squarely the problems in the construction of "Digital Ocean", feasible leap over type of development model will be sought for making the" Digital Ocean" plan;

(4) Following closely the forward scienctific and technological development and the latest development on international Digital Earth and related development on "Digital Ocean", looking for optimum linking point between the national needs and the scientific and technological innovation, a developing strategy for Chinas "Digital Ocean" will be adjusted in time.;

(5) Based on the conditions of the Nation, and following the principle of "to do something and not to do something", a feasible implementation plan and specific scenario should be formulated for making policies and regulation, construction of spatial data infrastructure, research on supporting technologies, prototype development and application demonstration.

II The Role of "Digital Ocean"

1. "Digital Ocean" will be a Guarantee for the safeguarding the national marine rights and interests

The war in the future will be the contest of high and new technologies, and also a confrontation of information technologies. Every link of construction of national defense, defensive at sea, military training, and weapon experiment needs support from the marine information system. Actually, the struggle for safeguarding marine rights and interests is also a contest of the possession of marine information and marine information technologies. Mass information, advanced marine information technologies, abundant expert systems and methodology databases will produce various types of negotiation scenario for maritime delimitation quickly, accurately and effectively to constantly ensure favorable positions in the diplomatic struggles for safeguarding the nation's marine rights and interests.

2. "Digital ocean" will be the motive power in promoting the development of science and technology

At the end of this century and at the beginning of the next century, many countries have launched and are going to launch ocean color and ocean dynamic satellites. Vast quantities of space-to-earth observation data collected from those satellites are bound to promote the organic combination of space technology, information technology and earth science. The implementation of "Digital Ocean" strategy is just such a synthetical combination of multi-disciplinary researches, which should rely on various branches of marine science and relevant theoretical and methodological technologies such as various types of marine application model, marine spatial information collection, scientific computing, mass data storage and compression, computer network graphic browsing, webGIS, knowledge intelligence and virtual reality technology studies. These will be the motive forces for the rapid development of marine science and technology. In the specific researches of marine science and technology, marine spatial information could provide oceanographers with information on basic fields of the ocean, such as information on bottom topography, hydrology, meteorology, biochemistry, etc. The study of "Digital Ocean" will surely promote the progress in the marine scientific and technological research.

3. "Digital Ocean" is a basis for integrated marine management and macro policy-making

In the field of marine supervision, through cruising and law enforcement, the evidence of unlawful activities can be quickly obtained and dealt with accordingly. For illegal exploration of marine resources, monitoring of oil-spill incident, assessment of damage and claim according to law, marine spatial information could be used to provide information for qualitative, positioning and quantitative science-aided decisions. For marine functional zoning, sea area use management, sea area boundary survey, examination and approval of coastal engineering projects, unified and high-quality marine spatial information is required. By using marine spatial information, the state of marine environmental quality, diffusion and floating of marine pollutants, as well as marine environmental improvement and protection plan could be well displayed. With support of marine spatial information, the distribution of marine fishery resources, the migration route, and spawning ground, and the fishing ground of major marine

economic fish species, as well as environmental background information such as watercolor and chlorophyll could be well displayed.

4. "Digital Ocean" is the optimum way to make full use of marine information resources

Through dozen years' efforts, China has accumulated a vast quantity of historical data. During the periods of Eighth Five-Year Plan and Ninth Five-Year Plan, various types of large- and medium-sized marine database have been set up one after another and produced digitized basic geographic maps and specialized maps in different scales. But at present, the ownership of quite amount of data is in confusion, the standard is inconsistent, compatibility is bad, the utilization ratio is low, causing a great waste of marine information resources. It is unfavorable for the development of common sharing of marine information in the future. The construction of the "Digital Ocean" will solve this problem once and for all.

5. "Digital Ocean" will provide Information highway with essential Marine Information Resource

In the era of information, the difficulties encountered are how to collect mass data and how to obtain the needed information from it. "Digital Ocean" could provide opportunity to make full use of and understand the mass data. Development of "Digital Ocean" in China should first proceed from the rapid construction of marine spatial data information, and incorporate data acquisition, processing, storage, transmission, management, utilization and service technology into one. It should take marine space with geographic position as a research target, marine spatial information data as a core, and realize the totally digitized and holographic storage of marine information resources. Then it should use spatial analysis and virtual reality technology, enabling the user to view directly the dynamic pictures of various marine real changes and its effects with multi-dimensional characteristics and multi-resolution, thus providing timely, accurate and effective marine spatial, dynamic information service on resources and environment.

III Major Study Contents of "Digital Ocean"

1. Study on the policies and regulations relevant to "Digital Ocean"

"Digital Ocean" is one of the important national strategic decisions and it is also one of the global marine information projects which will be constructed and shared by the government, industry and hi-tech institutions. Therefore, the first consideration is to make "Digital Ocean" relevant policies, laws and regulations. There are two key ideas for "Digital Ocean" concept. One is to use digital means for unified processing, representation of the ocean in order to understand the ocean directly perceived through senses, the other is to make the fullesl use of marine information resources and common sharing of marine information. At present, China is facing many serious problems in information sharing, such as data blockade, lack of regulations for data sharing. To solve this problem once and for all , the first and foremost thing is to enhance the understanding of data management and common sharing, and set up a data sharing mechanism with the support of the State.

The study contents of the "Digital Ocean" relevant policies, laws and regulations include: formulation of the national policies, laws and regulations for marine information sharing; study on methods and scope for confidential security of marine data and removal of confidentiality; study on formulating the principles and methods for marine information sharing (including classification and

classified management, principles of and scope for the sharing of marine information free of charge and on the pay basis, formulating regulations at the national level on marine basic information management.

2 Study on "Digital Ocean" Spatial Data Infrastructure

"Digital Ocean" is based on the information highway and relying on the marine spatial data infrastructure. That is to say, the "Digital Ocean" will be operated on the broad-band and high speed Internet. In order to accurately represent, describe and access to all the marine spatial information, which is related to geographic parameters, it is necessary to construct the "Digital Ocean" spatial data framework and carry out study on the "Digital Ocean" spatial data infrastructure.

The "Digital Ocean" spatial data infrastructure is one of the important components of the National Information Infrastructure. It is a bridge to link the "Digital Ocean" with the information highway. The "Digital Ocean" spatial data infrastructure mainly include the "Digital Ocean" spatial data framework, the "Digital Ocean" spatial data clearing house, the "Digital Ocean" data exchange standard and the "Digital Ocean" spatial data coordination, management and dissemination system and mechanism.

2.1 Research on the "Digital Ocean" spatial data framework

"Digital Ocean" spatial data framework is the core of the marine spatial data infrastructure. It contains very basic marine spatial data sets. The main contents of the marine spatial data framework include coastline, water depth, sea bottom topography, background information on marine resources and environment, offshore man-made structures, submarine cables and pipelines, sea area use, and coastal administrative divisions. The objectives of the marine spatial data framework construction is to set up a framework system with multi-scale, accurate accessing to and integration of marine spatial information which matches the positions of spatial coordinates and to provide platform for marine spatial data framework and marine spatial information service. On the "Digital Ocean" spatial data framework, a series of national spatial data base groups with different scales at the national level could be set up and utilized for various purposes.

The main contents of research on "Digital Ocean" spatial data framework are to develop multi-scale marine spatial data framework systems, including basic and public marine data sets and spatial geographic coordinates reference.

2.2 Construction of the "Digital Ocean" Spatial Data Clearing House

"Digital Ocean" spatial data clearinghouse is a wide area network system linking the marine spatial data acquisition, management and service. Though China has set up marine information web site, such as China Ocean Information Network (http//www.coi.gov.cn), because the marine spatial data is vast in quantity and requires a huge storage capacity and a fast network speed , the marine spatial data exchange network system needs to be further studied.

The main research contents of "Digital Ocean" spatial data clearing house include the construction of hardware and software system such as spatial data exchange network and data exchange network server, and the construction of metadata management system helping users to have access to and obtain the data.

2.3 Research on "Digital Ocean" Spatial Data Exchange Standard

Marine spatial data is multi-source with great varieties, the leading to a big difference between the marine spatial data model and its data structure. The compatibility of marine spatial data is bad. So, strict

unified marine spatial data exchange standard must be developed to ensure that the marine spatial data collection and management agencies follow the same standard, so that the data which enter the spatial data clearing house is compatible and successfully represented in the "Digital Ocean" spatial data framework and is commonly shared.

The major contents of "Digital Ocean" spatial data exchange standard include vector of spatial reference information and grid data (including network) exchange agreement, format, metadata and contents, and the standard include concept, quality report, transformation module, and the definition for spatial parameters and attributes.

2.4 "Digital Ocean" spatial data coordination, management, and dissemination system and organization

The research on "Digital Ocean" spatial data infrastructure should be led and coordinated by the related State agencies (the department concerned of the State government should set up a "Digital Ocean" leading group and full time personnel should be appointed to coordinate the work of "Digital Ocean"). A special organ should be set up on the basis of the existing national marine data and information management institutions responsible for the management and dissemination relating services of "Digital Ocean" spatial data. In addition, considering the specific characteristics of marine spatial data acquisition, processing and management, a special organ is needed to maintain, update and develop the spatial data.

3. Research on Supporting Technology of "Digital Ocean"

"Digital Ocean" is a multi-disciplinary and multi-technological marine combination. Its construction needs not only existing mature technology basis, but also related new theories and technologies to support it. These technologies include broadband network technology, remote sensing data acquisition technology, mass data storage and compression technology, interoperation technology, scientific computing, distributed object technology, distributed spatial database technology, spatial data storage technology, various application models, KDD, virtual reality technology, WebGIS technology, etc. The major technologies to be developed include:

3.1 Mass data storage, compression and management technology

The quantity of marine remote sensing data, multi-beam survey data, historical marine routine observation data are amazing. In the construction of "Digital Ocean", these data will finally evolve into a spatial related multi-media mixture. Therefore, the vast quantity of spatial digital data and the non-standard (spatial graphic, image, sound) information must be stored, extracted and managed efficiently. Relying only on the existing data management technology would not be able to meet the requirement. New technologies should be introduced, including mass storage and compression technology, massive spatial data management technology and object-oriented marine spatial database technology.

3.2 Marine data assimilation and composition technology

The acquisition of marine data is mainly from satellite remote sensing, coast remote monitoring, marine survey, station buoy observation, etc. The standard, precision and resolution of these multi-source data are not unified. Therefore, the research on multi-source data assimilation, especially 4-D assimilation technology is needed. At the same time, the satellite remote sensing data in different time phases and different bands need to be composed.

3.3 "Digital Ocean" application model

"Digital Ocean" can be used to support the decision making for integrated marine management. It will provide alternative options for major decisions on marine development plan, marine resources and environmental protection. So, it needs support of the comprehensive marine spatial data analysis technology. The theoretical basis of spatial data analysis is numerical application models of different types. These include marine spatial data model, marine numerical model, marine sustainable development model, assessment model, prediction model and forecasting model, etc.

3.4 "Digital Ocean" virtual reality technology

"Digital Ocean" is a technological integration of 4-D marine spatial information. The virtual reality technology is one of the very important technological measures to enhance the understanding of marine spatial information. By using a real-time interaction operational way, it brings the real ocean world before the eyes of the users. The research contents of virtual reality technology include 3-D cartoon technology, network multi-media technology, interaction 3-D visual technology and virtual reality technology.

3.5 "Digital Ocean" WebGIS technology

"Digital Ocean" WebGIS is an important measure to display audio-visually the ocean spatial data through Internet. It is an important technical support for "Digital Ocean" application and service. The main contents of the research include marine 4-D GIS technology, GIS super-chain technology, GIS interoperation technology, marine GIS information products production and real-time release technology.

4. Research on Marine Dynamic Geographic Information System

Along with the application of new ocean monitoring technologies and the rapid development of Internet, the vast quantity of marine information obtained by the oceanographers is unprecedented. The key problem is how to select the useful information from it, and how to handle these information in an appropriate way to let them be inter-connected and finally produce a understandable information to help us understand the ocean better. Obviously, using GIS technology to process, display and develop marine information in the best way to solve the above-mentioned problems. At present, the mature GIS technology is based on land, and widely used in city planning and various land-based research work. All these are 3-D systems, enabling the data to match with positions and form a series of overlapped layers, each layer describing one type of characteristics. However, the ocean has a very broad sense of marine spatial and temporal changes, and such phenomena as sea wave, tide, current, temperature, salinity, density, sound, light, and electricity are closely related to time. To describe these phenomena by using the above-mentioned systems, the map layer in the system will change continuously. This will be difficult for marine data to find a matching position. This is a fatal weakpoint of using a 3-D geographic information system to describe marine information.

Therefore, research and development of a dynamical 4-D (x, y, z, t) marine geographic information system is really important. This type of system could handle data on the spatial system which changes with ocean phenomena (time). Thus, the unique requirement of dynamic marine data management, display and development could be met. Of course, this system should have the capability to integrate and operate marine numerical model, and should have good man-machine interface, visible and interactive. The objective of this system research and development is to provide a GIS tool suitable for marine applications and provide capabilities to integrate multi-source data and model in the system, public analysis and

display framework. At the same time, the system should have the functions of 4-D presentation, display the processing of point, profile, vector, and grid data, multi-model operations including real-time fast time series (cartoon) and WebGIS.

5. Research on Marine Basic Information Field

The marine basic information field means the background field information of various marine parameters such as sea bottom topography, sea surface temperature, air pressure, sea surface wind field, sea temperature, salinity, density, current, sea wave, dissolved oxygen. It could not only provide oceanographers with forcing field, initial field and boundary conditions for numerical modeling and forecast, prediction model computation, but also meet the requirement of various marine scientific researches by making full use of the multi-source marine information. For instance, the US National Oceanographic Data Center designed World Ocean Data Atlas WOA82, WOA94 and WOA98 in 1982, 1994 and 1998 respectively. These products are widely used by marine scientists from various countries for ocean numerical model computation and marine scientific research. But the station points and the resolution of these data relevant to the China sea area can not meet the needs in the actual application in China. So, it is necessary to use a marine data assimilation, especially the 4-D assimilation technology, and data quality control method to analyze and process marine data obtained from different time, different space with different observation means to study, design and produce multi-resolution marine environmental basic field information products. It is of special importance at present when marine data sharing is still rather difficult.

Ⅳ. Tentative Ideas on the Prototype System Development of "Digital Ocean"

Based on the existing conditions and basis, it is geared to the actual circumstances to adopt a prototype method of the system engineering project for "Digital Ocean" research and development.

1. Overall Design of "Digital Ocean" Prototype System Development

1.1 "Digital Ocean" prototype system development

Overall planning and design of the "Digital Ocean" prototype system development include information acquisition, system objectives, system functions, information processing, visual transmission and on-line service countermeasures.

1.2 Research on "Digital Ocean" related standard and norms

One of the important goals of the research on the construction of "Digital Ocean" is to realize the sharing of marine information and the prerequisite of marine information sharing is to have unified marine information standard and norms. Though China has carried out research on marine information standard, unified standards at the national level are less, and the scope is narrow. So far, there is no unified standard for such important marine information like marine resources. So, the standardization work should be quickened to lay foundations for the research and construction of "Digital Ocean".

The major contents of the research on "Digital Ocean" related standard include: classification and coding of marine information, standard for marine data processing and quality control, standard for marine information metadata, standard for marine resources, environmental map legend and charting,

parameter system and coding for marine resources and environmental maps (GIS) with different scales.

2. Transformation of Existing Databases

Prototype system development of "Digital Ocean" should be based on the available databases. The existing databases should be transformed if used for the construction of "Digital Ocean". Specific transformations include:

2.1 Standardization

The existing databases should be transformed according to the national unified marine information standard and work on preprocessing, dealing with redundant data, and quality control of marine information, should be carried out.

2.2 Special Treatment

Upon completion of the database standardization, the data status should be analyzed. For the geographic characteristics of the data, if the graphic is used to represent spatial position, spatial distribution, and spatial relations of the data, the attribute data and interconnections of the data should be set up to make a spatial positioning. For statistical data, the statistical unit should be divided according to the standard of positioning.

2.3 Networking

The aim of networking is to serve the data sharing. The establishment of metadata base and re-establishment of an index are to provide network sharing on the Web classified inquiry and conditional inquiry.

3. The Construction of Marine Basic Information Database Group

As a core foundation of "Digital Ocean" the spatial database should be integrated, systematic and authoritative. Through tackling of key scientific problems during the period of Ninth Five-Year-Plan, the marine basic geographic information database with scale of 1:500000 has been established. In the light of the actual needs of marine development and management and the strategic requirement of "Digital Ocean ", marine basic geographic information databases with medium and large scales at the national level need to be established urgently.

3.1 The Establishment of Marine Basic Information Database Group

On the basis of marine basic geographic information database with scale of 1:500000, a marine basic geographic database with scale of 1:250000 could be established through the integration of historical data, transformation of existing database and update measures. At the same time, according to the needs of national marine management, and under the unified planning of the Nation, marine basic geographic information databases will be established for the major coastal areas. The contents of the marine basic geographic information database include coastline, sea bottom topography, water depth, offshore man-made structure, submarine pipelines, coastal administrative divisions, background field of marine resources and environment, socio-economy and marine industry development.

3.2 Development of Basic Products

Utilizing the achievements of marine spatial information database construction, a series of easy-to-use marine basic database products and understandable marine basic maps will be produced. The contents of marine basic products include spatial distributed information such as basic geography, marine

resources, environment, marine disasters, coastal socio-economy and marine economy.

4. Research on Information Acquisition and Updating System

"Digital Ocean" should be provided with a complete set of highly efficient unhindered marine spatial information acquisition and updating systems. It should have the functions of quality control and standardized processing, fast updating of mass information. This is an information engineering with fast technological up-grade, huge investment and constructed with overall planning of the State.

4.1 Construction of marine spatial information automatic acquisition operational system.

Initial marine information automatic acquisition operational system could be formed by making full use of the existing marine observation system, marine remote sensing information automatic acquisition, marine routine monitoring data automatic release and real-time receiving technology, as well as the high-speed, accurate information transmission network.

4.2 Construction of marine spatial information quality control and standardization operational system.

Theoretical and methodological study on marine multi-source information quality control and standardization will be carried out to solve the key technical problems on marine information automatic processing operational system for marine spatial information quality control and standardization.

4.3 Construction of operational system for automatic information updating.

Utilizing periodical components of 4-D spatial decomposition and composition technology, and assimilation and integration of multi-time phase information, the continuation and integrity of marine information in 4-D space can be realized. By solving the key technology for quick storage, safe copying and redisplay of mass spatial information, the operational system for automatic marine information updating will be formed.

5. Research on "Digital Ocean" Information Sharing and Service System

Every link of "Digital Ocean" data acquisition, transmission, processing, updating, sharing and service needs high-speed marine information networking system. The characteristics of mass quantity and decentralization of "Digital Ocean" data dicate the distribution nature of the "Digital Ocean" database group and the importance of information sharing service system. During the research and development of "Digital Ocean", the main research contents include:

5.1 Construction of "Digital Ocean" spatial data exchange website

The aim of this website is to provide a broadband, high-speed marine information-sharing platform, and provide service to "Digital Ocean". The spatial data exchange website will be operated relying on the Internet. The main contents of this research include the construction of spatial data exchange communication system, large marine spatial database management server, WWW server, FTP server system constructions, information service and release Web homepage design and establishment.

5.2 Research on "Digital Ocean" metadata network service system engineering

The objective of this research is to help data originators manage and maintain the spatial data effectively and set up data file, provide information on data storage, classification, contents, quality, and exchange network of the originators to the users, enabling them to have access to and acquire geographical spatial data. The main contents of this system include metadata collection of marine

information, establishment of metadatabase, development of metadata operating tools, connection of metadatabase with database and sharing on the Web, update and maintenance of metadata and quality control.

5.3 Research and development on "Digital Ocean" WebGIS and application model

The objective of this research is to realize audio-visual presentation and description of the marine spatial data on the Web, enabling the users to understand marine phenomena and real meanings of marine data. The major research contents include the construction of marine WebGIS, marine 4-D GIS, and GIS super-chain technology, application model on the Web, production and sharing service of marine special GIS information products on the web.

6. Research on "Digital Ocean" Application Demonstration

According to the objectives and present conditions of Digital Ocean development and in view of the focal fields such as marine environment, resources, economy and disasters, using technologies of multi-media, 3-D cartoon, virtual reality and WebGIS, research on marine information visualization application demonstration will be carried out, so as to accumulate experience and lay a foundation for the "Digital Ocean" research.

V. Domestic Research Basis

Through many years' efforts, China has done a lot of work and made much progress in the construction of marine technology infrastructure, marine information system, and marine information network, thus providing basis for the research and construction of Digital Ocean in China.

For the information source and information acquisition, China has set up marine monitoring network, connecting 60 coastal stations, ocean buoys, regional marine forecasting station, regional marine information centers, the National Marine Data and Information Service and the National Marine Environmental Forecasting Center. Automatic marine observational data processing on the marine survey vessels has been realized. Marine routine crusing and law enforcement activities by using marine surveillance vessels and planes have provided good conditions for the collection of marine monitoring information. The marine environmental monitoring network has more than 400 members, ensuring the sources of marine pollution monitoring data. The marine statistical information network has linked management and statistical units from 19 marine-related State government agencies and 11 coastal provinces and cities, enabling the collection of statistical information from socio-economic, population, marine industrial development and marine resources. The China Ocean Information Network has been set up and is operating well, providing sharing and service of various marine basic information and information products. The State Oceanic Administration has accumulated a huge amount of marine scientific investigation data. Department of Fisheries of the Ministry of Agriculture, Ministry of Communications, Ministry of Water Resources, the Navy and some major marine-related companies and industries have also collected basic information respectively. In addition, China is going to launch the ocean satellite No.1, which together with earth satellites of other countries, will form a common marine spatial data acquisition system, becoming one of the main information sources for the construction of "Digital Ocean".

In data sharing, from the technological point of view, data sharing basis and conditions are existing in China. The nations public phone network, the construction and development of group data exchange network and the national information highway have provided technical support for marine data sharing. In China, many marine-related institutions have set up information system networks, and relevant data service application systems, equipped with computer hardware and software of different grades. Some of the systems have been connected with the Internet, to provide information-sharing service.Wide-ranging international cooperation and exchange has enriched our marine data collection, providing a sound basis the establishment of the marine data sharing management agencies and their routine operational procedures.

The application of GIS in the marine field: Although the research and application of GIS in China started later than in other countries, the progress is obvious in development speed and the scope of popularization through dozen years' efforts and with the guidance by the national key laboratories. Several major types of products have been formed, such as resources and environmental information system, regional ecological information system, flood and draught disaster assessment information, city construction and tourism development information system, as well as multi-scale digital map databases. In the marine field, through key scientific problems tackling during the Ninth Five-year-plan period, a marine basic geographic information system with scale of 1:500000 has been set up. In addition, WebGIS research and development pilot work has been carried out for marine information sharing and some progress has been made.

Though China has done a great deal in the field of marine information technology and service, we should be a ware of where we fall short compared with the international marine information field, and understand that there is a long way to go for the construction of "Digital Ocean". The main problems are in the field of marine information acquisition, 3-D marine information network should be established to improve the space-to-earth observation system and to solve the slow updating of marine information; in information sharing, owing to lack of high-level data management scheme and information sharing policies, laws and regulations, and influenced by the sectoral interests, marine data loss has become prominent, and it is difficult to realize marine data sharing; The research and development on medium- and large-scale marine basic geographic information system should be quickened, especially for the development of marine basic information databases with scales of 1:250000, 1:50000 and 1:10000; We need to do more in the construction of marine spatial data infrastructure; We have to make more efforts on the research and development for marine information products visualization, construction of marine spatial database, marine WebGIS, etc. Therefore, at present, we must pay much attention to the research of "Digital Ocean" strategy, policies, laws and regulations, and emphasize tackling of the key problems such as "Digital Ocean" capacity-building and supporting technology, and put stress on the pilot research of "Digital Ocean" prototype system development and application.

Ⅵ. Recommendations

1. A leading group should be set up with leaders of State marine related governmental agencies as its members, to take charge of the leadership, organization, and coordination of "Digital Ocean" work.

2. Set up a "Digital Ocean" expert committee, responsible for the formulation of "Digital Ocean" development strategy, objectives, policies, and overall framework design, providing theory, method and technical guidance for the construction of "Digital Ocean".

3. Proceeding from the national development strategy make more investment and quicken the construction of China's information infrastructure.

4. Set up a special program and give priority to the research on "Digital Ocean" spatial data infrastructure, set up national marine spatial 3-D monitoring system, marine information circulation system and fast marine information updating system as soon as possible.

5. Formulate a requisite marine basic information resources management act, to ensure the safety of nation's marine land resources, and support for the accumulation, management and sharing service of marine basic information.

6. The State should make more investment on the marine basic public-good service, strengthen the research on policies, laws and regulations on marine information sharing, and quicken the steps of marine information sharing.

7. Devote major efforts to training technical personnel at different levels.

8. Strengthen international cooperation and exchange on marine information research.

9. Update the existing technical equipment to improve gradually the construction of "Digital Ocean" platform.

Research on the Distributional Features of and Interrelationships Between the Dissolved Oxygen, Salinity, pH Value and Nutrient Salts in the Honghai Bay Waters

Wang Xiaoping(王小平) Jia Xiaoping(贾晓平) Lin Qin(林钦) Li Chunhou(李纯厚)
Gan Juli(甘居利) Cai Wengui(蔡文贵) Wang Zenghuan(王增焕) Lu Xiaoyu(吕晓瑜)
(*South China Sea Fisheries Institute, the Chinese Academy of Fisheries Sciencies, Guangzhou 510300*)

Abstract In this paper, the environmental factors are surveyed of the mariculture waters of the Honghai Bay from the late spring to the early summer (June) in 1998. The distributional features and variation laws of dissolved oxygen, salinity, pH value and nutrient salts in the sea water are expounded. Also discussed are their relationships between each other. The results show that the contents of dissolved oxygen and pH value in the sea water increase with the increasing temperature from north (except for No.15~17 stations) to south (expect for No.6 station). At the same time it is affirmed that photosynthesis is the major cause of the high contents of dissolved oxygen and pH value. And the nutrient salt shows a negative correlation with salinity. The total content of phytoplankton obviously increased with the reduction of nutrient salts from north to south.

Keywords Honghai Bay, dissolved oxygen, salinity, pH value, nutrient salt, distributional features

1. Introduction

Situated in the sea area of East Guangdong in the northern South China Sea, the Honghai Bay is affected by the Zhujiang River and Hanjiang River, which supply it with rich nutrient salts. The longshore currrents and upwellings in East Guangdong also exert greater influence upon it in different periods, and the suitable temperature and rich nutrient salts in the sea area promote the growth of plankton in large quantities, thus making the Honghai Bay a major producing area of mariculture in East Guangdong. In order to establish various types of technical models for the optimum and long-scale culture in the culture sea area of the South China Sea and raise the level of automation for culture management and environmental control of the culture water bodies, research has been carried out on the environmental factors and ecology in the cultivated waters of tidal-flat, shallow sea, reef flat and ponds in the cultivation demonstration sites, mainly the Honghai Bay Since 1996. Based on the data from the late spring to the early summer (June) of 1998, this paper discusses the distributional features of chemical elements in the cultivated waters of shallow sea and reef flat as well as their relationship between each other.

2. Surveyed Area and Methods of Analysis

2.1 Surveyed area

In the cultivated waters of the Honghai Bay (22° 39′ ~22° 51′ N, 115° 7′ ~115° 27′ E), 17 survey stations are set up , among which the stations Nos.1~4 are for the reef-flat culture zone and Nos.5~17 are for the shallow-sea culture zone. For the station locations, see Fig.1.

2.2 Methods of analysis

The dissolved oxygen is measured with the Model YSI-55 hand dissolved oxygen meter, with a maximum error of ±0.03mg/L in the analysis of samples, the pH value with the H5-Checkeri pH meter, with an error of about 0.01 pH units, and the nutrient salts and salinity are measured according the "Specifications of Oceanographic Survey"[1] issued by the State Oceanic Administration in 1991.

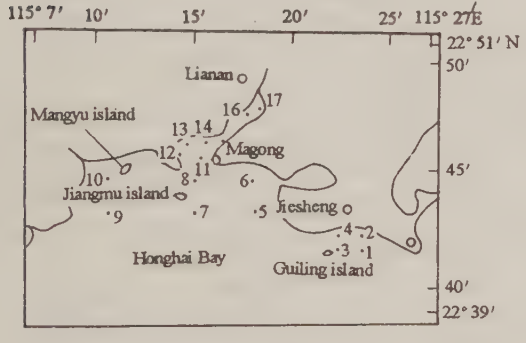

Fig.1 Map of station locations

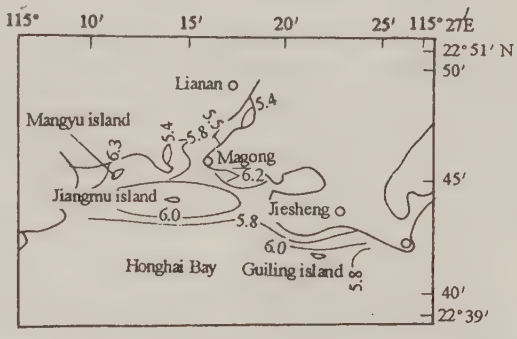

Fig.2 Planar distribution of the surface DO contents (mg/l) in the sea area of the Honghai Bay in June, 1998

3. Survey Results

3.1 Content of dissolved oxygen and its planar distribution

In June, the content of surface dissolved oxygen in the cultivated waters of the Honghai Bay varies in the rang of 5.43~6.26 mg/L, with an average of 5.80mg/L. Fig.2 shows its planar distribution, i.e., the content of surface dissolved oxygen is mostly in massive distribution, higher in the south and lower in the north. The trend of distribution is that in the south the higher content zones on the east and west sides decrease towards the outer bay, while in the north, (except station No.12), the content of oxygen increases from the low content zone in the north to beyond the bay mouth, which is roughly identical with the fact that sea temperature (Fig.3) rises from the east side of the south to beyond the bay mouth and that in the north it drops from the north to the bay mouth. The maximum oxygen content occurs in the station No.6 to the east of the bay mouth and the station No.10 to the west of the bay mouth, with a magnitude of 6.26 mg/L, while the minimum value occurs in the stations Nos.16 and 17 to the north of the bay mouth, with a magnitude of 5.43mg/L.

3.2 Planar distribution of seawater pH value and salinity

In June, the seawater pH value in the Honghai Bay varies in the range of 7.86~8.22, with an average of 8.12. It can be seen from Fig.4 that the pH value of the surface seawater possesses a distributional

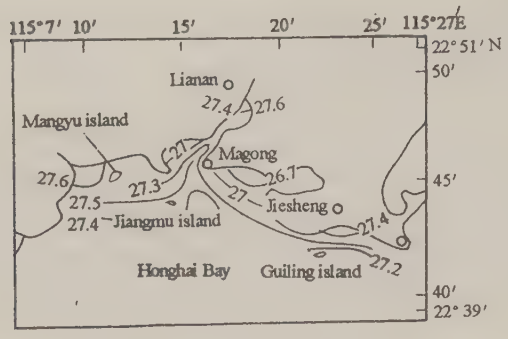

Fig.3 Planar distribution of the surface temperatures in the sea area of the Honghai Bay in June, 1998

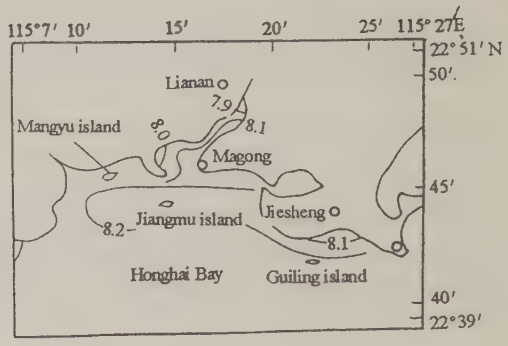

Fig.4 Planar distribution of the surface pH in the sea area of the Honghai Bay in June, 1998

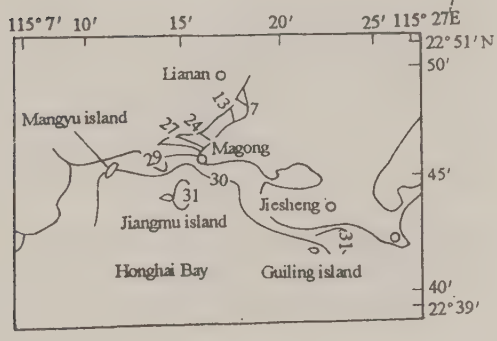

Fig.5 Planar distribution of the surface salinity in the sea area of the Honghai Bay in June, 1998

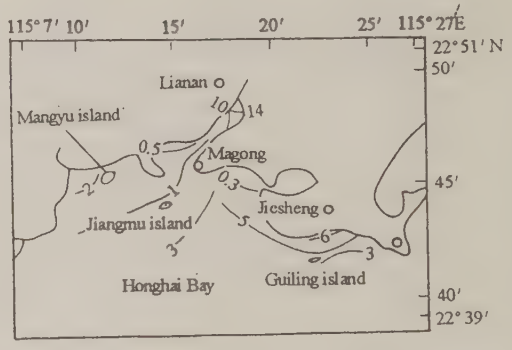

Fig.6 Planar distribution of the surface NO_3-N (μ mol/l) in the sea area of the Honghai Bay in June, 1998

feature of being low in the north and high in the south and that with the dropping of latitude, the pH value gradually rises from north to south. Fig.4 also shows that there occurs a 8.10 contour line for the pH value to the north of the bay mouth while the pH value from the south to the southeast outside the bay mouth is within the range of the 8.20 contour line, which is simply the result of being affected by photosynthesis in late spring and early summer. The surface salinity in June varies in the range of 6.62~31.89, with an average of 27.648. It is clear from Fig.5 that the surface salinity in the bay is characterized by being low in the north and high in the south and that, with the dropping of latitude, the salinity value tends to gradually increase from north to south. The maximum value of salinity occurs in the stations Nos.7 and 8 in the central bay mouth and the stations Nos.1, 2 and 4 by the southeast of the bay mouth, with a salinity value of over 31.23 while the minimum value in the station No.17 to the north of the bay mouth, with a salinity value of only 6.62.

3.3 Planar distribution of nutrient contents

3.3.1 Nitrate (NO_3-N)

The content of NO_3-N in the surface seawater of the Honghai Bay in June is within the range of 0.00~

13.76 μ mol/L, with an average of 3.13 μ mol/L. It can be seen from Fig.6 that in its planar distribution, the content of NO_3-N is mostly in a massive shape and that the highest content occurs in the waters of the stations Nos.16 and 17 in the north, reaching 10.01 μ mol/L and 13.76 μ mol/L respectively, while the lowest value occurs in the station No.12 to the north of the bay mouth, with a magnitude of 0. The distribution trend for the concentration of NO_3-N is roughly decreasing from southeast to northeast (except the stations Nos.16 and 17 in the north). This result shows that such a distribution condition of NO_3 -N is related to the influence of the coastal runoff.

3.3.2 Nitrite (NO_2-N)

The content of NO_2-N in the surface water of the Honghai Bay in June varies between 0.08 μ mol/L and 1.77 μ mol/L, with an average of 0.44 μ mol/L. It is clear from Fig.7 that the surface water contour line is trending from south to north and that the high value zone occurs in the stations Nos.16 and 17 in the north, the content reaching 1.80 μ mol/L while the low value zone in the stations Nos.3~5 and 10 on the east and west sides of the bay mouth, the content reaching 0.14 μ mol/L. The distribution of the content is characterized by being high in the north and low in the south as well as by a greater gradient; The concentration tends to decrease from the north to the waters between the central bay mouth and the east and west sides while the content of NO_2-N in the waters of the stations Nos.1, 2 and 4 near Guiling Island is similar to that in the waters of various stations in the bay.

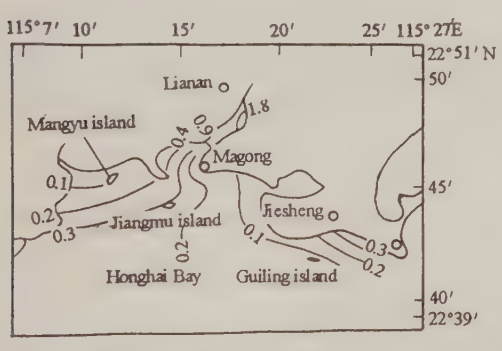

Fig.7 Planar distribution of the surface NO_2-N (μ mol/l) in the sea area of the Honghai Bay in June, 1998

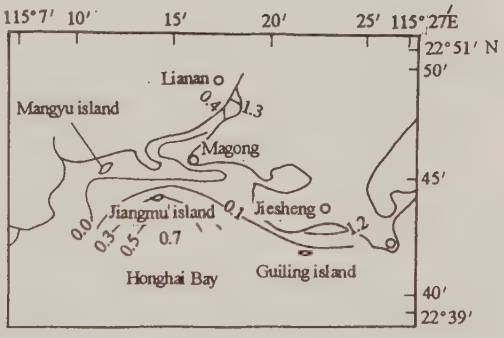

Fig.8 Planar distribution of the surface NH_4-N (μ mol/l) in the sea area of the Honghai Bay in June, 1998

3.3.3 Ammonia-nitrogen (NH_4-N)

The content of NH_4-N in the surface seawater in June varies within the range of 0.0~1.32 μ mol/L, with an average of 0.31 μ mol/L. Fig.8 shows that the NH_4-N contour line in the surface water trends from south to north and its content is highest at the bayhead in the north and lowest to the west by north of the bay mouth. The highest value occurs in the station No.17 at the bayhead with a content of 1.26 μ mol/L, secondly is the value occurring in the stations Nos.2 and 4 near Guiling Island, which is 1.22 μ mol/L while the lowest value occurs in the waters between the west and to the north of the bay mouth (except the stations Nos.16 and 17), with a content of 0. The concentration of NH_4-N tends to be distributed centring around the station No.7 in the bay and decrease in the direction of northwest~northeast (except the stations Nos.16 and 17).

3.3.4 Phosphate (PO_4-P)

The content of PO_4-P in the surface seawater in June ranges from 0.06 μ mol/L to 0.76 μ mol/L, with an average of 0.32 μ mol/L. It can be seen from Fig.9 that the PO_4-P contour line in the surface water trends roughly from south to north and its content is also higher in the north and slightly lower in the southeast. The highest value occurs in the station No.12 north of the bay mouth, the content amounting to 0.76 μ mol/L while the content of PO_4-P in the waters near the stations Nos.2~5 in the east by south is slightly lower, which is 0.12 μ mol/L. The content tends to increase from the southeast to the waters north of the bay mouth (except the stations Nos.16 and 17), with a greater gradient in the north and a smaller one in the south.

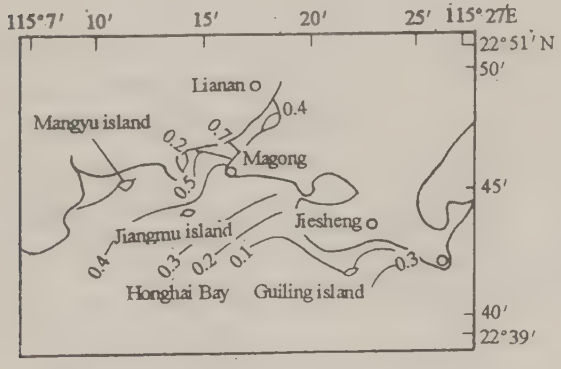

Fig.9 Planar distribution of the surface PO_4-P (μ mol/l) in the sea area of the Honghai Bay in June, 1998

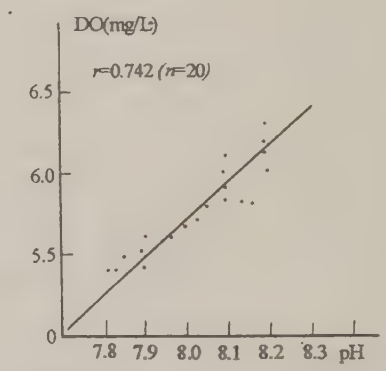

Fig.10 Relationship between DO and pH in the sea water of the Honghai Bay in June, 1998

4. Discussion

4.1 Relationship between pH value and temperature in the sea water

When the seawater temperature rises, CO_2 escapes to the air and the decrease of CO_2 in the seawater causes the pH value of seawater to rise. Gieskes[2] gives the effect of seawater temperature on the pH value:

$$pH_{t2} = pH_{t1} + a(t_1 - t_2) \quad (1)$$

According to Formula (1), in June, the water temperature in the waters of the Honghai Bay increases 0.3~0.2 ℃ (except station No.6) from 27.0 ℃ north of the bay mouth (except the stattions Nos.15~17) to 27.6 ℃~27.2 ℃ in the southwest and the east by south, but the maximum effect of seawater temperature on the pH value would not exceed 0.06 pH units. In fact, however, the pH value rises from 0.8 in the surveyed area to the north of the bay mouth (except station No.17) to 8.20 from southwest to southwest in the south of the surveyed area. Such a change range of pH is evidently not simply the result of the changes in seawater temperature. The more important factor contributing to this rise of pH value is photosynthesis.

4.2 Relationship between dissolved oxygen and pH value in the seawater

The results of analysis show that the content of oxygen in the studied sea area in late spring and early summer (June) is roughly low in the north and high in the south, which is mainly attributable to

photosynthsis. Photosynthesis should follow the following equation:

$$106CO_2+16NO_3^-+HPO_4^{2-}+122H_2O+18H^+ \rightarrow C_{106}H_{263}O_{110}N_{16}P+13O_2 \quad (2)$$

Equation (2) indicates that, apart from nutrient elements such as N, P etc., the process of photosynthesis absorbs large amounts of CO_2. The reduction of CO_2 in the seawater leads to the relative increase of the proportions of HCO_3^- and CO_3^{2-}, thus causing the pH value to rise[3]. To further confirm that such a phenomenon does exist in the sea area of the Honghai Bai, a regression analysis is made of the content of the surface dissolved oxygen and the pH value in the bay, which has obtained satisfactory results (Fig.10). Fig.10 suggests that the content of dissolved oxygen and the pH value are in a linear distribution, with the related coefficient $r = 0.7418$ (n=20), which proves from another angle that photosynthesis is a contributing factor to the higher content of dissolved oxygen and pH value.

4.3 Relationship between nutrient salts and salinity

The content of nutrient salts in sea water decreases or increases generally with the higher or lower salinity. The relationship between nutrient salts and salinity can be seen from Table 1. The results of regression show that there exists a close negative correlation between nutrient salts and salinity in the surface and that especially the relationship between NO_2-N, NO_3-N and salinity is closer, which indicates that nutrient salts decrease with the increase of salinity.

Table 1 Relationship between nutrients and salinity in the waters of the Honghai Bay in June, 1998

Relationship	*y -x*	Layer	*Regression equation (y=a+bx)*	*Related coefficient (r)*
Between nutrient and salinity	C_{NO2}-S	surface	*y=2.4524-0.0726S*	-0.9651
	C_{NO3}-S	surface	*y=15.246-0.4383S*	-0.8019
	C_{NH4}-S	surface	*y=1.0173-0.02579S*	-0.3622
	C_{PO4}-S	surface	*y=0.6193-0.00976S*	-0.3357

Table 2 Comparison of nutrient content (μ mol/L) and biomass of phytoplankton* ($\times 10^4$ ind./m^3)

Item	Stations 1~10 in the south	Stations 11~17 in the north
NO_2-N	0.20	1.13
NO_3-N	3.10	6.19
NH_4-N	0.39	0.43
PO_4-P	0.22	0.53
PHYTO.	576	126

* PHYTO.—phytoplankton;Data is provided by the division of Cultivation and stock Enhancement of the Institute

4.4 Relationship between nutrient salts and total biomass of phytoplankton

Research findings suggest that the content of dissolved oxygen and the pH value in the sea water of the surveyed area both increase with the dropping of latitudes and the rise of water temperature (except the stations Nos.15~17); The case with the content of nutrient salts is just the opposite, from which it may be concluded that this is caused by the gradual intensification of photosynthesis from north to south. To further verify this conclusion, we have introduced the total biomass of phytoplankton and chosen the

average content of nutrient salts and the total biomass of phytoplankton in the surface at stations Nos.11~17 in the north of the surveyed area and stations Nos.1~10 in the south of the survey area to be listed in Table 2.

It can be seen from Table 2 that the content of nutrient salts in the studied sea area is higher in the north than that in the south while the total biomass of phytoplankton is much higher in the south than that in the north. If the average values are taken respectively from the 10 stations in the south and the 7 stations in the north, NO_2-N in north 5.5 times that in the south, NO_3-N in the north is over twice that in the south, NH_4-N in the north more than doubles that in the south and PO_4-P in the north is 2.5 times that in the south while the total biomass in the south is 4.6 times that in the north. However, whether the decrease in the content of nutrient salts from north to south or the increase in the total biomass of phytoplankton from north to south are both a gradual process. Due to limited space, this paper cannot list the data in all the station sites and can only make a comparative study between the south and the north. Besides, the content of nutrient salts and the total biomass of phytoplankton are also affected by the distance from the coast as well as rivers and bay mouth water body. But the results in Table 2 show that the total biomass of phytoplankton obviously increases with the decrease of nutrient salts from north to south.

Among the factors affecting the content of nutrient salts, pH value, salinity and distribution of nutrient salts, apart from the causes mentioned above, there are also such contributing factors as coastal water systems, e.g., East Guangdong coastal current, the South China Sea surface water, Daye River, Lijiang River and continental runoff of the Huanggang River as well as the open-sea water systems like the upwellings. The decrease and increase of these factors plays a major role in affecting the high or low of the above-mentioned chemical elements, especially their seasonal variations.

References

1 State Oceanic Administration, Specifications of Oceanographic Survey, Beijing, China Ocean Press, 1991, 4~20

2 Gieskes J M. Effect of temperature on the pH of seawater, Limnol., 1985, 14(5): 679~684

3 Boto K G et al. Dissolved oxygen and pH relationship in northern Australian mangrove ways, Limnol. Oceangr., 1981, 27(6): 1176~1178

4 Sousa S N, De S Y S Singval. Chemical oceanography of the Arabian Sea: part 6. Relationship between nutrients and dissolved oxygen in the Central Basin, INDIAN J. MAR. SCI., 1986, 26(3): 153~161

Study on Basic Hydrologic and Meteorological Parameters in the Ice-covered Bohai Sea*

Wang Keguang (王可光) Wang Caixin(王彩欣) Wu Huiding(吴辉碇)
(*National Marine Environmental Forecasting Center, Beijing, 100081*)
Wu Shuli(吴术礼)
(*China Offshore Oil Engineering Corporation, Tianjin, 300452*)

Abstract Based on the sea ice investigation in Liaodong Bay and observation on Platform JZ20-2 in January, 1997, the basic hydrologic and meteorological parameters in the Bohai Sea are studied. These parameters consist of solar short wave radiation, long wave radiation, wind velocity, air humidity and some thermal properties of the sea ice. The following is obtained: (1) solar short wave radiation is an important factor affecting the energy balance in the Bohai Sea, and the simplified form of Laevastu (1960) formula can be used to calculate it in the Bohai Sea, (2) the air humidity is about 50% above the sea ice surface, and about 90% above seawater surface in winter according to the observations, (3) wind velocity and air temperature is another two important factors affecting energy balance, the stronger the wind is and the lower the temperature is, the more energy of the sea surface loses, (4) the net long wave loss of the sea surface is almost static in winter, (5) in the Bohai Sea, the thermal conductivity and latent heat of seawater condensation can be regarded as constant, but the specific heat is varying within a sizable range.

Keywords the Bohai Sea ; radiation ; heat flux ; heat balance

1. Introduction

The Bohai Sea is an internal continental sea of China. It is not only an important sea area to exploit offshore oil and gas, but also an important channel. In recent years, with the vigorous development of production, the offshore activities become more and more frequent. But every winter, the Bohai Sea area will appear to freeze in different degree, the existing and movement of sea ice will bring into great harmness to offshore activities. Especially during the severe icebound in 1969, the "2nd sea well" living platform, equipment platform and drilling platform were all pushed over. The seat reinforcing bar of "1st sea well" platform was cut off; 58 passenger liners were destroyed in different degree at Tanggu Port in one month, among which some ships hull were severely deformed and cracked, sea water entered into the cabins, which suffered very great losses.

The Bohai Sea ice is the one-year ice, ice period is about 3~4 months. With the cold air moving from north to south in each winter, the temperature of seawater begins to drop down, and sea ice begins to appear. Under the continuous effect of cold air, ice condition becomes more and more severe and becomes severest by the last ten days of January or the first ten days of February, after that, with the weather turning warm, the ice condition gradually lightens, until the sea ice disappear completely.

As the ice in the Bohai Sea, its emergence and disappearance and its movement are determined by local hydrologic and meteorological conditions. In the local sea area, the appearance of sea ice may be from dynamic factor, or may be from thermodynamic factor, but mostly is influenced by both factors. For the whole Bohai Sea, the severe ice condition is mainly determined by thermodynamic factor. At present, the operational forecast of sea ice is mainly based on the statistic relationship between sea ice thermodynamic process and atmospheric force, and uses the hydrologic and meteorological data to forecast the ice condition of the Bohai Sea and the northern Yellow Sea. With the exploration and exploitation of oil and gas in winter and the development of offshore transport, sea ice forecast is pressed for quantity and objectivity. On the basis of sea ice thermodynamics, dynamics and rheology, considering the characteristics of the Bohai Sea hydrologic, meteorological and ice condition, a ice dynamic-thermodynamic model for the Bohai Sea was put forward. The model successfully simulated growth, decay and drift of the sea ice. Combined this model with atmospheric model, the Bohai Sea and northern Yellow Sea ice is numerically forecasted with the aid of real time satellite remote sensing data. In addition, the sea ice numerical forecast must further consider the thermodynamic process and the coupled influence between them(Wu et al, 1992, 1997; Bai et al, 1998). The basic hydrologic and meteorological factors in the Bohai Sea and the relevant processes during ice period are analyzed and studied by use of the date from ice breaker survey and JZ 20-2 platform in Jan. 1997. And energy budget at the air-sea and ice-sea surfaces in the ice covered area is calculated for providing the thermodynamic part of sea ice model, in order to satisfy the demands of sea ice forecast and the Bohai Sea engineering design and operation.

2. Basic Hydrologic and Meteorological Parameters During the Bohai Sea Ice Period

According to the observed result, some basic hydrologic and meteorological parameters during the Bohai Sea ice-covered period will be emphatically studied in the following, which includes solar short wave radiation, long wave radiation, wind velocity, humidity and thermal properties of sea ice etc.

2.1 Solar short wave radiation

Solar short wave radiation is the most important factor affecting the energy balance of different areas in the earth, much studies on it have been made. The solar short wave radiation reaching at the ground can be divided into two courses, that is, solar short wave radiation reaching atmospheric upper boundary and penetrating the atmosphere from the atmospheric upper boundary to the ground.

Radiation of solar short wave radiation reaching at the atmospheric upper boundary can be expressed as follows

$$S' = \frac{D_0}{D} S_0 \sinh \qquad (1)$$

where, D_0 is average distance from the sun to the earth, D is the distance from the sun to the earth in any day of a year, S_0 is the solar constant, choosing 1367W/s^2, and h is the solar height angle. It can easily be known from the knowledge of astronomy,

$$\sinh = \sin\varphi \sin\delta + \cos\varphi \cos\delta \cos\omega \qquad (2)$$

where, ϕ is geographic latitude, δ is the solar declination with variation between +23.5 ° and -23.5 ° in a year, for the sake of simple, usually choosing $\delta = 23.5° \sin(d / 365)$, in which d is the number of the day in a year from equinox, ω the hour angle , choosing 0 when the sun is at the meridian (high noon) , its daily variation is 2 π , that is 360. Because solar height angles equal to 0 at sunrise and sunset, it can be obtained from Eq. (2),

$$\sinh = 0 = \sin\varphi \sin\delta + \cos\varphi \cos\delta \cos\omega_0 \tag{3}$$

that is,

$$\cos\omega_0 = -tg\varphi tg\delta \tag{4a}$$

In the Bohai Sea area, $\varphi = 40$ ° is chosen as the representative latitude value. In winter season, $\delta \in [-23.5°, 0°)$, $\cos\omega_0$ is always positive, so

$$\omega_0 = \pm \arccos(-tg\varphi tg\delta) \tag{4b}$$

In midwinter day $\delta = -23.5°$, and $\omega_0 = \pm 68.6°$ which is equal to 4h34min, that is, the sunrise time is 7:26, and the sunset time is 16:34.

In addition, ω is equal to 0 at the high noon, here solar height angle $h = 90° - \varphi + \delta$. Solar height angle of the Bohai Sea area in the midwinter day is about 26.5 ° , it is the smallest solar height angle in this area.

After solar short wave radiation into atmospheric layer from atmospheric upper boundary, it is weakened by atmospheric absorption and dispersion. Vapor, ozone and carbon dioxide are the main absorption substances of short wave radiation. For the complexity of atmospheric absorption and dispersion, a simple parameterization method of atmospheric effect on solar short wave radiation is usually adopted in practical application. For example, Laevastu (1960) adopted the following formula to calculate ground solar short wave radiation,

$$S_1 = \frac{S_0 \sin^2 h}{(\sinh + 2.7)e \times 10^{-7} + 1.085\sinh + 0.10} \tag{5a}$$

where e is vapor pressure , its unit is hPa , the value of e usually smaller than 10hPa in winter , therefore, the first term in the denominator can be neglected comparing with the other two terms in Eq. (5a), so,

$$S_1 = \frac{S_0 \sin^2 h}{1.085\sinh + 0.10} \tag{5b}$$

Table 1 Observed values of short wave radiation at JZ20-2 platform in January 1997 (W/m^2)

28	Hour	7:00	7:35	8:00	8:30	9:15	10:05	10:45	11:10	11:45	12:00	12:35	13:00	14:00	16:00	16:3
	Radiation	0.1	15.6	93.7	170	277	388	460	498	526	553	537	524	439	176	102
29	Hour			8:00	8:35	9:00	10:05	10:30	11:00	11:50	14:00	15:00	15:30	16:30	17:10	18:0
	Radiation			98	183	265	411	438	460	510	395	221	125	39	9.1	0

The observed values of solar short wave radiation of 28 and 29 January, 1997 at JZ20－2 platform are showed in Table 1 , when the weather is cleary. The solid line is the calculated valuesby Eq. (5b) in

Fig.1, solid angles denote the observed values in 28, and hollow angles show the observed values in 29. From Fig.1 it can be seen that the calculated values by Eq. (5b) fairly correspond to the observed values. Therefore, the Eq. (5b) can be used to calculate the solar short wave radiation in the model. It is regretted that the effect of cloud on the solar short wave radiation can not be examined by the observed data, for it is sunny and no cloud in the two days. It can be corrected for cloudy days as follows (Hoffert et al, 1979),

$$SW=(1-0.66c^3)S_1 \qquad (6)$$

where c is total cloud cover.

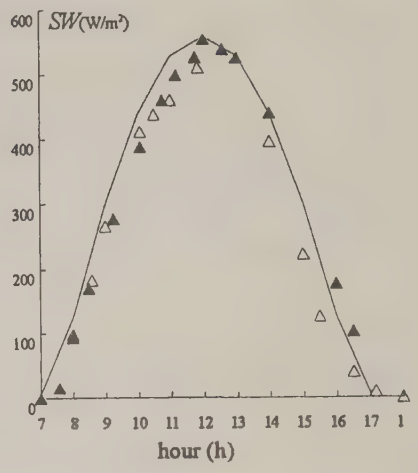

Fig. 1 Comparison of the solar short wave radiation theory values with the observation

2.2 Wind velocity and relative humidity over sea

Wind is an important factor of sea ice growth, decay and drift. The wind frequency of NE, NNE, N and NNW reaches 50% or so, and the total wind frequency of SSW, SW, W and S is about 30% in January 1997 in JZ20-2 area. Its speed is usually 5～10m/s, and the largest wind speed ever reached 18.8m/s on January 1.

According to the observation, variation of relative humidity over sea is larger but shows certain law. In general, the relative humidity is about 35~55% when ice concentration reaches 10 as shown in Table 2. In the last ten days of January 1997, the sea ice concentration in the Liaodong Gulf was very large according to the data of National Center for Marine Environment Forecast. The sea ice concentration of JZ20-2 area is mainly 10 or so as shown in Table 2.

Table 2 Observed values of ice concentration and relative humidity (%) at JZ20-2 platform in January 1997

Date	27			28				29			
	12:00	15:00	18:00	8:00	11:10	13:00	16:00	8:00	11:00	14:00	18:00
Ice concentration	7	10	10	10	10	10	10	9	9	10	10
Relative humidity	87	50	54	52	46	37	53	42	49	35	45

It is also found from observation that open water or lead has larger effect on relative humidity, which is dependent on the wind speed and direction. It can be seen from Table 2 that relative humidity reaches 87% at 12:00 27th. At that time, the open water lies in the windward direction of JZ20—2 platform, and the water vapor was transported to the apparatus at the platform by wind, which made the measured relative humidity very high. On the contrary, the open water just lies in the leeward direction of the platform on the morning of 29th, the measured relative humidity is lower than 50%, which is similar to the condition when all of the sea is covered by ice. Therefore, we think open water basically has no effect on humidity on this condition.

Temperature variation in a day can produce some effect on relative humidity. Relative humidity in a

day can reach minimum at 14:00~15:00 o'clock if sea ice concentration keeps at 10. Because the temperature reaches maximum at that time, but the vapor in the atmosphere has only a little variation at the same time.

2.3 Sensible heat flux and latent flux over water surface and ice surface

Adopting the observed wind speed and relative humidity, we can estimate sensible heat flux and latent heat flux over water surface and ice surface. According to the bulk scheme:

$$\begin{cases} F_H = \rho a C_p C_H V_a (T_a - T_s) \\ F_L = \rho a L C_E V_a (q_a - q_s) \end{cases} \quad (7)$$

where, V_a, q_a, T_a are respectively wind speed, specific humidity and air temperature at 10m over sea. In the Bohai Sea area, the typical value of wind speed is $5 \sim 10$m/s; specific humidity can be got by $q = 0.622e / p = 0.622 Esat(Ta) r / p$, where r is relative humidity, $E_{sat}(T_a)$ is saturation vapor pressure with air temperature T_a, and can be got by Magnus empirical formula. C_H, C_E are sensible heat and latent heat transportation coefficient, usually chosen as constant, for example, $C_H = 1.3 \times 10^{-3}$, $C_E = 1.4 \times 10^{-3}$. T_s and q_s are temperature and specific humidity of water surface or ice surface, in mixing area of ice and water, especially when ice-covered area appears lead, the temperature on water surface can be determined as ice point, and it is chosen as -1.8℃ in the Bohai Sea area. The temperature on ice surface is dependent on ice thickness and air temperature variation rate. C_p is air specific heat at constant pressure, and its value is 1004 J/(kg.K), L is ice sublimation heat and chosen as 2.834×10^6J/kg.

It is known from the above that the relative humidity over ice surface is about 50%, and about 90% over water surface. Air density$_a$ is chosen as 1.3kg/m^3. Specific humidity over water surface or ice surface q_s can be taken as saturated and is only determined by its surface temperature. Sensible heat flux and latent heat flux can be calculated by air temperature T_a, surface temperature on water or ice T_s and wind speed V_a.

The variation of sensible heat flux and latent heat flux on water surface with T_a, T_s and V_a is shown in Fig.2 and Fig.3. The temperature on water surface T_s is chosen as -1.8℃ in the figures. It can be seen

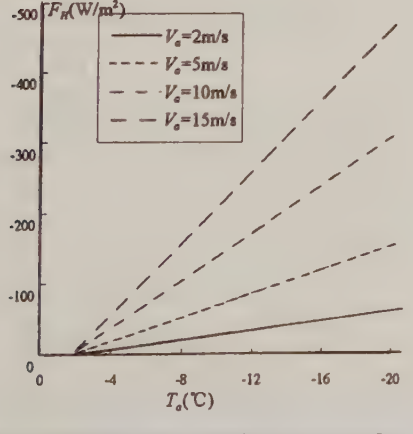

Fig. 2 Sensible heat flux variation on water surface

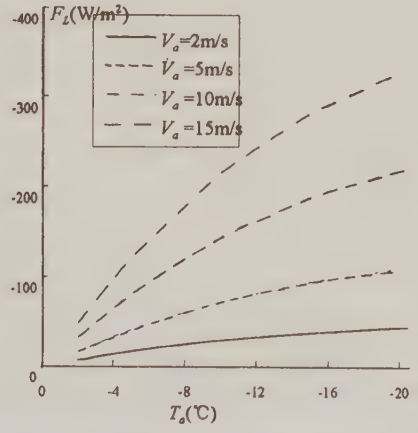

Fig. 3 Latent heat flux variation on water surface

from the figures that absolute value of sensible heat flux and latent heat flux on water surface increase with wind speed increasing and air temperature dropping. The sensible heat flux appears linearity relation with temperature, and the latent heat flux also approximately appears linearity relation with temperature. When the air temperature is -10℃ and wind speed increases from 2m/s to 15m/s, sensible heat flux and latent heat flux all approximately increase from 20W/m^2 to 200W/m^2. Its variation is very large.

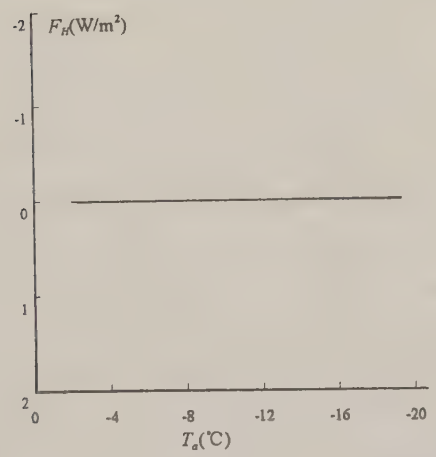

Fig. 4 Ice surface sensible heat flux variation (ΔT=0)

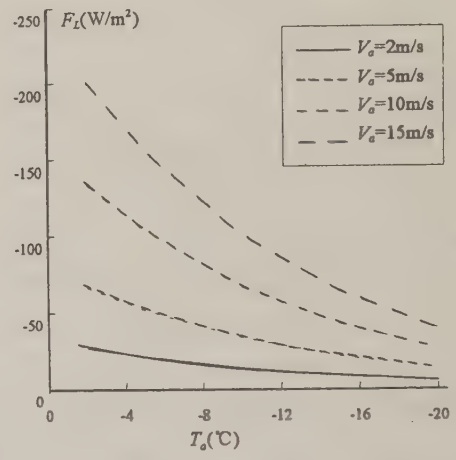

Fig. 5 Ice surface latent heat flux variation (ΔT=0)

The variation trend of sensible heat flux and latent heat flux on the ice surface with *Ta*and *Va* is shown in Figs.4 ~ 7. Ice surface temperature is equal to air temperature, that is, in the Fig.4 and Fig.5. The sensible heat flux is always equal to 0 in this condition, but the latent heat flux has obvious variation with temperature and wind. The ice surface temperature is higher 2℃ than air temperature in Fig.6 and Fig.7. It can be seen from the figures that the sensible heat flux increases only with wind velocity increasing when the difference between the ice temperature and air temperature is constant, but the latent heat flux still changes with wind speed and air temperature. However, it should be pointed out that the ice surface temperature can't be got by explicit formulation, and in fact it is the result of energy balance.

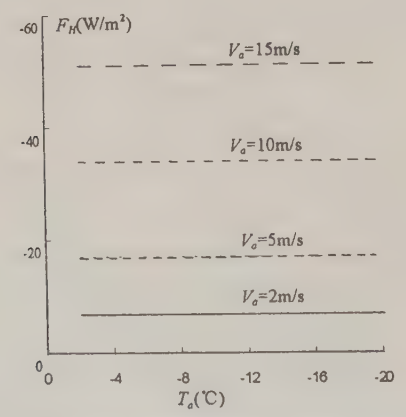

Fig. 6 Ice surface sensible heat flux variation (ΔT=2℃)

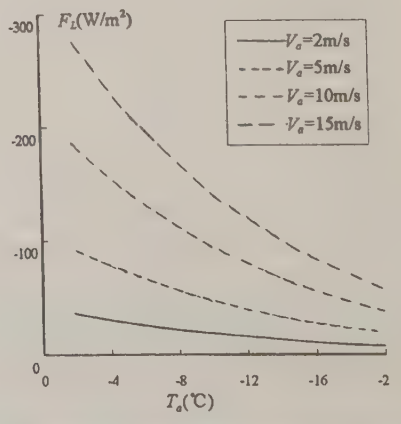

Fig. 7 Ice surface latent heat flux variation (ΔT=2℃)

2.4 long wave radiation

In the investigation, long wave radiation wasn't observed, and we would discuss a little about it in this section considering whole energy balance of the Bohai Sea area. Generally long wave radiation includes long wave radiation coming from atmosphere, and long wave radiation of water surface or ice surface. When studying water surface or ice surface heat balance, only net long wave radiation into water surface or ice surface is concerned, Haney(1971), Hoffert etc (1979) and Wu Huiding etc (1984) all adopt parameterization form, that is,

$$Rw = \varepsilon w \sigma T w^4 (0.39 - 0.05\sqrt{e})(1 - 0.76c) \quad (8)$$

where R_w is net long wave radiation on water surface, and for ice cover, R_i, ε_i and T_i will take the place of R_w, ε_w and T_w, e is vapor pressure, ε_w and ε_i are water surface and ice surface long wave radiation rate respectively, σ is boltzmanns constant. When the underlying surface is water surface and ice surface respectively, the variation of long wave radiation for different synoptic condition on different surface is shown in Fig.8. It can be seen from the figure that long wave radiation is extremely insensitive to air temperature. Radiation variation is only about 10W/m^2 when surface temperature variation is 10 ℃. But it is very sensitive to cloud amount, radiation amount will increase from 20W/m^2 to 100W/m^2 or so as cloud amount varies from 0 to 10. Because of uncertainty of cloud distribution in space-time, the effect of cloud amount on the long wave radiation is quite uncertain.

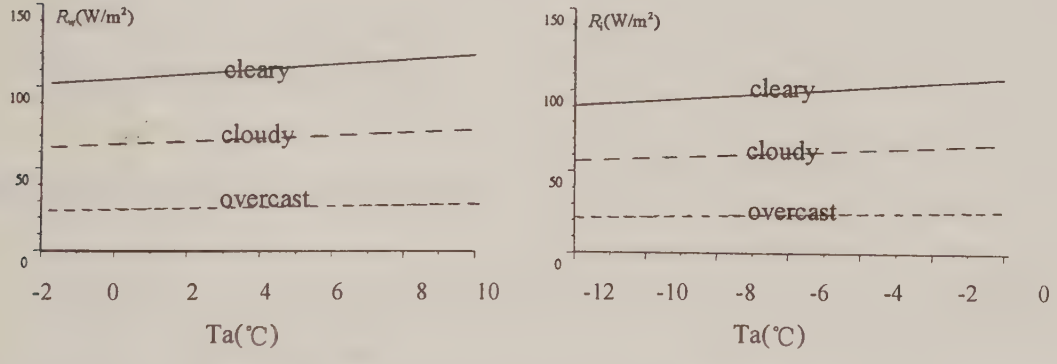

Fig. 8 Variation of long wave radiation with air temperature for different weather on different underlying surface

2.5 Sea ice specific heat and thermal conductivity

Specific heat and thermal conductivity are two main sea ice thermal properties. Because there is not only pure ice, but also brine and air bubble, their properties are very complex. Pounder(1964) adopted the following formula to calculate specific heat of pure ice and brine,

$$C_i = 2.111 + 0.0075T \quad (9)$$

$$C_b = 4.2 + 0.092T \quad (10)$$

where the subscript i and b denote pure ice and brine, respectively. The temperature T is measured by centigrade scale. The relation of brine quality of unit quality sea ice with ice temperature and salinity is,

$$M_b = 0.001S(1 - 54.11/T) \tag{11}$$

and the pure ice quality is $M_i = 1 - M_b$, neglecting the air bubble quality.

The ice around the brine bubble will melt as sea ice temperature rises for the brine concentration balance under the new temperature. The specific heat of sea ice, T, should consider the effect of variation of the pure ice quantity, as well as the specific heat of pure ice and brine, that is,

$$C = M_i C_i + M_b C_b + L_T \frac{dM_b}{dT} \tag{12a}$$

where $L_T = L_0 + (C_w - C_i)T$, in which C_w is the specific heat of water, L_0 is the melt latent heat of the pure ice. Those parameters are introduced into the formula and small quantity is neglected, we can obtain,

$$C = 2.111 + 18S/T^2 \tag{12b}$$

Where S is sea ice salinity. The variation of C with temperature and salinity is shown in Fig.9. It can be seen from Fig.9 that the specific heat of sea ice continuously reduces with decrease of temperature and salinity, and approximates the specific heat of pure ice finally. Salinity is about in the range of 2.6 ~ 5.0 according to measurement of Yang Guojin etc. (1988), considering that ice point is -1.8℃ in the Bohai Sea, the maximum value of C is about 30 kJ/(kg.K), however specific heat of pure ice is only 2kJ/(kg.K) at this moment, which is approximately 1/15 of the specific heat of the Bohai Sea ice. The difference has very large effect on heat balance.

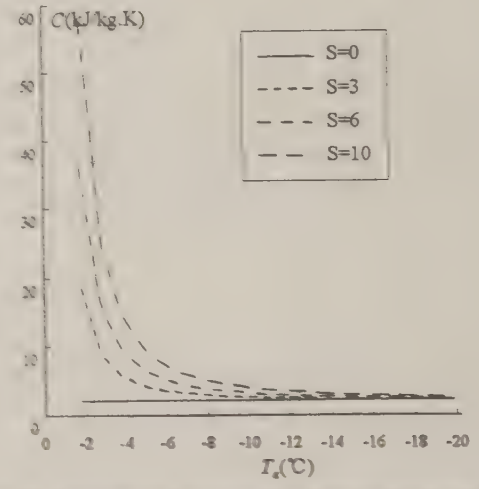

Fig. 9 Relationship between C and temperature and salinity

Based on the study of Untersteiner (1961), heat conductivity coefficient of sea ice is,

$$k = 2.03 + 0.117\, S/T \tag{13}$$

the value of k is between 1.71 ~ 2.03 W/(m.K) from Eq. (13), it can be simply chosen as constant in general calculation for its variation not large.

2.6 Freezing point, melting point and condensation latent heat of sea ice

When winter comes, with cold air continuous invasion, sea ice appears and continuously thickens and widens in a part of the Bohai Sea area. The ice begins to melt and finally disappears with air temperature rising in the next spring, this is the typical course of one-year ice. Compared with fresh ice, freezing of sea and melting of ice aren't a reversible process, because the brine in the ice continuously decreases with time.

While freezing, the ice-water interface temperature usually keeps a certain temperature, which is called freezing point. According to sea ice constituents discussed in the above, the latent heat can be calculated when seawater per mass freezes. Because salt separates from the brine while freezing, the

condensation latent heat is released by pure ice when fresh water per mass freezed, that is, in the Bohai Sea,

$$Qn = Mi \cdot L_T \cong 333 + 18S/T \qquad (14)$$

where T=—1.8℃, S = 5 and then Q_n=283J/g.

When air temperature continuously dropping down, the upper layer of ice floe releases heat and reduces the temperature, and its specific heat can be determined by Eq.(12b). Sea ice continuously separates salt with temperature dropping down, the salt discharges into seawater under ice floe and makes sea ice salinity continuously reduce. It can be easily known from Eq.(12b) that specific heat continuously decreases at this moment, and sea ice temperature raises more easily during melting period.

When air temperature increases, the ice around the brine bubble will gradually melt to keep balance with the brine bubble phase, that is to say, when the temperature increases, sea ice is always melting but begins to melt at one moment. That means melting point of sea ice isnt deterministic. But generally speaking, the freezing point of seawater at sea surface is only determined by salinity, and the sea temperature is equal to its freezing point while sea ice melts. So we prescribe that melting point temperature is equal to the freezing point. The melting latent formula same as (14) can be obtained similarly to the freezing. Because the sea ice salinity is lower than that of the freezing ice at that time, it can be easily known that the melting heat is larger than condensation heat according to formula (14). When the salinity of sea ice is 3, the melting heat Q_r is 303J/g. It can be seen from the calculated result that, although the continuous decrease of sea ice salinity makes the melting heat of ice point larger than condensation heat, the difference between them is very small. In fact, the freezing and the melting can be looked as reversible. The melting heat and the condensation heat can be chosen as 300J/g for the Bohai Sea. This shows that the sea ice per unit area with thickness of 2cm needs the condensation latent heat of 6.1×10^6J.

3 Sea-air Energy Balance of the Ice-covered Sea

According to the ice conditions in the Bohai Sea during ice period, the sea surface can be divided into two parts, the open water area and the ice-covered area. In fact, the lead or polynya will appears in the ice-covered area for inhomogeneity of ice velocity field. In this paper, the sea-air energy exchange relationship is given under certain hydrological and meteorological conditions.

3.1 Energy balance at the water-air interface

For the open water without ice, the net energy flux into the mixed sea layer, as shown in Fig. 10, is

$$Q_{ws} = F_H + F_L + R_w + F_{sww} + F_w \qquad (15)$$

Where Fw is the sea heat flux into the mixed layer, $Fsww$ is the net solar short wave radiation flux at sea surface, provided all the solar radiation to sea surface SW except the portion reflected to atmosphere, i.e.,

$$Fsww = (1-\alpha_w)SW \qquad (16)$$

where α_w is reflection rate at the sea surface, choosing as 0.1. The temperature variation for 28th January is approximately expressed as, $T_a = T_{a0} + 2\sin\omega$, where T_{a0} = -5℃, Tw is -1.8, 1 and 3℃, respectively. Fig.

11 shows the net heat flux variation with water temperature at sea surface. It can be seen that the net heat flux at high noon is positive under this condition, and decreases with the temperature increase at the sea surface. The water temperature variation at sea surface has great effect on the net heat flux at sea surface. It is shown in Fig. 11 that the net heat flux changes 30W/m^2 as sea temperature increase 1℃.

The effect of air temperature variation on the net heat flux at sea surface is shown in Fig.12. It is shown in Fig.12 that the net heat flux at sea surface will reduce about 100W/m^2 as air temperature drops down 5℃, and the maximum net heat loses from the sea surface is 450 W/m^2 for the air temperature $Ta = -15 + 2\sin\omega$ ℃, and its daily average is about 250 W/m^2.

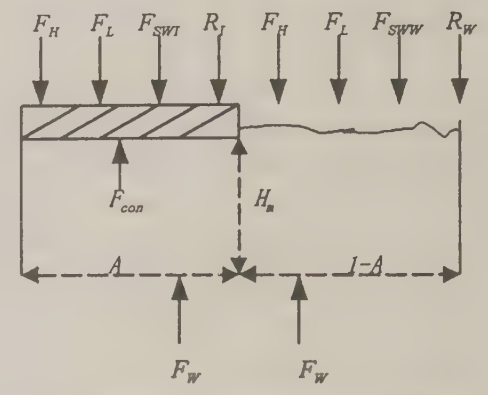

Fig. 10 Sketch map of energy flux

Seawater of the whole layer fully mixes in winter season because the Bohai Sea is a super-shallow sea. For seawater of depth H_m per unit area, the temperature drop is

$$\Delta Tw = \frac{Qws \cdot \Delta t}{Hm \cdot Cw} \qquad (17)$$

where Q_{ws} is the net heat flux at the sea surface, $C_w^{'}$ is the sea water specific heat per unit area, choosing 4.1 × 10^{6}J/(m.K), H_m is the mixed layer thickness, and Δ t is time difference. The variation rate of the sea surface temperature is shown in Fig.13 for water depth of 10m, sea surface water temperature of 1℃, and different air temperature. It can be seen form the figure that the rate of the sea temperature with the net heat flux at sea surface is basically consistent with the net heat flux at sea surface.

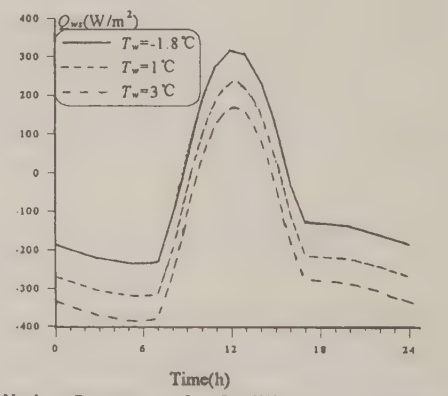

Fig. 11 Net heat flux at sea surface for different water temperature

In addition, if net loss of the heat flux is 100～250W/m^2 for the sea water temperature of -1.8℃, it can be estimated that freezing of 2cm thickness sea ice costs about 4～17h.

3.2 Energy balance at the ice-air interface

For the ice covered sea surface, as shown in Fig.10, the net energy flux is,

$$Qis = F_H + F_L + Ri + Fswi + Fcon \qquad (18)$$

where, F_{con} is the convective flux upward through ice, F_{swi} is the solar short wave absorbed by the ice surface, which is expressed as the following with Semtners(1976) parameterization method:

$$Fswi = (1 - 0.4I_0)(1 - \alpha_I)SW \qquad (19)$$

where, I_0 is the short wave penetrability at the ice surface. Maykut and Untersteiner(1971) assumed that I_0= 17%; α_I is the short wave albedo relative to ice thickness, as shown in Tab.3. According to the

observation at the Bayuquan, Li Zhijun etc (1989) got the result that the difference of ice temperature and air temperature is about 5℃ from the ice surface to 3cm in the ice layer and their variation is in-phase. In fact, the variation of ice temperature lays behind the variation of air temperature, but we still assume that their variations are in-phase in this paper. And we also assume that the difference of the ice surface temperature and the air temperature are constant in a day. According to the observed data in the Bohai Sea, the heat flux variation is shown in Fig.14 for the mean air temperature of -10℃, the wind speed of 10m/s, the ice thickness of 20cm, and the differences of the ice surface temperature and the air temperature of 0℃, 2℃ and 5℃ respectively. It can be seen from Fig.14 that the variation trend of the net heat flux at the ice surface and sea surface is basically identical, but the flux is different quantitatively. Assuming the ice temperature is 2℃ higher than the air temperature, the heat flux of different ice thickness at ice surface is shown in Fig.15. It can be seen from the figure that the maximum variation is about $100W/m^2$ and it decreases with solar height angle decreasing. The heat flux at the ice surface is independent on the ice thickness before sunrise and after sunset, without considering F_{con}.

Table. 3 The relationship of the short wave albedo of ice with ice thickness(after Weller, 1972)

Thickness(m)	0.05	0.1	0.2	0.3	0.4	0.6	0.8
a_1	0.27	0.32	0 36	0.39	0.41	0.44	0.46

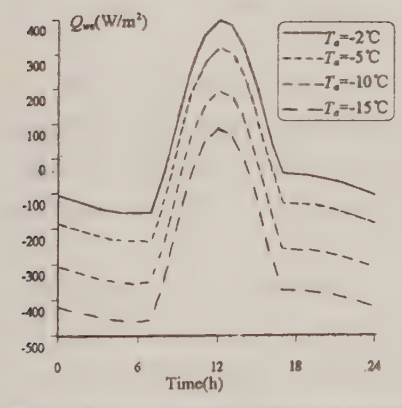

Fig. 12 Net heat flux at sea surface for different air temperature

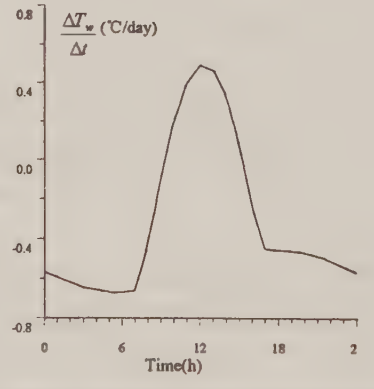

Fig. 13 Sketch of temperature variation rate at the sea surface (T_w=1℃)

4 Conclusions

From the above analyzing and studying by the use of the observed data in the Bohai Sea, the following is summarized.

(1) The solar short wave radiation has an important effect on the surface heat balance in the Bohai Sea. Not only its flux is large, but also its variation is marked. It is the most important factor causing sea surface energy unbalance. The simplified Laevastu(1960) formula is available for calculating the solar short wave radiation of the Bohai Sea area.

(2) According to the observation, the atmospheric relative humidity at the ice surface is about 50%, and the relative humidity at the water surface is about 90%.

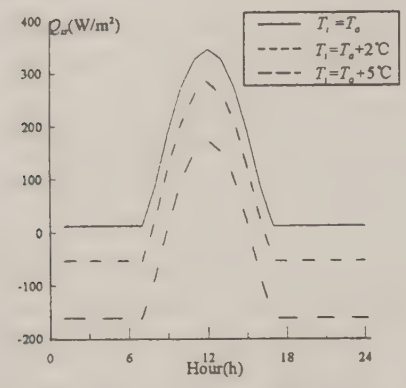

Fig 14 Net heat flux for different temperature differences at ice surface

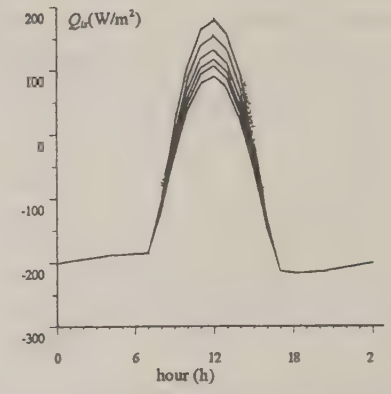

Fig 15 Net heat flux of different ice thickness at the ice surface (The numbers attached to the curves denote the conditions of the different ice thickness from 0.05m to 0.6m as shown in Tab 3)

(3) The wind velocity and the air temperature are the other two important factors making the heat budget unbalanced at the sea surface. The lower the air temperature is and the larger the wind velocity is, the more heat losses at the sea surface. The low temperature and gale are the direct reason for sea ice to grow in the Bohai Sea during January 1997.

(4) The long wave radiation flux at the sea surface is more steady, and is usually about 100W/m^2 in winter. The flux varies with the air temperature and the sea surface temperature, but its variation range is less than 30W/m^2, in general.

(5) The sea ice salinity decreases with the time during freezing, it effects the specific heat, conductivity and condensation latent heat of sea ice, but during freezing the sea ice salinity decreases with the time. In the Bohai Sea, however, the conductivity and condensation latent heat of sea ice vary little, and they can be taken as constant, but the specific heat flux varies largely, which should be paid much more attention.

The study above provides the basis for the mathematical treatment of the thermodynamic process in the sea ice model, and provides the basis for choosing calculation formula and parameters of heat budget at the interfaces of ice-atmosphere and water-atmosphere, and provides the basis for further determining the sea ice growth function in the sea ice model.

References

Bai Shan, Wu Huiding, (1998)Numerical sea ice prediction in China. *Acta Meteologica Sinica*, 56(2):139～152

Haney R L. Surface thermal boundary condition for ocean circulation models. J Phys. Oceanogr.,1,241, 1971

Hoffert M I and Storch J. A scheme for computing surface fluxes from mean flow observations. Boundary-Layer Meteoro.,17:429, 1979

Laevastu T. Factors affecting the temperature of the surface layer of the sea. Soc. Sci. Fenn. Comm. Phys. Math.,.25, 1960

Li Zhijun, etc. Measurement and analysis for ice temperature and other physical properties of the fast level ice in Liaodong Bay,*Acta Oceanologica Sinica*, 4: 525~533, 1989

Maykut G A. and Untersteiner N. Some results from a time-dependent thermodynamic model of sea ice. J. Geophys.

Res.,76,6,1550~1575, 1971

Pounder E R. Physics of Ice. Pergamon Press,1964,151

SemtnerA J.A model for the thermodynamic growth of sea ice in numerical investigation of climate. J. Phys. Oceanogr.6, 375~389,1976

Untersteiner N. On the mass and heat budget of Arctic sea ice. Arch. Meteorol. Geophys. Bioklimatol., A, 12,151~182, 1961

Weller G.Radiation flux investigation. Aidjex Bull.,1972 , 14,28-30.(Available as PB 220/859, Nat. Tech. Info. Serv., Springfield,Va.)

Wu Huiding, Wang Zhilian, Sea ice thermodynamic process and its numerical simulation. See: Series of science and computation, *Numerical calculation for physical oceanography*, Feng, S. and W. Sun ed. Henan Science and Technology Press. pp. 361-428, 1992

Wu Huiding, Bai Shan and Zhang Zhanhai, Numerical simulation for dynamical processes of sea ice.*Acta Oceanolog ica Sinica,* Vol. 16, No. 3, pp. 303-325, 1997

Wu Huiding, etc. Numerical model for atmospheric boundary layer,*Acta Meteologica Sinica*, 42, 290, 1984

Yang Guojin and Jochmann P. Ice Survey 1988 in the Liaodong Bay. E182/88,Hamburgische Schiffbau-Versuchsanstalt, Hamburg,2.5-2.6,2.37-2.39, 1988

Analysis of the Sedimentary Characteristics and Origin of the "Old Red Sands" in the Coastal Areas of Southeast Fujian

Zeng Congsheng (曾从盛) Chen Jucheng(陈居成) Wu Yougong(吴幼恭)
(*Institute of Geography, Fujian Normal University, Fuzhou 350007*)

Abstract The "Old Red Sands" are widely distributed and typically developed over the coastal areas of Southeast Fujian, but there are different views on their origin. Based on the overall field investigations and a series of lab studies, the paper suggests that the "Old Red Sands" are mainly formed by the beach wind-drift sands and ,locally, by slope wash and alluviation.

Keywords Old Red Sands, sedimentary characteristics, origin, coastal areas of Southeast Fujian

In the coastal area to the south of the Minjiang River mouth are widely distributed a kind of mainly red, medium-fine sandy, and semi-consolidated sediments commonly called the Old Red Sands. Research on this kind of unique Quaternary sediments started as early as the early 1960s, but so far there are a number of controversies on its origin[1] . Based on the overall field investigation and a series of lab studies made on the Old Red Sands in the coastal areas of Southeast Fujian in recent years, this paper makes an analysis and discussion on its sedimentary characteristics and origin.

1 Sedimentary Structures and Tectonics of the Old Red Sands

1.1 Grain-size characteristics and grain forms

A total of 62 grain-size analytical samples have been collected from the emerged section of Old Red Sands in the coastal areas of Southeast Fujian and, for the convenience of comparison, 6 beach sand samples from Liushui, Pingtan and Ciaotou, Changle. According to the granulometric analysis, the mean grain size (Mz) is 1.88~6.09 ϕ, with an average of 3.39 ϕ, and in general, they are mainly the fine sands (accounting for about 38.23% on an average) and medium sands (accounting for about 19.6% on an average). Individually, the Old Red Sands sections in Humian of Putian, Xiangzhi of Jinjiang and Sonxia of Changle are dominated by the medium sands (acccounting for about 31.33% on the average) and fine sands(acccounting for about 24.34% on an average) while the Old Red Sands in Nanjing of Zhangpu are mainly silt (acccounting for about 33.66% on an average) and clay (acccounting for about 18.95% on an average). Analysis of the modern beach sand samples from Ciaotou of Changle and Liushui of Pintan shows that, although the beach sands are mainly fine and medium sands, the content of extremely coarse sands and gravels is higher than that in the Old Red Sands and it is particularly obvious that the Old Red Sands contain much fine-grained matter such as silt and clay, in which the content of clay is 0.3%~40.2%, with an average of 14.2% while the modern beach sands contain very little silt and no clay. The presence

of much clay matter in the Old Red Sands is mainly due to the weathering of their unstable minerals such as andesinite in the late stage of sedimentations of the Old Red Sands, because in the Old Red Sands sections whose red colour turns from dark to light from top to bottom, all its content of clay without exception deceases from top to bottom. For instance, in the 7m-thick Old Red Sands section in Ciaotou of Changle, the contents of clay in the upper, middle and lower parts amount to 23.84%, 5.82% and 2.73%, respectively; and the contents of clay are 6.31%, 3.15% and 1.33% in the 5.6m-thick Old Red Sands section in Xiangzhi of Jinjiang at the burying depths of 1.3m, 3.6m and 4.6m, respectively. In an Old Red Sands Section in Dongsheng of Dongshan, the upper part is in orange colour while the lower part is reddish brown, obviously representing the sedimentation in the old and new stages. The content of clay in the upper part is 0.67% while that in the lowwer part is 8.44%, thus indicating that the content of clay in the Old Red Sands is colsed related to the degree of weathering.

The standard deviation (σ_1) of the Old Red Sands is 9.86~4.39, with an average of 2.21, among which those in between 1.00~9.00, 2.00~4.00 account for 48.89% respectively, belonging to the fairly poor ~ very poor sorting. The σ_1 of the modern beach sands is 0.46~0.99, with an average of 0.75, which belongs to the medium level of sorting while the σ_1 of modern eolian sands is between 0.16 and 1.19, wiwth an average of 0.58, among which, those in between 0.35~0.71 account for 52.38%, being fairly well sorted~very well sorted. As far as the standard deviatiion is concerned, the Old Red Sands are not so well sorted as the modern beach sands and eolian sands.

The skewness (SK_1) of Old Red Sands is in between -0.18 and 9.56, with an average of 0.66, of which the positive skewness occupies 95.56% while theSK_1 of modern beach sands is in between -0.51~-0.33, with an average of -0.37, all being negative skewness.

The kurtosis (Kg) of Old Red Sands is in 0.58~ 11.27 with an average of about 3.06, most being very narrow kurtosis (those of >3.00 occupy 24%) and part being the medium to narrow kurtosis (those of 0.9 ~1.5 occupy 13.3%) and the very narrow kurtosis (those of 1.50~3.00 occupy 24%) while the beach sands are dominated by the medium to narrow kurtosis (occupying 75%), with the very narrow kurtosis and the extremely narrow kurtosis missing.

There is now still a divergence in opinion as to whether the scatter diagram of size parameters can accurately reflext the characteristics of the sedimentary environment. It can be clearly seen from the scatter diagram for the Old Red Sands and the modern beach sands in the coastal areas of Southeast Fujian (Fig.1) that on the scatter diagrams of1/4 ϕ size parameters of Mz v. σ_1, Mz v. Kg and Sk_1 v. Kg, the two can very well be differentiated from each other.

The probability accumulative curves of the Old Red Sands (Fig.2) are mostly the three-section type, part are four-section and two-section types, which are mainly the skip components (the content reaching 80%~90%), mostly depicting a skipping ensemble. The saltation components have narrow intervals in between and large slopes (62° ~76°); the content of roll components is low and some are even missing; the content of suspended components is high, reaching generally 20%~40% and the maximum of 60%, far higher than that of the modern coastal wind-drift sand (generally not higher than 2%[2]).

Statistical analysis of the quartz particles roundness degrees of the Old Red Sands, dune sands and beach sands in the coastal areas of Southeast Fujian indicates that the rounded, subrounded and acute angular particles account for 6.78%, 83.75% and 9.46% respectively in the Old Red Sands; 9.88%, 75% and 16.67% in the dune sands; and 0%, 70% and 30% in the beach sands, all of which are dominated by

the subrounded particles, but in the Old Red Sands and dune sands there occur small amounts of rounded particles while in the beach sands there occur very few or none of the rounded particles, but there are obviously more subangular ones than those in the farmer two. This shows that the degrees of roundness in the Old Red Sands, and the dune sands are close, both better than that in the beach sands.

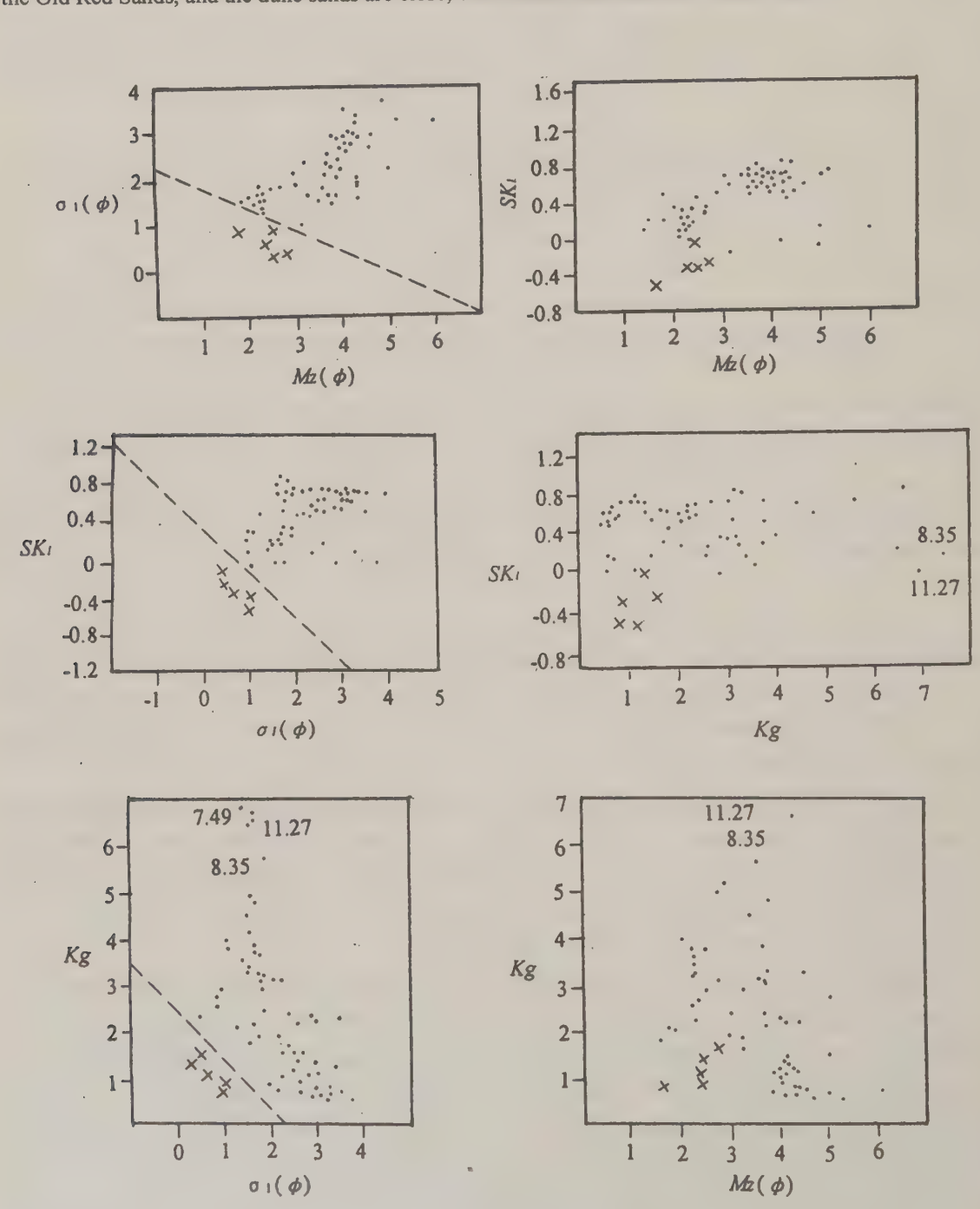

Fig.1 Scatter diagram of Old Red Sands in the coastal areas of Southeast Fujian

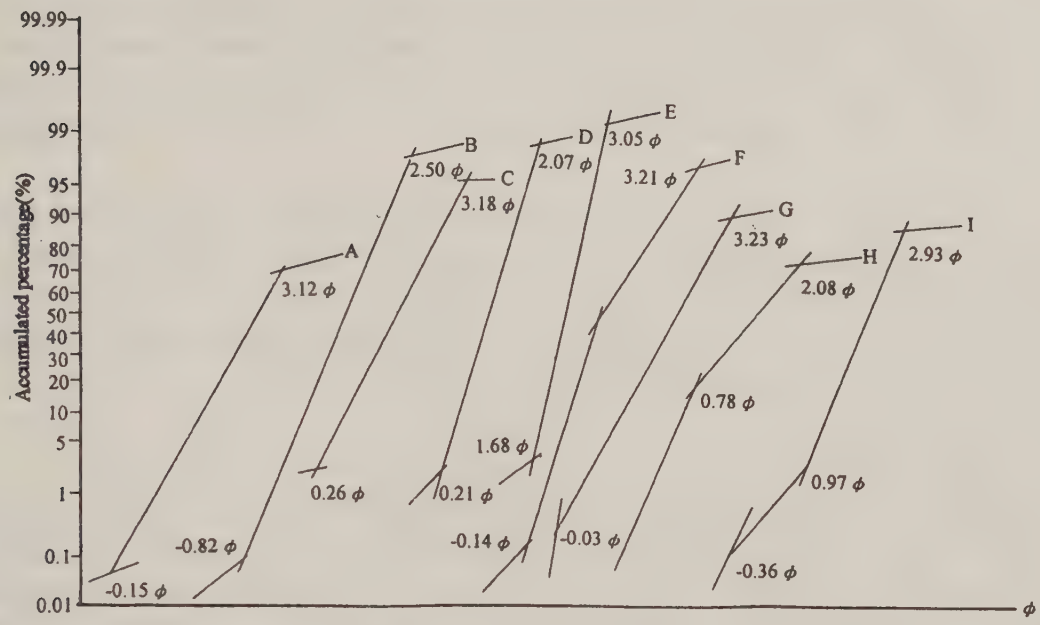

Fig.2 Diagram of probality accumulative curves of the Old Red Sands in the coastal areas of Southeast Fujian

A—Ciaotou, Changle(FZ9702); B—Qingfeng, Pingtan(FQD-17); C—Qingfeng(FQD—33); D—Qingfeng, Pingtan(FQD-61); E—Liushui, Pingtan(FLD-7); F—Liushui, Pingtan(FLD-7); G—Jingsha, Pingtan(FZS-9701); H—Humian, Putian(FH9702); I—Nansai, Weian(FHN9702)

Different sedimentary environments may leave different surface structural characteristics on the surface of quartz particles. It is generally believed that on the surface of the eolian quartz particles there are typical butterfly pits, pitting, snaking ridges and upper convolute cleavage lamellae, etc. Are there typical grain surface structural characteristics in the coastal wind-drift sands? Pye believes[3] that due to the fact that tyey are transported by the wind force for a shorter distance and time, the quartz particles in the coastal dune cannot form the surface structural characteristics uique in the coastal dune environment and most of the particle surface only inherit and transform the characteristics of the beach sands (V-shape pits, triangular corroded pits) and in the meantime, are superimposed with the characteristics of the eolian environment (butterfly pits, impact pits and frosting, etc.), which indicates that the coastal dune is the product of transport and transformation of the beach sands by wind force. Observation and analysis by the scanning electron microscope of quartz particles in grain sizes of 0.25~0.5mm of the Old Red Sands in the coastal areas of Southeast Fujian indicates that the surface structures which represent the eolian environment such as butterfly pits, pittting, crescent impact pits, upper convolute cleavage lamellae, etc. are commonly seen and among them, the occurrence rate of the butterfly pits is 28.71% and that of the pitting 11.67%. The occurrence rate of the V-shaped pits representing the underwater environment reaches 48.9% and the plane of parallel cleavage characteristic of the marine-built environment may also be seen. The chemical action on the surface of quartz particles is very common, including both the obvious phenomena of chemical dissolution and the typical action of chemical precipitation. Chemical

dissolution is mainly represented by the solution pits and solution grooves with an occurrence rate of 68.9%, indicating that it has been subjected to seawater dissolution for a long time. Chemical dissolution occurs in the forms of siliceous scates and siliceous membranes, with an occurrence rate of 12.1%, 13.5% and 10.57% respectively, indicating that it has been subjected to the further chemical action in the terrstrial environment.

The surfaces of quartz particles in the modern eolian sands in the coastal areas of Southeast Fujian have the similar cheracteristics to those of the Old Red Sands, while the surface structural characteristics of the eolian environment such as butterfly pits are not found in the modern beach sands, but the characteristics of the underwater environment such as V-shape pits (with an occurrence rate of 65%) are obviously more than those in the Old Red Sands and the modern wind-drift sands.

1.2 Sedimentary tectonics

Affected by the late-stage weathering, the sedimentary bedding is mostly not distinct and generally manifested in the block structure. In some sections, low-angle cross-bedding may be seen and the high-angle cross-bedding and wedge-type bedding may also be found (e.g. in the Qingfeng and Jingsha sections of Pingtan). Generally, the redder the Old Red Sands are, the higher the degree of weathering is and the more indistinct the bedding is. For most vertical sections of the Old Red Sands, their colour changes from dark to light from top to bottom, i.e., from the reddish brown or red colour in the upper part gradually downwards to the dark orange or orange and even to the greyish white. But in some Old Red Sands sections (e.g. in Keren of Jinjiang), distinst sedimentary layers of red~yellow~red~yellow are found from top to bottom.

The Old Red Sands mostly overlie unconformably the granite or its crust of weathering (patterned layer) while some part of them underlie the sliderock (e.g. in Liuao of Zhengpu) or the Quarternary littoral -facies epidermis (e.g. in Qianhu of Zhangpu). Between the Old Red Sands there have developed peat strata or clay strata rick in organic matter, but they are mostly distributed with in a limited scale and often lens-shaped. In the deeply weathered Old Red Sands, there are often thin-bedded ferruginous zone of enrichment or iron pan. It should be noted that some previous studies suggested that the iron pan is the first-order interface of dissected eolian deposit, but actually the formation of the iron pan in the Old Red Sands is related to the fact that the Old Red Sands have been subjected to the intense weathering and leaching, and is not the primary sedimentary interface.

1.3 Characteristics of mineral assemblage

The light minerals in the Old Red Sands are mainly quartz and feldspar, with the content of the former reaching 75% on the average and that of the latter (mainly the high albite and small accounts of potassium feldspar) about 20% on the average. The general feature of the heavy mineral assemblage is that the contents of more stable minerals such as ilmenite, magnetite, leucoxene, zircon, tourmaline, etc. are generally high, and higher than those in the modern beach sands. For instance, in the Old Red Sands section in Ciaotou of Changle, the contents of ilmenite, magnetite, leucoxene, zircon, and tourmaline reach 24.3%, 27.1%, 18.4%, 7.8% and 6.5% respectively on the average while in the beach sands they are 3.4%, 18.2%, 5.4%, 2.5% and 3.7% respectively on the average. The contents of unstable minerals in the

Old Red Sands such as amphibole, garnet, chlorite, epidote, etc. are generally very low or even missing. For example, in the Old Red Sands section in Ciaotou of Changle, its upper part basically does not contain amphibole and its lower part only contains 0.5% on the average while the beach sands contain 15.5% on the average.

1.4 Geochemical and paleontological characteristics

In differentiating the marine and continental deposits, paleontology is often taken as the main identification marker. In the recent 20 years, the geochemical method of using microelements to identify the marine and continental sedimentary environments has been attached widespread importance. In this respect, the contents and their ratios of the six elements B, Ga, Rb, K, Sr and Ba are often used to make the differentiation. We have detected the microelements in part of the Old Red Sands samples taken from Linshui Qingfeng of Pingtan, Eweishan of Putian and Keren of Jinjiang. Except that the content of Ga in the two samples from Liushui Pingtan and that of Ba in one sample from Eweishan of Putian and Liushui of Pingtan each indicate the transitional facies, all the rest contents and values of ratio point to the continental facies (see Table 1).

Table 1 Contents of microelements (10^{-6}) in the Old Red Sands in the coastal areas of Southeast Fujian and their values of ratio

Sample No.	Sampling Location	B	Ga	B/Ga	Sr	Ba	Sr/Ba	K
FL9701	Liushui, Pingtan	23.65	19.13	1.2363	31.30	254.45	0.1230	730.40
FL9702	Liushui, Pingtan	19.52	15.44	1.2642	54.16	272.06	0.1880	1 238.40
FL9703	Liushui, Pingtan	8.46	8.90	0.9506	27.96	296.05	0.094	295.40
FL9705	Liushui, Pingtan	8.96	7.89	1.1356	35.31	330.00	0.107	417.40
FQ9701	Qingfeng, Pingtan	15.72	13.60	1.1559	17.72	184.50	0.096	377.50
FM9702	Eweishan, Putian	14.02	9.53	1.4758	38 81	386.80	0.100	486.40
FJK9701	Keren, Jinjiang	16.83	12.33	1.3650	20.35	164.15	0.124	319.00

Analysis of the total chemical contents in the Old Red Sands indicates that the various total chemical contents are in the order of SiO_2~Al_2O_3~TiO_2~MgO~FeO from high to low, which is similar to the total chemical contents assemblage characteristics in the granite crust of weathering, but the content of SiO_2 in the Old Red Sands is higher than that in the granite crust of weathering, But the content of Al_2O_3 is obviously lower, thus making the silicon-aluminium-iron ratio in the Old Red Sands (generrally larger than 15) is much larger than that in the latter (generally smaller than 10). This suggests that the weathering of the Old Red Sands is lighter as compared with that of the granite crust of weathering. As far as the change of the vertical section of the Old Red Sands is concerned, the silicon-aluminium-iron ratio increases from top to bottom, indicating that the degree of weathering in the upper part of the Old Red Sands is generally higher than that in its lower part. The value of ratio of FeO/Fe_2O_3 in the Old Red Sands is all very small, generally below 0.1, which shows that the Old Red Sands have been long subjected to

the oxidized environment.

Possibly due to the larger sediment particles in the Old Red Sands and the effects of weathering in the later stage, the Old Red Sands are poor in paleontological fossils. According to the report of research findings [4], the lower part of the Old Red Sands sedimentary section in Honghutou, Putian contains individual fossils of foraminifera and marine ostracoda. Sporopollen analysis of the Old Red Sands section in Qianhu, Zhangpu[5] indicates that in the upper Old Red Sands layer only are detected the pollen of Pinus and Hemlock, and, in the lightly weathered lower part, only sporo-pollen of Pinus, Hemlock, Carya, Birch, the grass family and Pteridium, etc. are seen.

2. Discussion on the Origin of Old Red Sands

Based on the above-mentioned sedimentary structure and tectonic characteristics of the Old Red Sands in the coastal areas of Southeast Fujian and in the light of their distribution and geomorphological features [6], it may be believed that the Old Red Sands in the coastal areas of Southeast Fujian mainly originate from the eolian environment, i.e., they are the product of ancient wind-drift sand deposition formed by the wind-driven beach sand and subjected to rubefication after long-term weathering and leaching. Therefore, the Old Red Sands have both the characteristics of eolian deposition and the brand of sea beach sedimentation.

It is generally believed that the eolian sands are well sorted while the Old Red Sands deposition is poorly sorted. Both the modern coastal wind-drift sands and the beach sands are better sorted than the Old Red Sands. This is mainly due to the fact that in the later stage of the Old Red Sands deposition, the weathering action causes the fine-sized matter such as clay to increase significantly in them and also has something to do with the mixing of the decomposed rock debris on the mountain slope.

The probability accumulative curves of the Old Red Sands display mainly the three-section type of rolling, skipping and suspension. The skip components mostly depict a skipping ensemble, which is obviously different from the beach sands which are a four-section type and the skip components mostly present the characteristics of a double-skipping ensemble. The scatter diagram of grain size parameters also points to some differences between the Old Red Sands and the beach sands.

Most quartz particle surfaces of the Old Red Sands have the typical form of wind action such as butterfly pits, etc. and the obvious traces of under water action such as the V-shaped pits. The fact that the edges of the V-shaped pits are mostly rounded fully shows that the Old Red Sands are mainly the product of the beach sands being transported and transformed by wind. There are round particles occurring both in the Old Red Sands and the modern dune sands, but very few or none in the beach sands, which indicates that the higher degree of roundness in the Old Red Sands is the result of further transportation by wind on the basis of the beach sands.

Although being subjected to the weathering action, the depositional bedding in the Old Red Sands is not obvious, but there exist multi-level sedimentary interfaces, which are a major feature of eolian sedimentation.

It can be seen from the assemblage characteristics that compared with the neighbouring beach sands, the stable heavy minerals increase in the Old Red Sands while the unstable minerals decrease. The

enrichment of stable minerals may also suggest that the Old Ted sands deposition has been further subjected to the stronger transportation on the basis of the beach sands while the decrease of unstable minerals is related to their wear and tear in the second-time transport and the weathering action in the later stage.

Analysis of the contents of related microelements in part of the Old Red Sands sections and their values of ratio indicates that the Old Red Sands should be the continental deposit.

To sum up, it is clear that the Old Red Sands in the coastal area of Southeast Fujian are mainly formed by the beach sands being transported by wind and accumulating. But for the Old Red Sands in individual lacations, there exist some differences in their origin. For instance, the Old Red Sands in Songxia, Changle are accumulated at the front edge of a small alluvial and pluvial fan, and they are not only coarse in grain size, but the most poorly rounded Old Red Sands section found in the coastal areas of Southeast Fujian, indicating that they are obviously formed by alluviation and pluviation; The Old Red Sands in Nanjing, Zhangpu are the most poorly sorted ones found in the studied area, and they are dominated by silt and clay, which are mixed up with a fairly large number of well-rounded gravels, indicating they are mainly formed by alluviation. The low parts of the Old Red Sands sections in Jingsha, Pingtan and Eweishan, Putian, the upper part of the Hutou Old Red Sands section in Liuao, Zhangpu and the Old Red Snads section near the foot of a mountain on the southwest side of Qingfeng, Pingtan are all intermingled with many alluvial slope detrital gravels, thus possessing the mixed feature of eolian accumulation and slope wash.

The direct and indirect sedimentary datings of the Old Red Sands (see Table 2) indicate that the Old Red Sands in the coastal areas of Southeast Fujian were mainly formed during the Quartenary Wurm glacia l stage, which may be roughly divided into the two major relatively concentrated stages of formations: 60~45kaBP and 30~10kaBP, (if further subdivided, the latter may be divided into the two stages of 30~25kaBP and 20~10kaBP except that the Old Red Sands were distributed in a limited way in the stage of 30~25kaBP), and the Old Red Sands were most widely distributed during the 20~10kaBP. The peat layer and ancient soil were mainly developed during the Wurm glacial stage, when were also developed the alluvial and pluvial Old Red Sand in Songxia, Changle and other locations, indicating that, under warm and wet conditions, the large-scale activity of wind-drift sands in the coastal areas were somewhat weakened.

3. Conclusion

It may be concluded from the research on the Old Red Sands in the coastal areas of Southeast Fujian that:

a) The Old Red Sands are a kind of mainly red, medium-fine sandy and semi-consolidated sediments.

b)The Old Red Sands are generally manifested in block structure and their depositional bedding is mostly not distinct, which is related to the weathering action in their later stage of deposition. Most of the vertical sections of Old Red Sands change from dark to light in colour from top to bottom. The higher the degree of weathering is, the redder the colour is.

Table 2 Datings of the Old Red Sands in the Coastal Areas of Southeast Fujian

Location	Buried Depth(m)	Sample	Age(aBP)	Method	Data Source
Liushui, Pingtan	10.73	Old Red Sands	58000±5000	TL	This paper
Qingfeng, Pingtan	6.00	Old Red Sands	54000±5000	TL	This paper
Keren, Jinjiang	11.59	Old Red Sands	54000±5000	TL	This paper
Dongshen, Dongshan	4.00	Old Red Sands	49000±5000	TL	Wang Yuzhou, 1990
Xiakeng, Weian	3.70	Clay among the Old Red Sands	>42000	^{14}C	Chen Yuantian, 1991
Songxia, Changle	1.50	Old Red Sands	42000±5000	TL	Wang Yuzhou, 1990
Houlou, Pingtan	Elevation 15	Old Red Sands underlying peat	>41670	^{14}C	Zheng Jingwen et al., 1982
Xilou, Pingtan	Elevation 17	Old Red Sands underlying clay	39230±2130	^{14}C	Zheng Jingwen et al., 1982
Ciaotou, Changele	0.75	Old Red Sands	37000±4000	TL	This paper
Houlou, Pingtan	Elevation 17	Old Red Sands underlying peat	32665±1980	^{14}C	Zheng Jingwen et al., 1982
Ciaotou, Changle	1.50	Old Red Sands	32000±4000	TL	Wang Yuzhuo, 1990
Pinghai, Putian	Elevation 16.7	Peat within the Old Red Sands	31490±1300	^{14}C	Chen Weiguang et al., 1986
Shenhu, Jinjiang	8.90	Old Red Sands	30000±3000	TL	Wang Yuzhou, 1990
Nansai, Weian	2.50	Old Red Sands	27200	ESR	This paper
Eweishan, Putian	5.30	Old Red Sands	26000±2500	TL	This paper
Keren, Jinjiang	5.93	Old Red Sands	25700	ESR	This paper
Nanjing, Zhangpu	1.20	Old Red Sands	25500	ESR	This paper
Liuao, Zhangpu	1.40	Old Red Sands	25000±2000	TL	Wang Yuzhuo, 1990
Qingyan, Jinjiang	Elevation 21	Clay	22590±780	^{14}C	Chen Weiguang et al., 1986
Xiakeng, Weian	Elevation 19	Clay among the Old Red Sands	22404±615	^{14}C	Chen Yuantian, 1991
Liushui, Pingtan	5.88	Old Red Sands underlying peat	22070±510	^{14}C	This paper
Eweishan, Putian	1.50	Old Red Sands	22000±2000	TL	This paper
Liushui, Pingtan	5.19	Old Red Sands	18500±1500	TL	This paper
Yuandan Port, Xiamen	Elevation 23	Old Red Sands above peat	16000±650	^{14}C	Cai Lizhu,1988
Keren, Jinjiang	4.90	Old Red Sands	15200	ESR	This paper
Liushui, Pingtan	1.99	Old Red Sands	12500±1000	TL	This paper
Riwenkeng, Putian	0.60	Old Red Sands	12500	ESR	This paper
Riwenkeng, Putian	Elevation 30	Old Red Sands underlying peat	12250±192	^{14}C	Dingxianghuan, 1998
Qingfeng, Pingtan	0.29	Old Red Sands	12000±1000	TL	This paper
Eweishan, Putian	0.30	Old Red Sands	11000±1000	TL	This paper
Keren, Jinjiang	1.22	Old Red Sands	10000±1000	TL	This paper
Liushui, Pintan	0.20	Old Red Sands	9500±800	TL	This paper
Jingsha,Pintan	1.60	Old Red Sands	9000	ESR	This paper

c) There are some peat layers or ancient soil layers developed in the Old Red Sands, which belong to the interdune deposition of coastal dunes under warm and wet climatic conditions while the existence of some ferruginous enriched thin layers or placons is the result of long-term weathering and leaching of Old Red Sands after deposition.

d) The Old Red Sands contain more clay materials, which is mainly due to the weathering of unstable minerals such as fledspar.

e) The Old Red Sands deposit is poorly sorted, which is related to the increase of clay materials and the intrusion of the slope decomposed rock debris.

f) The skewness of Old Red Sands is mostly positive, but in a few cases, it is negative. The probability accumulative curves are mainly the three-section type and the skip components mostly present a single skip ensemble. The interval between the skip components is narrow, the slope is large and the content is high.

g) The quarze particles of the Old Red Sands are well rounded, mostly in subrounded and rounded shape. The surface microstructures have both inherited and transformed the characteristics of beach sands and been superimposed with the traces of wind action.

h) Except a few which indicate the transitional facies, the majority of microelements and their values of ratis point to the continental deposit.

i) The Old Red Sands in the coastal areas of Southeast Fujian are mainly formed by the beach sedimentary sands being transported by wind and, locally, by alluviation, eolian accumulation and slope wash.

j) The deposition of the Old Ted Sands in the coastal areas of Southeast Fujian may roughly be divided into two major relatively concentrated stages of 60~45 kaBP and 30~10kaBP. And if further divided, the latter may be further subdivided into the two stages of 30~25 kaBP and 20~10kaBP, and the Old Red Sands formed in the stage of 20~10kaBP are the most widely distributed.

References

1. Zeng Congsheng, Chen Jucheng and Wu Yougong (1997).*The Taiwan Straits*, A Summary of Researches on the Old Red Sands in the coastal Southeast China, 16(3): 363~370.
2. Wu Zheng et al. (1995), Research on the Wind-drift Sand Geomorphology in the Coastal South China, Beijing Science Publishing House, 57~68.
3. Pye K. (1983), Coastal Dune, Prog. Phys. Geogr., 7(4): 431~557.
4. Zhang Hunan, Yao Qingyuan, Zhao Xitao (1985), Discussion on the Origin and Times of Old Red Sands Deposition in the Coastal Areas of South Fujian and East Guangdong, *Marine Geology and Quaternary Geology*, 5(1): 47~57.
5. Zheng Xiaoyun (1997), Some Problems Concerning the Frontal Lake Sections in the Coastal Area of South Fujian, *the Taiwan Straits*, 16(2): 117~127.
6. Chen Jucheng, Zeng Congsheng and Wu Yougong (1998). Distribution and Sedimentary Geomorphology Features of the Old Red Sands in the Coastal Areas of Southeast Fujian, *the Taiwan Straits*, 17(1): 50~54.

The Verification of the Resonance Prediction Method for Great Earthquake Motion and its Prediction

Zheng Wenzhen(郑文振)
(*National Marine Data and Information Service, State Oceanic Administration, Tianjin China*)

Abstract More than 200 great (strong) earthquakes are examined in this thesis on the basis of the method for prediction of movement resonance of great earthquakes; and through the table of about 20 disastrous or representative earthquakes among them, it is proved that there is still room for breakthrough in the prediction of great (strong) earthquakes. At the end of 1996, I predicted that there would be a great earthquake with magnitude between 7.5 and 8.4 and a series of great earthquakes in Japan Trench in the following 1 or 2 years, and later this prediction was realized. Further study on this method resulted in the formula of epicentre prediction. Recently I also worked out that we can reduce the time of great earthquake prediction and epicentre prediction through the study of the early earthquakes with magnitude of $M \geqslant 4$. Written predictions on 7 earthquakes with magnitude of $M \geqslant 6$ between January, 1998 to September 10, 1998 are proved successful in varying degrees, which will solve the poser set by some authorities in international earthquake research field — 'Short-time earthquake prediction is impossible on the basis of contemporary scientific technology'.

Keywords Great earthquake; Earthquake prediction; Resonance prediction method

1. Introduction

The cause and occurrence of great earthquakes is always an international poser in natural science. Because of that, the prediction of great earthquakes is also a contemporary poser, which requires scientists to make great efforts. Through my 20 year's continuous analysis and study on the data of great (strong) earthquakes at home and abroad, I advanced a new theory on the cause and occurrence of great earthquakes in September 1996. From the movement during the seismic upsurges we can learn that the energy from the outerarea movement is the predominant energy source of great earthquakes. The resonance will occur when two or more than two great earthquake energy sources, whose speed has changed through the transmission of faults of the earth's crust, meet at approximately the same speed, and a great earthquake will take place at the meet point. The theory of the movement and resonance of great earthquakes provides new theoretical foundation for the new method of earthquake prediction, and it helps me work out the method for predict of movement resonance of great earthquakes (see Bibliography 1).

2. The Verification of the Method for Prediction of Movement Resonance of Great Earthquakes

From the catalogue of different countries' formal historical earthquake data which I have collected, we can see that attention was only give to disastrous great earthquakes and earthquakes in the ocean which caused tsunamis. We have fewer records of earthquakes in deserted areas or in the ocean, especially in the South Pole. THere is hardly any record of earhquakes to the south of 60° S. In fact there must have been great earthquakes near the South Pole in history. This can be proved by the great earthquake of magnitude 7 near the South Pole (62.9° S, 152.6° E) on March 25, 1998. In earthquake catalogues and earthquake diagrams in Cina and Japan, much attention is give to internal earthquakes, but those in neighbouring countries are lacking of enough attention. In fact, many of great earthquakes in Japan came from its neighbouring countries, and many in our country also came from our neighbouring countries or districts. Therefore in the study of great earthquake prediction, we should study not only internal great earthquake movements but also those in neighbouring countries and districts, even the law of great earthquake movement throughout the world.

Since earthquake study is not my major subject, I spend most of the time on oceanic study. My collection of earthquake data catalogue was not so complete before, and it became an obstacle in my earthquake study. Through these two years' work, I applied the method for prediction of movement resonance of great earthquakes to predict great earthquakes with the utilization of great earthquake data 10 to 20 years before then. More than 200 great earthquakes at home and abroad were verified, and the results were quite satisfactory, and they proved that breakthrough can be made in great earthquake prediction. Because of the limitation of the length, only a few disaastrous or representative great earthquakes are listed here in Table 1.

In 1996 I put forward that great earthquakes with magnitude $M \geqslant 7$ are caused by the resonance of 2 or more than 2 energy movements of great earthquakes. Through two years' study, I find that earthquakes with magnitude $M \geqslant 6$ are also caused by such resonance, and even some earthquakes with magnitude $M < 6$ result from it, too.

3. The Result of the Method for Prediction of Movement Resonance of Great Earthquakes

According to an article in USA *Times* on September 15, 1997: It Never Works. It took Japan 30 years to set up its earthquake prediction system, but it took just 20 seconds to destroy this system. On January 17, 1995, a great earthquake with magnitude of 7.2 attacked Kobe without any indications, which cost 6400 lives··· Professor Nanzhifu in the Earthquake Institute of Tokyo University said, 'It would be great if we can predict accutately a great earthquake, but Kobe Earthquake tells us that that is impossible.' The earthquake with magnitude of 7 on January 17, 1994 in Los Angeles, USA, which caused great damage, was also failed to be predicted. Old international authorities believe that great earthquakes in the world are mainly independent events, and this has done great harm to mankind. Even now, the poser of the cause and occurrence of great earthquakes is still not solved yet. The prediction of great earthquakes is far from being realized even though different countries spend at least millions of US

Table 1 The verification of some disastrous or representative great earthquakes

Actual condition of great earthquakes						Verification of the prediction	
Date	Epicentre			Magnitude (Dichter scale)	Damage degree or caualties	Difference in time (day)	Epicentre difference (km)
	Longitude (° N)	Latitude (° E)	Place				
1994.12.7	33.8	136.0	South sea of Japan	8		Several days	200
1996.3.8	37.4	114.9	Longyao, Hebei,China	6.8	About 10000 people	Several days	150
1996.3.13	24.1	122.6	Taiwan, China	7.8		Within a month	150
1996.3.22	37.5	115.1	Ningjin, Hebei,China	7.2	Serious	Several days	100
1970.1.5	24.0	102.7	Tonghai, Yunnan,China	7.7	Thousands of pe ople	Several days	150
1974.5.11	28.2	103.9	Yongshan,Yunnan,China	7.1	Serious	Within a month	370
1975.8.15	53.5	169.0	Aleutian, Islands	7.2		Within a month	370
1976.7.28	39.6	118.2	Tangshan, Hebei,China	7.8	240000 people	Severa; days	300
1976.8.17	4.1	125.1	Philippines	8.1	8000 people	10 days	50
1976.11.15	39.4	117.9	Ninghe, China	6.9	After shock of Tangshan Earthquake	Several days	50
1978.1.14	34.6	141.0	Southeast Tokyo, Japan	7.2	Serious	Several days	150
1992.8.19	42.1	73.9	Kirghiz	7.5		Within a month	100
1994.1.17	34.9	118.8	Los Angeles, America	7.0	Disastrous	Several days	220
1994.10.4	43.7	146.8	Hokkaido, Japan	7.9	Disastrous	Several days	220
1995.1.17	34.5	134.9	Kobe&Osuha, Japan	7.2	6430 people	Within 23 days	150
1996.2.3	27.2	100.3	Lijiang, Yunnan, China	7.0	309 people died, 700 wounded	Several days	200
1996.9.6	21.9	121.9	Yilan, Taiwan, China	7.1		Within 10 days	260
1997.2.28	30.0	68.3	Pakıstan	7.3		Within 25 days	200
1997.11.8	35.2	87.3	Mani Tibet, China	7.5		Within 18 days	280
1998.5.4	22.7	125.6	Ryukyu Islands	7 7		Within 17 days	340
1998 8 20	30.5	140.5	LBird Island, Japan	7.1		Within 18 days	250

Some epicentre different in this table are emended with the utilization of the latest data of earthquakes with magnitude M≥4 before these great earthquakes.

dollars blindly in this field. One school in USA, with Galley as the representative, believes that short-time earthquake prediction is impossible on the basis of contemporary scientific technology.

I think that we should stick to the right theory on the cause and occurence of great earthquakes and make deep study of earthquake data. Through the utilization of the theory on the cause and occurrence of great earthquakes, we need time to probe the earthquake law of our country and of the whole world, and make prediction and verification with this law. Through the practice of the verification of predictions, we should stick to the right and correct the wrong, and advance our knowledge. Gradually we will perfect our study to find the law in earthquake prediction, and breakthrough will be made to solve the poser of great earthquake prediction. On accordance with the theory ' practice is the only standard for the judgement of truth', here I list some of my predictions and their results in these two years.

3.1 The prediction and result of earthquakes in the Japan Trench

My paper *Study on the Genesis and Occurrence of Great Earthquakes and Their Prediction* was published in page 39 to 44 in the first issue of the 16th volume of *Ocean Journal* in February 1997. In that paper, I pointed out that great earthquakes in near future will mainly move to the Japan Trench (including an area from North Philippine in the south to Chijima Island in the north). I estimated that great earthquakes will take place within one and a half years; as for the accuracy of time (when will be M 7.5~8 earthquake, I know fairly well.), early in November 1997 I wrote to one colleague in Japan, ' A great earthquake will happen from November 11 to December 16th, 1997 in Japan or the far-east coastal area of Russia, which will probably be of magnitude M≥7.5' .

Later, a great earthquake with magnitude of 8 took place on December 5, 1997 in Russian Kamcatskij Sea waters; on December 6 and December 8 there respectively happened an earthquake with magnitude of 7. The prediction was made 36 days before the earthquakes happened, which was near short-time prediction. With the data of the earthquake with magnitude of M≥4 before December 5, it could be predicted that Russian Kamcatskij Sea Waters was the first earthquake area, and the time prediction would be limited within the several days around December 4.

Earthquakes with magnitude of 7.7 took place on May 4, 1998 in Yishigaki Sea near Okinawa. It was lucky that all these four earthquakes with magnitude of M≥4 happened in the sea and none of them caused seismic sea wave. And I don't think it is necessary to spend much time on the several earthquakes with magnitude of M≥6 and M≥5 during that period.

On May 15, 1998 I made another written prediction report to departments such as the State Oceanic Administration, in which I stated that Japan Trench was still at the upsurge period of great earthquakes. I wrote, 'There would be at least two earthquakes with magnitude of M≥6 (including one with manitude of 7.1~8) from then on to March 1999. One earthquake will be on the land in the coastal area, which will cause casualities in Japan. One most possible time of the first earthquake will be from now on to September, and the other will be between December and February, 1999. (I am now collecting and waiting for the data of earthquakes with magnitude of M≥4 from September to Novermber in China and Japan, and I hope that a prediction more accurate in time and place will be made later.).'

Later on May 31, 1998 an earthquake with magnitude of 6.1 happened in Sannliku Sea in Japan, and another took place on August 20, 1998 on the Bird Island 410 kilometres south to Kannto, Japan; on September 3 an earthquake with magnitude of M≥6 took place in Yiwateken County, Japan. (Because I

learned it from CCTV News, I was not quite sure about the exact magnitude and the date, but I was sure that it was on the land, for I saw the destroyed road on TV). The predictions of the Japan Trench were successful. (This can be proved by Mr. Xu Daoyi's letter from Japan on December 15, which affirmed the success of my prediction on December 5).

On May 8, 1999 an earthquake with magnitude of 8.5 happened in Russian Kamcatshij Sea, which was the greatest earthquake in the past ten years (noted by the writer on May 12). The predicted date is just 8 days away from May 8.

3.2 The prediction and result of earthquakes in north China

On November 7, 1997 I reported in written form to the State Earthquake Analysis and Prediction Center, 'There will probably be an earthquake with magnitude of $M \geqslant 6$ between November 11, 1997 and January 11, 1998 in north China. Possibly epicentre: (1) Within a circle with Chaoyang in Liaoning Province as the centre and with a radius of 200 kilometres,… or (2) Within a circle with Tumotezuoqi in Inner-Mongolia as the centre and with a radius of 200 kilometres;…'

Later is January 10, 1998 there was an earthquake in Shangyi, Zhangbei in Hebei Province; 47 people died and 2000 were wounded, …

Zhangbei is about 200 kilometres from Tumotezuoqi, Inner-Mongolia. Both the time and the magnitude of the earthquake conformed to the prediction, therefore the prediction was successful.

On April 30, 1998 I reported in written form to the State Oceanic Administration and the State Earthquake Bureau, 'There will possibly be earthquakes with magnitude 5.7~6.7 between May to August 31, 1998 in north China … or (2) Within a circle with Qingshuihe as the centre and with radius of 200 kilometres …'

Later three earthquakes with magnitude of $M \geqslant 3$ took place in Fengtai, Beijing from May 31 to June 1, 1998; on June 2 one with magnitude ML=5.7 happened in Zhangbei; on July 11, 1998 one with magnitude 5 happened in Yongji, Shanxi Province; on July 27 three continuous earthquakes with magnitude 4~5 took place in Zhangbei. According to ML Magnitude the magnitude 5.7 just reached the prescribed minimum of the prediction, and it would be a little higher than the minimum with the addition of several earthquakes with magnitude 4~5 in this period. If we apply to the magnitude MS=5.4, it would be even lower than the prescribed minimum. Qingshuihe in prediction (2) is about 200 kilometres away from Zhangbei.

3.3 The prediction and result of earthquakes from the edge of Xinjiang to the Caspian Sea

On April 30, 1998 I reported in written form to the State Earthquake Bureau, 'Great earthquakes with magnitude 7~8 may happen from now on to August from the edge of Xinjiang to the Caspian Sea. The magnitude will be lower if earthquakes happen in Xinjiang in our country. Possible epicentres are: (1) Within a circle with 41° N, 74.7° E as the centre and with a radius of 300 kilometres; or (2) Within a circle with 35° N, 50° E in Iran (or near 30.6° N, 57.8° E in the area where an earthquake with magnitude of 7.5 happened on March 15, 1998; or (3) Near Afghanistan and Pakistan.

Result: An earthquake with magnitude 6.2 happened on May 29, 1998 in Pishan (37.5° N, 79.2° E), Xinjiang in our country; on May 30, 1998 one with magnitude 7.1 happened in Afghanistan (35.7° N, 70.5° E), in which 3000 people died; on July 9, 1998 one with magnitude of 5.9 happened in Iran (37° N, 49° E); on July 28, 1998 one with magnitude 5.5 happened in Baicheng (41.5° N, 81.6° E),

Xinjiang; on August 2, 1998 one with magnitude 6.0 happened in Jiashi (39.6° N, 77.5° E), Xinjiang; on August 27 one with magnitude 6.6 happened in Jiashi (39.6° N, 77.9° E), Xinjiang. Earthquakes with magnitude 6 and 6.6 in August, 1998 in Jiashi were all within the 300 kilometres around the 41° N, 74.7° E in epicentre prediction (1), therefore the prediction was successful. If we make corrections with the latest data of earthquakes with magnitude $M \geqslant 4$, the difference in epicentre prediction will be reduced to within 200 kilometres, and the time will be limited within August.

3.4 Three successful epicentre and time prediction of earthquakes with magnitude $M \geqslant 6$ in Southwest Tibet

On April 30, 1998 I reported in written form to the State Earthquake Bureau, 'Earthquakes with magnitude 6.1~7.1 will take place from now on to September in Tibet or South Asia. Possible epicentre in Tibet is: (1) Within a circle with 30° N, 87.3° E as the centre and with a radius of 300 kilometres; …'

Result: On July 20, 1998 an earthquake with magnitude 6.1 happened in Xietongmen (29.8° N, 87.7° E), Tibet; on August 25 one with magnitude 6.0 happened in Shenzha (30.4° N, 88.5° E), Tibet; on September 4, 1998 one with magnitude 6.2 happened in Dingri (28.5° N, 87.6° E).

The great American writer Mark Twain (1835~1910) have said, 'if you ask me when the great earthquake will take place, I can answer without hesitation that I do not know.' I used to think that epicentre prediction (of course combined with time prediction) was the most difficult problem for me. After further study in the method for prediction of movement resonance of great earthquakes, I have worked out the formula of epicentre prediction of great earthquakes, recently I also worked out the more accurate prediction of time and epicentre of great earthquakes with the utilization of data of earthquakes with magnitude $M \geqslant 4$ before them. Calculation according to the formula resulted in the prediction that there would be at least two earthquakes with magnitude 6.1~7.1 between May and September, 1998 in 30° N, 87.3° E in Tibet. And later the earthquake with magnitude 6.1 on July 20 in Xietongmen (29.8° N, 87.7° E) was less than 50 kilometres from the predicted epicentre (30° N, 87.3° E). This is a successful example in epicentre prediction, which is really hard to achieve. Early in April a person of the same trade in Geology Research Bureau asked whether there was any tendency of great earthquake at that time. I answered that earthquakes with magnitude 6.1~7.1 will happen between the middle of August and the beginning of September, and that the epicentre will possibly be within the circle with 30° N, 87.3° E in Tibet as the centre and with a radius of 300 kilometres. And later an earthquake with magnitude of 6.0 happened on August 25, 1998 in Shenzha, Tibet and one with magnitude of 6.2 happened on September 4 in Dingri, both of which were less than 200 kilometres away from the predicted epicentre. In his letter in October, 1998, he said, 'The prediction was quite successful, especially on the epicentre.' This prediction can be regarded as the beginning of the breakthrough of the poser set by some authorities in international earthquake research field— 'Short-term earthquake prediction is impossible on the basis of contemporary scientific technology.'

3. Conclusion

From the written prediction report with the appliance of the method for prediction of movement resonance of great earthquakes, we can see that:

(1) As for the prediction that future upsurge of great earthquake will take place at the end of 1996 in the Japan Trench, five great earthquakes with magitude M≥7 took place in the Japan Trench in these two years, which proved that this prediction was right. It was lucky that all these great earthquakes happened in the ocean and none of them caused seismic sea wave.

(2) Preliminary formula for the calculation of the position of epicentre

All the epicentre differences in the verification of the 20-odd great earthquakes in Table 1 result from the formula, and some are corrected with the latest data of earthquakes with magnitude M≥6 in Tibet were very successful, which was a great progress in new prediction method.

(3) No earthquakes with magnitude M≥7 have happened in the mainland in our country since January, 1998 to now (September 10 1998). All the eight (one exception was the earthquake with magnitude 6.0 on March 19 in Atushi, Xinjiang, for at that time my study of earthquakes in Xinjiang has not started yet) destructive earthquakes are: one with magnitude of 6.2 in Zhangbei, one with magnitude of 6.2 in Pishan, two with magnitude of M≥6 in Jiashi and three with magnitude M≥6 in Tibet. This method has made written and successful (in various degrees) preedictions of these earthquakes. Some predictions are near the short-time prediction. (According to the standard set by the State Earthquake Bureau, short-time earthquake prediction refers to the prediction of earthquakes in certain place within one or two months).

Edmund Halley (1656~1742) predicted that the comet (Halley Comet) will appear again at the end of 1758 or in 1759, and later in May, 1759 the Comet reappeared, which was an amazing achievement in astronomy history. In 1996 the author made successful prediction on one of the greatest earthquakes in these years — the earthquake with magnitude of 8 on December 5, 1997 in Russian Kamcatskij Sea waters. What Halley predicted was the comet in the air, and the author's prediction of great earthquakes is more complicated than that. Halley's predicted time was at the end of 1758 or in 1759, and that of this great earthquake prediction was 36 days. Halley opened a new area in Comet study, and this success in prediction of great earthquake with magnitude 8 will the same significant as his achievement.

Bibliographies

1. Zheng Wenzhen, Study on the Genesis and Occurrence of Great Earthquakes and Their Prediction,*The Oceanic Journal*, 1997,16(1) P39~44

2. State Earthquake Bureau, Brief Catalogue of the World's Great Earthquakes 1904~1972 (magnitude M≥7),1976. 2

3. State Earthquake Bureau, Brief Catalogue of China's Earthquakes, Earthquake Publishing House, 1977

A Three-dimensional Forecasting Model for Oil Spill

Sun Yinglan(孙英兰) Wang Lixia(王丽霞) Sun Changqing(孙长庆)
(*College of Environmental and Physical Oceanography, Ocean University of Qingdao, 266003*)

Abstract A 3-D forecasting model for oil-spill is developed using the finite difference method to numerically solve the shallow water equation. The instantaneous flow distribution in the studied area is calculated and the trajectory of the oil-slick centroid is predicted by means of Lagrange's method. The computed results agree with the observed data well, this shows that this 3-D forecasting model has high accuracy.

KeyWords 3-D model; oil - spill; forecasting model; Lagrange method; finite difference

1 Introduction

Studies of the processes and principles of the spread and drift of oil-slick on the sea[1,2] have been done by a number of researchers in China and the methods employed by them are mainly full-dynamic numerical model[2] and Fays method[3,4]. The drift velocity of the oil-slick is determined with the empirical formulation as follows:

$$\vec{v}_0 = \vec{v} + k\vec{v}_w$$

where $\vec{v}_0$ is drift velocity of the oil-slick centroid; $\vec{v}$ is the sea water velocity; $\vec{v}_w$ is the wind velocity; k i s an empirical constant (i. e the wind factor, with a domain of 0.02~0.05). As for the parameterization of $\vec{v}$, it is obvious that the surface water velocity should be used as a substitute for it. Thus the current field in the sea area must be computed with 3-D model, not a 2-D one.

At present, there are quite a few numerical methods available for solving the 3-D hydrodynamics equations, among them the 3-D various layers model[5,6] used in this paper, the current resolution model[7,8] and the vertical spectoanalysis model[9,10] are relatively popular.

2 The physical model

2.1 The 3-D equations for tidal wave motion and solution conditions

This physical model, taking into consideration of the heat and salt effects and the spacial variation of density, uses a subgrid scale (SGS) energy of the small scale turbulence, which is undistinguishable to the model grid and includes the energy and momentum exchange among the subgrids.

Choosing right-hand coordinate system in the "f-plane", letting Plane XOY coincides with the average sea level with a axis x, positive eastward, a axis y northward, and a axis z upward The governing equations of motion are as follows:

$$\frac{\partial u}{\partial t}+\frac{\partial (uu)}{\partial x}+\frac{\partial (uv)}{\partial y}+\frac{\partial (uw)}{\partial z}-fv+\frac{1}{\rho}\frac{\partial p}{\partial x}-\frac{1}{\rho}\nabla\cdot\vec{\tau}_x=0 \qquad (1)$$

$$\frac{\partial v}{\partial t}+\frac{\partial (uv)}{\partial x}+\frac{\partial (vv)}{\partial y}+\frac{\partial (vw)}{\partial z}+fu+\frac{1}{\rho}\frac{\partial p}{\partial x}-\frac{1}{\rho}\nabla\cdot\vec{\tau}_y=0 \qquad (2)$$

$$\frac{\partial P}{\partial z}+(\rho-\rho')g=0 \qquad (3)$$

The continuity equation:

$$\Delta\cdot\vec{v}=0 \qquad (4)$$

The balance equations for salt and heat:

$$\frac{\partial S}{\partial t}+\nabla\cdot(\vec{v}S)-\frac{\partial}{\partial x}(D_x\frac{\partial S}{\partial x})-\frac{\partial}{\partial y}(D_y\frac{\partial S}{\partial y})-\frac{\partial}{\partial z}(E_m\frac{\partial S}{\partial z})=0 \qquad (5)$$

$$\frac{\partial T}{\partial t}+\nabla\cdot(\vec{v}T)-\frac{\partial}{\partial x}(D_x\frac{\partial T}{\partial x})-\frac{\partial}{\partial y}(D_y\frac{\partial T}{\partial y})-\frac{\partial}{\partial z}(E_m\frac{\partial T}{\partial z})=0 \qquad (6)$$

The equation of subgridscale energy density:

$$\frac{\partial e}{\partial t}+\nabla\cdot(\vec{v}e)-\frac{\partial}{\partial x}(D_x\frac{\partial e}{\partial x})-\frac{\partial}{\partial y}(D_y\frac{\partial e}{\partial y})-\frac{\partial}{\partial z}(E_e\frac{\partial e}{\partial z})+D_e-S_e=0 \qquad (7)$$

State equation:

$$\rho=\frac{5890+38T-0.375T^2+3S}{(1779.5+11.25T-0.0745T^2)-(3.8+0.01T)S+0.698(5890+38T-0.375T^2+3S)} \qquad (8)$$

where u, v, w are the current velocity components in x , y and z directions, respectively; $\vec{v}$ is the current velocity vector, $\vec{v}=\vec{i}u+\vec{j}v+\vec{k}w$; f is the Coriolis parameter; t is the time; p is the pressure; S is the Salinity;T is the temperature; ρ is the density;e is SGS subgridscale energy density; E_m is the vertical diffusion coefficient of mass; E_e is the vertical diffusion coefficient of energy; $\vec{\tau}_x,\vec{\tau}_y$ are the components of the stress vectors; D_x, D_y are the horizontal diffusion coefficients for heat and mass; D_e is the dissipation of subgridscale energy; S_e is the source of subgridscale energy; $\nabla=\vec{i}\frac{\partial}{\partial x}+\vec{j}\frac{\partial}{\partial x}+\vec{k}\frac{\partial}{\partial z}$, the gradient vector;

At the surface, $z=\zeta$

$$\omega=\frac{\partial\zeta}{\partial t}+u\frac{\partial\zeta}{\partial x}+v\frac{\partial\zeta}{\partial y} \qquad (9)$$

$$p=p_a,(\tau_{xz},\tau_{yz})=(\tau_x^s,\tau_y^s) \qquad (10)$$

At the bottom, $z=-h$

$$\omega + u\frac{\partial h}{\partial x} + v\frac{\partial h}{\partial y} = 0 \tag{11}$$

$$(\tau_{xz}, \tau_{yz}) = (\tau_x^b, \tau_y^b) \tag{12}$$

in which, ζ is the water elevation calculated from the static level; h is water depth from the static level; P_a is atmospheric pressure; $\vec{\tau}^b = \vec{i} \cdot \tau_x^b + \vec{j} \cdot \tau_y^b$, friction stress at the bottom; $\vec{\tau}^s = \vec{i} \cdot \tau_x^s + \vec{j} \cdot \tau_y^s$, the wind stress at the surface.

The initial conditions:

$$t = 0, u = v = w = \zeta = 0 \tag{13}$$

The land boundary condition:

$$v_n = 0 \tag{14}$$

The open boundary condition:

$$\zeta = \zeta^* \tag{15}$$

2.2 Trajectory equation for the oil-slick centroid

As mentioned above, the velocity vector of the oil-slick centroid is:

$$\vec{v}_0 = \vec{v} + k\vec{v}_w \tag{16}$$

Let the initial position vector of the oil-slick centroid be $\vec{S}_0$, and the new position vector Δt time later be $\vec{S}$. Hence:

$$\vec{S} = \vec{S}_0 + \int_{t_0}^{t_0+\Delta t} \vec{v}_0 dt \tag{17}$$

3 The difference equation and the determination of the exchange coefficients

For the finite difference equation see references[5,6].

3.1 Computation of the oil-slick centroid track

In accordance with expression (17), Δt can be divided into n time steps. Note as: $0 < t_1 < t_2 < \cdots < t_n = \Delta t$. Hence, the new position vector at time t_i is

$$\vec{S}_i = \vec{S}_{i-1} + \int_{t_0+t_{i-1}}^{t_0+t_i} \vec{v}_{0(i-1)} dt \qquad (i = 1,2,\cdots,n) \tag{18}$$

If $\vec{S}_{i-1}$ are not at the gird points, the velocity vector $\vec{v}_{0(i-1)}$ will be determinated with interpolate on from the four grid points, immediately adjacent to $\vec{S}_{i-1}$. If one of the points is a land point, the velocity vector will be $\vec{O}$.

3.2 The determination of exchange coefficients and other parameters

3.2.1 Vertical exchange coefficient for momentum

$$E = \rho L\sqrt{e}\exp(m\frac{g}{\rho}\cdot\frac{\partial\rho}{\partial z}/e\cdot L^2) \tag{19}$$

3.2.2 Vertical exchange coefficient for mass

$$E_m = \alpha_4 L\cdot\sqrt{e}\cdot\exp(r\frac{g}{\rho}\cdot\frac{\partial\rho}{\partial z}/e\cdot L^2) \tag{20}$$

3.2.3 Vertical exchange coefficient for energy:

$$E_e = \alpha_1\cdot L\cdot\sqrt{e}\cdot\exp(m\frac{g}{\rho}\cdot\frac{\partial\rho}{\partial z}/e\cdot L^2) \tag{21}$$

3.2.4 Horizontal exchange coefficient for mass, momentum and energy

$$A = r\left|\frac{\partial\omega}{\partial x}+\frac{\partial\omega}{\partial y}\right|(\Delta l)^3 \tag{22}$$

$$\Delta l = \sqrt{\Delta x^2+\Delta y^2}$$

3.2.5 Generation of the SGS energy

at the bottom layer:

$$S_e = g\cdot\sqrt{u^2+v^2}/C^2 \tag{23}$$

at the middle layer:

$$S_e = \alpha_3\cdot L\cdot\sqrt{e}\cdot\left[(\frac{\partial u}{\partial z})^2+(\frac{\partial v}{\partial y})^2\right] \tag{24}$$

at the surface layer:

$$S_e = L\cdot\sqrt{e_0}\cdot\left[(\frac{\partial u}{\partial z})^2+(\frac{\partial v}{\partial y})^2\right] \tag{25}$$

3.2.6 Dissipation item of SGS energy

$$D_e = \frac{a_2\cdot e^{\frac{3}{2}}}{L} \tag{26}$$

In the above formulae, a_1, a_2, a_3, a_4, m, r are constants; r' is an empirical coefficient; ω, the vorticity; e_0, wind velocity function; $L=\nu'\cdot z(1-z/d)^{1/2}$, in which, ν' is Von Karman Constant, z is the vertical distance from the bottom to the calculation point, d is the vertical distance from the bottom to the surface of the sea.

4 Case study

For the application of the above-mentioned physical model and difference method, the shallow-sea and tidal-flat area (Oil Exploration Development Zone of the Shengli Oil Field) is chosen as the sea area for the computation.

4.1 The computation domain and the arrangement of the computation grids

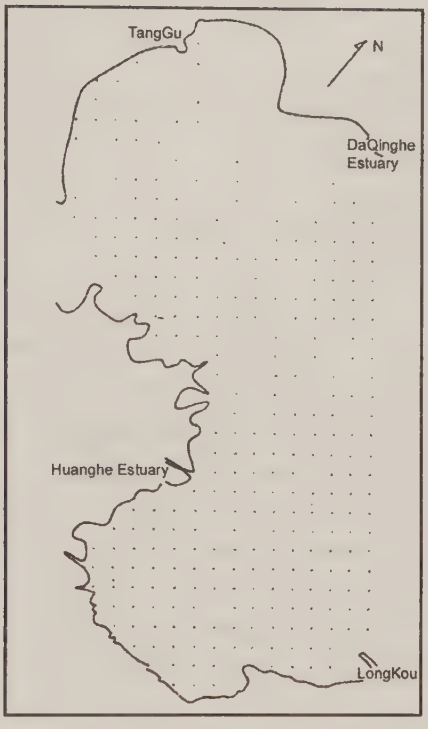

Fig. 1 Distribution of computation grids

The computation domain is the sea area west of the line between Longkou and the estuary of the Daqing River (see Fig.1). The grid spacings are as follows, $\Delta x = \Delta y =$ 8km; the thickness of the three vertically divided water layers from surface to bottom are 4m, 5m, and the remaining water depth, respectively.

The other parameters are as follows:a_1=0.8, a_2=a_3=0.08, a_4= 0.1,m_1=0.4, m_2= r = 0.8;s=30.5, T=19.5 ℃(S and T are the defined constants in the computation domain due to without temperature-salinity field data); the time step Δt= 124 Sec.

4.2 Determination of the elevation at the boundary

Because a precise forecast of practical significant of the moving path of the oil-slick centroid and its shore-reaching time is of to the environmental protection and aquaculture, it is very important to determinate precisely the forced water elevation at the boundary.

If only the water elevation of the average tide M_2 were given as the forced water elevation at the boundary, the accuracy of the result would fail to meet the precise requirement. Therefore we use the combination of the boundary water elevations of the six component tides: M_2, S_2, O_1, K_1, M_4, MS_4, as the forcing at the boundary, i.e.:

$$\zeta(t) = \sum_{c=1}^{6} D_c H_c \cos(\sigma_c t + d_c - g_c) \tag{27}$$

where D_c, d_c(c =1,⋯ ⋯6) represent the astronomical harmonic constants of each component tide,

respectively; H_c, g_c, σ_c(c=1,⋯ ⋯ 6) are the amplitude, tidal epoch and circular frequency of each component tide, respectively.

4.3 Preset of the wind field

The wind velocity and wind direction in the sea area should be revised according to the data forecasted by the local weather authority.

4.4 The computation results and the analysis of them

4.4.1 The forecasted instantaneous current field

According to the expression (27) given above, it can be seen that the calculated current is an instantaneous current field. Fig.2～Fig. 6 illustrate the surface flow field obtained by inputting the data of the instantaneous boundary water elevation on Mar.31, 1991. Fig.2 shows that most of the computed area is in ebb tide except for the part near the coast of Longkou, where is in flood tide. Fig.3 shows that the computed area is in flood tide, with the area inside the Bohai Bay being a strong current district, the area off the estuary of Xiaoqing river being a week current district. In Fig.4 the computed area is still in flood tide except the area off the estuary of Xiaoqing river, with the strong current area in the Bohai Bay while the week current district off the Xiaoqing River mouth. In Fig.5 most of the sea area is in flood tide, Fig.6 illustrates a flow distribution almost in reverse to that in Fig.3.

The computed results show that when six component tides are used to forecast the instantaneous flow field of the computed area on March, 31,1991 the current flow distributions show the feature of the anomalous semidiurnal tide and rather like the feature of the semi-diurnal tide. It also shows that the sea area off the estuary of Xiaoging River is a weak current district.

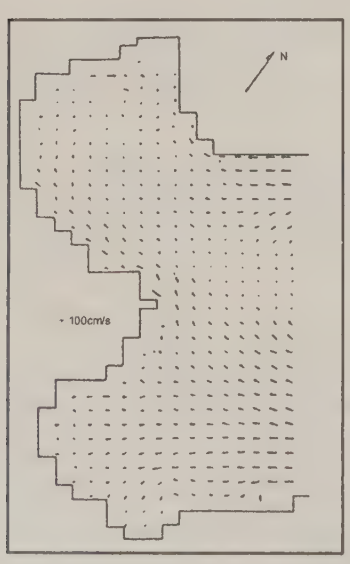

Fig. 2 Surface layer tidal current field at 11 hr. on March 31,1991

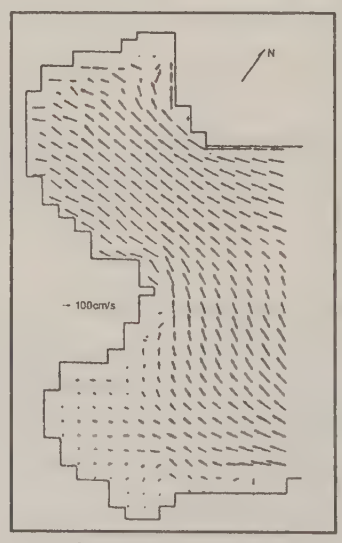

Fig. 3 Surface layer tidal current field at 13 hr. on March 31,1991

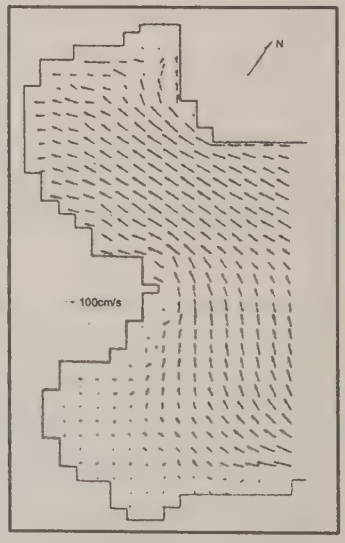

Fig. 4 Surface layer tidal current field at 15 hr. on March 31,1991

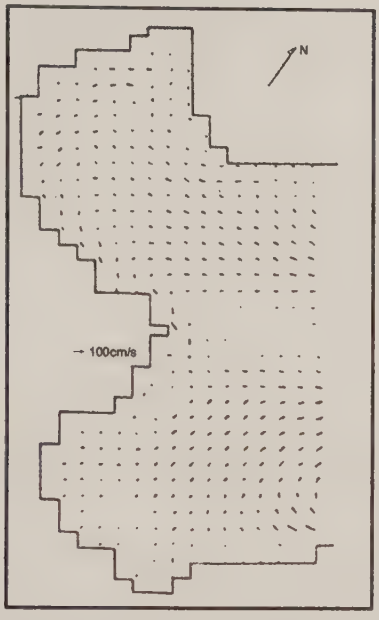

Fig. 5 Surface layer tidal current field at 17 hr. on March 31,1991

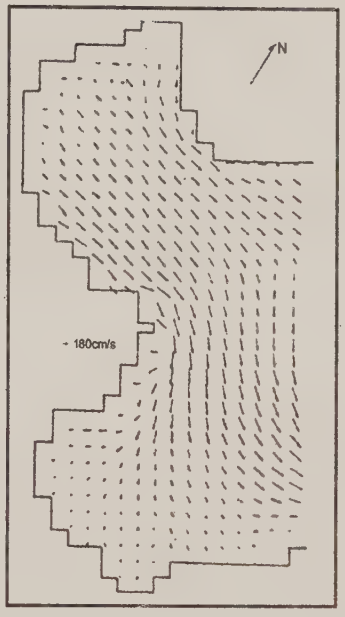

Fig. 6 Surface layer tidal current field at 19 hr. on March 31,1991

4.4.2 The forecast of the track of the oil-slick centroid

An oil-dropping experiment on the site was made on Mar 31,1991 by drooping 400kg oil onto the sea to test the accuracy of the numerical simulation. The solid curve in Fig.7 is the trajectory of main oil-slick measured by GPS meter and the accuracy reaches the scale of the meter.

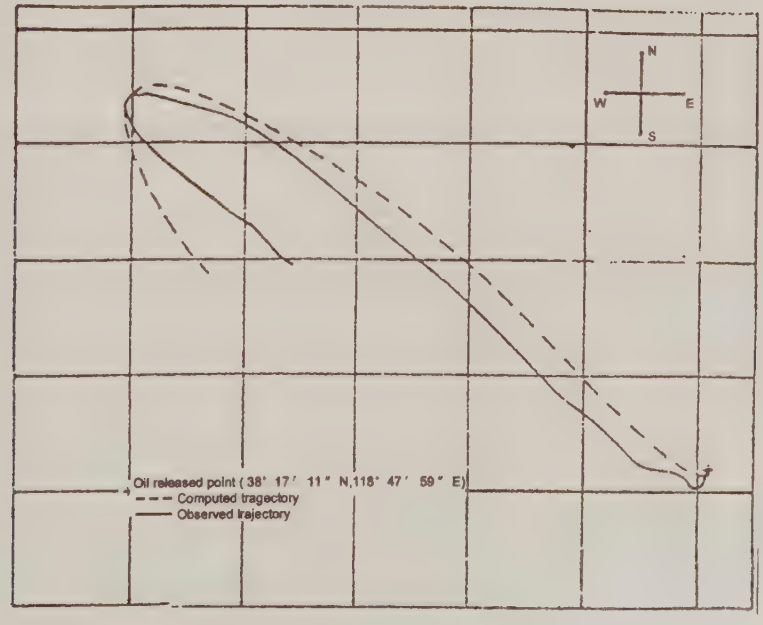

Fig. 7 The movement trajectories of oil slick center

Using the instantaneous flow distribution and the forecasted wind distribution, we have calculated the velocity vector of the oil-slick centroid (wind factor is 0.0235) with (16) and the moving track of the centroid with (17). In Fig.7 the dashed curve (note: the grid spacing is 2km) is the computed moving track. The figures show that the maximum error between the computed results and the observed data is about 1.54km, the mean error is about 0.54km; and the shifting position of the oil-slick centroid agree swell with the measured one. It proves that the 3-D numerical forecasting model for the trajectory of the centroid of the oil-slick is of fairly high accuracy. By analogy this model can be used to forecast the moving trajectory of the oil-slick centroid over a long time.

Reference

1. Zhang Yongliang et al. The Mathematical Model for Oil Spills Pollution and Its Application Research. Environmental Science Research,1991, 4(30:7-17.

2. Yuan Yeli et al. A Full Dynamical Numerical Model for Oil Slicks Motion. Numerical Computation in Physical Oceanography, edited by Feng Shize, Sun Wenxin. Henan Science and Technology Press, 1992:429-473.

3. Fay, J. A., The Spread of Oil Slicks on a Calm Sea. Oil on the Sea, Plenum Press, New York, 1969, PP53-63.

4. Murray, S. P., The Effects of Weather Systems, Currents, and Coastal Processes on Major Oil Spills at Sea. Pollutant Transfer and Transport in the Sea, Volume II, PP169-227.

5. Leendertse, J.J., Liu, S. K., A Three-dimensional Model for Estuaries and Coastal Seas. Volume I , Principles of Computation, R-1417-Owrr. Rand Corp., Santa Monica, California, 1973, PP1-58.

6. Sun Yinglan et al. The numerical Simulation to the 3-D Baroclinic Field of Coastal Seas. I. The Numerical Computation for Tidal Current in the Bohai Sea. College Journal of Qingdao Ocean University, 1990, 20(3):11-24.

7. Tang Yongmin et al. The Current Resolution Method for the 3-D Shallow-sea hydrodynamical model. Journal of Ocean, 1990,12(2);149.

8. Sun Wenxin et al. A numerical Solution in 3-D Shallow-sea Hydrodynamics-Current Resolution Method. Numerical Computation in Physical Oceanography, edited by Feng Shize, Sun Wenxin, Henan Science and Technology Publishing House, 1992: 100-195.

9. Heaps, N. S., On the Numerical Solution of the 3-D Hydrodynamical Equations for Tides and Storm Surges. Mem., Soc. R. Sci. Liege, 6.2, 1971, PP144-180.

10. Zheng lianyuan. The numerical Computation for the 3-D (潮致) Lagrangian Residual Current and Its Application in the Bohai Sea. Journal of Ocean University of Qingdao,1992,22(1):39-49.

11. Wang Hui et al. The numerical Computation for the 3-D Pollutant Transport Locus in the Bohai Sea. Journal of Ocean University of Qingdao.

Distribution and Sources of Polycyclic Aromatic Hydrocarbons (PAHs) in the Surface Seawater of the Western Xiamen Harbor

Liu Yan(刘岩) Zhang Zulin(张祖麟) Hong Huasheng(洪华生)
(Research Lab of Marine Ecological Environment, Ministry of Education, Xiamen 361005
Environmental Science Research Centre of Xiamen University, Xiamen 361005)

Abstract The concentration of PAHs in the surface seawater of the western Xiamen Harbor has been analysed in the paper. The PAHs concnetration at 9 station locations varies greatly within the range of 106.1ng/L ~ 4365ng/L. But PAHs pollution is slight as compared with that in similar areas in other parts of the world. PAHs stem mainly from oil pollution, urban and industrial discharges, and combustion of fuels.

Keywords PAHs; surface seawaters; western Xiamen Harbor; distribution

PAHs is a universally existent important matter polluting the environment and is strongly carcinogenic, thus arousing the attention of more and more people. It has been listed as a priority pollutant by the EPA of the United States and it exists mainly in coal, petroleum and all kinds of natural fuels. The PAHs pollution in the marine environment is mainly resulted from human activities, such as leakage of oil wells, maritime transportation, petroleum shipping, urban surface water runoff, and discharge of industrial waste water as well as sedimentation with atmospheric particles of the waste gas after implete combustion, which may carry PAHs into the marine environment. In recent years, many scholars at home and abroad have analysed and studied the distribution and sources of PAHs in the marine sediments, but the PAHs in the marine surface water body has rarely been studied systematically. This paper makes an investigation and study of the PAHs in the surface seawater of the western Xiamen Harbor and analysis its concentration and sources of pollution.

1 Sampling and Methods of Analysis

1.1 Description of sampling

The sampling was done on Jul. 20, 1998 in the sea area of the western Xiamen Harbor (see Fig.1). Nine stations were deployed in the area, among which the station No.9801 was located at the bay far away from the coast, the stations Nos.9802, 9803 and 9804 were in the harbor near the coast; Nos.9807 and 9808 in the bay of the harbor, Nos.9809 and 9804 in the main channel, and Nos.9810 and 9811 at the estuary. The sampling depth is 1m.

1.2 Analysis of water samples

Sample 1L of water with a sampler and filter it with the 0.7 μ m glass-fiber filter membrane to obtain part of the solution, and add into it 10 μ L PAHs—three kinds of MIX internal standards (50 μ g/mL). Pass the sample through the SPE mini-column (Supelclean TMENVITM-183mL) and eluate it with 3mL

of ethyl acetate; Condense N_2 to 100 μ L and put it into the sample; Detect and analysis PAHs by GC-FID.

1.3 Determination procedures of GC-FID

Instrument setting parameters: HP5890E gas chromatograph; chromatographic column: 50m 0. 22mm0.25 μ m, BPX-5 capillary column; initial temperature: 60℃ (stablizing for 2 min), sample inlet A temperature: 280℃, detector A temperature: 360℃; programmed temperature: 60℃~120℃, 10℃/min, 120 ℃ ~325 ℃ , 3 ℃ /min, constant temperature 5min; carrier gas: high-purity nitrogen, constant current volume by using the electron pressure controller (EPC): 483mL/min; sample feed column: non-distributary sample feed of the HP7673 automatic sample feeder: 1 μ L; operating time: 81.33min; data acquisition and processing using HP3365 chemical work station.

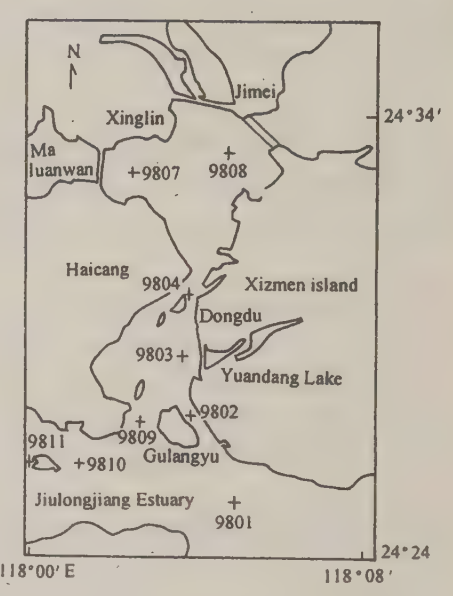

Fig.1 Diagram of sampling locations in the western Xiamen Harbor

2 Results and Discussion

2.1 Results

The analytical results of PAHs in the seawater of the western Xiamen Harbor are listed in Table 1 and Figs.2 and 3. For the convenience of analysis and comparison, the contents of DOC and POC in the seawater are tested and analysed, the results of which are listed in Table 2.

Table 1 Contents of various components of PAHs in the surface seawater of the western Xiamen harbor (ng/L)

station	Can	Flu	Phe	An	Fluo	Py	B[a]A	Chry	B[b]F	Dba	∑PAHs
9801	Nd	Nd	62.1	Nd	Nd	Nd	Nd	37.7	Nd	30	129.8
9802	Nd	8.2	64.2	Nd	Nd	Nd	174	Nd	61.5	108	415.8
9803	Nd	Nd	484	461	Nd	3420.6	Nd	Nd	Nd	Nd	4356.6
9804	Nd	12	58.7	31	71	56.4	Nd	Nd	Nd	150	379.2
9807	Nd	11	30.7	Nd	5.4	10.3	30	Nd	37.4	62.6	187.9
9808	127	16	20	13	24	11.5	Nd	Nd	Nd	79.4	291.9
9809	18	6.6	36.9	14	19	11.6	Nd	Nd	Nd	Nd	106.1
9810	Nd	Nd	35.4	21	Nd	481	Nd	Nd	Nd	Nd	538.2
9811	Nd	4.7	Nd	Nd	22	72.9	Nd	Nd	Nd	39.4	139.4

Note: Nd—not detected, None of Na, Ace, B[k]F, B[a]P, Ind, BgP have been detected.

2.2 Discussion

2.2.1 Total volume distributional features

It can be seen from Table 1 that the pollution levels of PAHs differ in various station sites in the western Xiamen harbour and the total PAHs values at 9 station sites vary from 106.1ng/L to 4365.6ng/L, among which the pollution level is higher in the stations Nos.9802, 9803 and 9804 which are close to the urban district, the content of ∑ PAHs is highest in the station No.9803, reaching 4365.6ng/L and successively decreases towards the two sides (9802, 9804) by a large margin (415.8ng/L~4365.6ng/L~379.2ng/L). Situated right at the waste water outlet of the Yuandang Lake, the content of PAHs in the station No.9803 is much affected by the discharge of land industrial waste water and urban domestic sewage. As the seawater in the harbor does not flow smoothly, the waste water from the outlet of the Yuandang Lake is discharged slowly to the either side and the stations Nos.9802, 9803 and 9804 differ greatly in the level of PAHs pollution. Comparatively speaking, the station No.9801 which is far away from the coast is significantly subjected to the effect of open sea water, so the content of ∑PAHs is lower (129.8ng/L). At the station No.9810 situated in the estuary, there are motorized vessels engaged in harvesting operations all the year round and there is waste water discharged from the land in the upstream, so the content of ∑PAHs is higher (538.2ng/L). The content of ∑PAHs is the lowest at the station No. 9809 lying in the main channel, the cause of which awaits further investigation. The stations Nos. 9807 and 9808 are situated in the inner bay, where the content of ∑PAHs is lower, 187.9ng/L and 291.9ng/L respectively, the cause of which awaits further investigation.

Table 2 Contents of ∑PAHs(ng/L), DOC, POC(mg/L) in the surface seawater of the western Xiamen harbor

Station	9801	9802	9803	9804	9807	9808	9809	9810	9811	Total
∑PAHs	129.8	415.8	4365.5	379.2	187.9	291.9	106.4	538.2	139.4	6554.2
DOC	2.15	1.96	1.318	1.638	3.231	2.271	1.697	0.641	1.969	16.88
POC	0.715	0.617	0.626	0.507	0.582	0.614	0.554	0.452	0.896	5.565

2.2.2 Structural distribution of PAHs and analysis of its sources

It can be seen from Table 1 that among the sixteen PAHs separated and identified from the surface water of the western Xiamen harbor, Na, Ace, B[k]F, B[a]P, Ind and BgP have not been detected and the rest 9 PAHs of different kinds are detected in different samples; The contents of phenanthrene (Phe) and pyrene are the highest, in which the content of Phe mainly ranges from 30ng/L to 60ng/L, the highest being at the station No.9803 (484ng/L); The content of pyrene is most uneven, ranging from none to 3420.6ng/L, and the distribution at each station site is identical with that of the total PAHs. Then come An, Fluo and Dba, among which An ranges from none to 461ng/L, Fluo from none to 71ng/L and Dba from none to 108ng/L. The contents of all others are very low.

With respect to the sources of PAHs pollutants, various scholars have made appropriate researches. Lee et al. (1977) determined the PAHs in the air-borne dust in the cities and defined the total PAHs combustion product (COMB) as the sum of the contents of 9 individual compounds: Fluo, Ba, Py, B[k]F, B[a]P, B[e]P, Ind, BP, Chry[1]. See Table 4 for COMB at various stations in the surface water of the western Xiamen harbor. The sources of PAHs in the surface water of the western Xiamen harbor may be analysed on the basis of the value of ratio of ∑COMB/∑PAHs. The values of ratio of ∑COMB/∑PAHs at the stations Nos.9803, 9810 and 9811 are all larger than 50%, so PAHs mainly originate from COMB.

The proportionality of ∑COMB/∑PAHs at the station No.9804 is 33.6%, which just close to the main channel of sea transportation and the sewage discharge outlet on land, so the PAHs is the result of combined action of oil pollution and COMB. The values of ratio of ∑COMB/∑PAHs at the rest stations are all below 30%, so the main source of PAHs is offshore oil pollution.

2.2.3 Relationship between PAHs and biological action in the surface water of the western Xiamen harbor

It can be seen from Table 2 and Fig.2 that PAHs has a good negative correlation with DOC and POC in the surface water of the western Xiamen harbor. At the station No.9803, the ∑PAHs value is highest and the contents of DOC and POC, especially that of DOC is lowest while at the station No.9807 the value of ∑PAHs is very low, but the contents of DOC and POC, especially that of DOC is highest. The stations Nos.9807 and 9808 are located in the cultivation zone and it may be inferred that the organisms in the water play some role in adsorbing and degrading PAHs, the cause of which may have to await further investigation.

Table 3 Structural parameters of PAHs in the surface seawater of the western Xiamen harbor

Station	COMB(ng/L)									∑COMB
	Flu	Py	Ba	Chry	BF	B[e]P	Ind	BB	∑COMB	/PAHs
9801	Nd	Nd	Nd	37.3	Nd	Nd	Nd	Nd	37.7	0.291
9802	Nd	Nd	Nd	Nd	61.5	Nd	Nd	Nd	61.5	0.148
9803	Nd	3420.6	Nd	Nd	Nd	Nd	Nd	Nd	3420.6	0.783
9804	71	56.4	Nd	Nd	Nd	Nd	Nd	Nd	127.4	0.336
9807	5.4	10.3	Nd	Nd	37.4	Nd	Nd	Nd	53.1	0.283
9808	24	11.5	Nd	Nd	Nd	Nd	Nd	Nd	35.5	0.189
9809	19	11.6	Nd	Nd	Nd	Nd	Nd	Nd	30.6	0.105
9810	Nd	481	Nd	Nd	Nd	Nd	Nd	Nd	481	0.893
9811	22	72.9	Nd	Nd	Nd	Nd	Nd	Nd	94.9	0.681

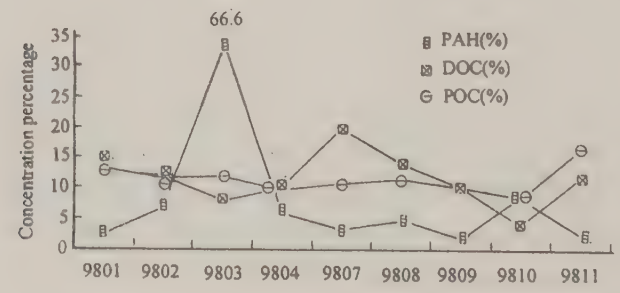

Fig.2 Correlation relationship between ∑PAHs and DOC,POC in the surface seawater of the western Xiamen harbor

3. Conclusion

a) By comparing the contents of ∑PAHs in the nearshore (9803, 9804), offshore (9801) and

estuarine areas, it may be assumed that the farther the area is from the coast, the smaller the effect of seawater is and the lower the value of ∑PAHs is; In the nearshore and estuarine areas where the effect of human activities is greater, the value of ∑PAHs is relatively higher. This tallies with the research findings of P.J.Law et al. in England and Wales.

b) The contents of ∑PAHs in the surface water of the western Xiamen harbor is uneven, varying between 106.1ng/L and 4365.6ng/L, which is still in the category of slight pollution. The sources of pollution are: oil pollution, COMB and the industrial waste water and domestic sewage discharged into the sea.

c) The content of dissolved organisms (DOC, POC) in the seawater has a good negative correlation with the content of PAHs, which may be related to the role of organisms in absorbing and degrading PAHs.

References

1 R. J. Law et al. Polycyclic Aromatic Hydrocarbones (PAHs) in Seawater around England and Wales.*Marine Pollution Bulletin.* 1997, 34(5): 306~322

2 Zhang Luoping, Analysis of Contents and Sources of PAHs in the Surface Sediments in the Western Xiamen Harbor and Victoria Harbor of Hongkong, 1996, 18(4): 120~124

Preliminary Research on the Characteristics and Causes of Formation of Seiches in the Bays

Wu Shaohua(吴少华) Wang Xinian(王喜年) Dai Mingrui(戴明瑞)
(*National Marine Environmental Forecast Center, Beijing 100081*)

Abstract The Haizhou and Daya bays are chosen as basins for seiche research in this paper. By reducing the astronomical tide, we obtain residuals which include seiches from the original observed tide curve of two representative gauges of the Haizhou and Daya bays, with a time resolution of 1min. We have further made a statistical analysis of the characteristics of the seasonal distribution of seiches and by making a comparative analysis of the seiches and the corresponding weather system, studied the origin of seiches. The research findings are of important reference value for the ocean engineering design and the storm surge forecast.

Keywords seiches; cause of formation; spectral analysis; Daya Bay; Haizhou Bay; seasonal variation

1. Introduction

The worldwide research on seiches has by now a history of nearly 100 years, starting from the early century (Chrystal G., 1904). As far as the research methods are concerned, a theoretical and statistical method was applied to study the characteristics of seiches before the 1960s. Although since the early 1970s, the dynamic numerical method has become a means of studying seiches[1~7], the statistical method is now still an important means of seiche research[8].

With the Hiazhou Bay of Jiangsu province and the Daya Bay of Guangdong province chosen as the areas for research on seiches, the paperr reduces the original observed tide curve of two representative gauges of the Haizhou and Daya bays and, having reduced the astronomical tide, obtains residuals with a time resolution of 1min, which contain the seiche oscillation. Analysis shows that the magnitude period and distribution in different seasons of the seiches in the Haizhou and Daya bays are as follows: the seiches in the Haizhou Bay are most serious in summer, secondly in spring and autumn, and lastly in winter, and those in the Daya Bay occur most frequently and seriously in summer while they seldom occur in October~January. By making a comparison of the weather systems corresponding to the typical processes of seiche, a preliminary analysis is made of the origin of the typical seiches in the Haizhou and Daya bays, which suggests that the seiches in the Daya Bay are mainly caused by the typhoon and the cold air going southwards while those in the Haizhou Bay are mainly resulted from the temperate cyclone going out to sea and the typhoon. In the context of the data used for research, the largest seiches in the Daya Bay and the Haizhou Bay are all caused by the typhoon. The seiches in the bays are generally resulted from the sudden change in local air pressure and wind, or maybe from the oscillations propagated

from the open sea through the bay mouth.

2. Data

The original observed tide curve or the time series of tidal level observation with high sampling density must be used in sorting out the data of observed seiches. Through sorting out and analysing the data, an overall understanding of the magnitude, period, frequency of occurrence, and the forcing that causes the seiche.

This paper adopts the original observed tide curves of the Lianyungang gauging station in January, April, August and November of 1997 in the Haizhou Bay. These four months represent the four seasons of winter, spring, summer and autumn. April and November are just the two time intervals when the effect of the coastal temperate weather system is most frequent and seious around Lianyungang. According to climatological statistics, August is the month when the typhoon affects Lianyungang most frequently. Hit by the typhoon No.9711 during Aug. 19~20, 1997, the highest tidal level at the Lianyungang gauging station reached the maximum value since 1950; January is the month when the strong cold air or the cold wave gale affects the area most frequently and seriously. For the Daya Bay, the original observed tide curve for the whole year of 1968 was adopted and this year there were 6 typhoons affecting the area.

3. Processing of the Data

In the original observed tide curve, the seiche oscillation is superimposed on the positive and negative set-ups caused by the astronomical tide oscillation and the metrorological factors. Therefore, the seiche oscillation may sometimes be clearly seen from the observed tide curve, while sometimes, the existence of seiches may be clearly identified only after the astronomical tide has been reduced. In this study, we adopt two methods to judge the existence of seiches for the observed tide curve of each day.

One is the method of eye observaiton. For the observed tide surve of a particular day where there exists obvious periodic oscillation, we compare it with the observed tide curves of 2~3d around it. If the observed tide curves several days around it all have almostly the same oscillaiton at the same time interval of each lunar day, such oscillation is generally caused by the non-seiche factors. If such oscillation does not occur in the observed tide curves around it and, there exists obvious oscillation only in this day, it can be assumed that there exists a seiche in this day.

The other is the mehtod of reducing the astronomical tide. For some seiche oscillations, it is very hard to identify their existence from the observed tide curve when they are superimposed on the astronomical tide. But if the past of the astronomical tide is removed from the observed tide curve, the seiche oscillation may be clearly identified. In this study, such work of reducing the astronomical tide is done for each day's observed tide curve. The digitalizer is used to digitalize the original observed tide curve and the surface height series are obtained at a sampling interval of 1min through computer processing. Then, the astronomical tide is forecasted, giving a value every 1min and the residuals (positive and negative set-ups) that can indicate the existence of seiches are obtained by the above-mentioned observed tidal level minus the forecast of astronomical tide in the corresponding period. Taking the time interval between the adjacent significant peak values of the seiche oscillation or that between the adjacent

significant valley values as the period of oscillation, the height of seiche is taken as the vertical distance between the adjacent peak and valley.

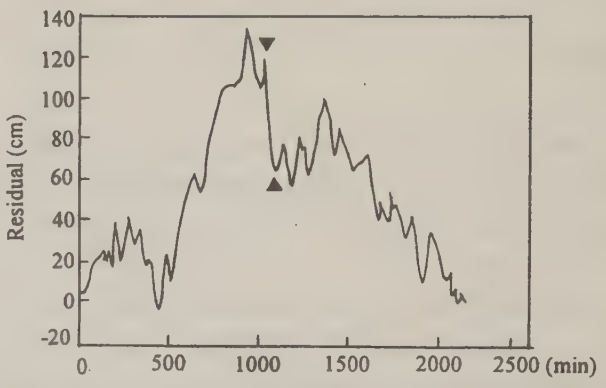

Fig.1 Curve of the residuals (observed tided level minus the forecast of astronomical tide) at the tidal station of Lianyuangang (1997-08-19, 00:00~1997-08-20, 12:00)

4. Statistical Analysis of Seiches

4.1 Haizhou Bay

The following results have been obtained from the statistical analysis of the data of January, April, August and November in 1997 in Lianyungang:

a) The more significant seiches generally occur around the high or low water time when the tidal level changes slowly and there is period of flood slack. In Lianyungang, the tidal range is great and the tidal level changes significantly around the half tide level, which is probably the reason why the seich is not significant.

b) Fewer seiches have occurred around the coastal Lianyungang. According to the statistics of these four months, there only occur 2~3 seiches each month.

c) In these four months, the maximum seiche magnitudes are in their proper order from big to small: summer > spring > autumn > winter. The detailed results are: (1) In summer (August), there are two significant processes of seiche: one occurring on Aug. 19 with a maximum seiche value of 58cm (see Fig. 1, in which the wave motion pointed to by two triangles is the seiche oscillation chosen while the vertical distance between the adjacent peak and valley pointed to by the two triangles represents the height of seiche, the same below.) and coming along with the typhoon (see Fig.2 for the corresponding weather map); the other occurring on August 3, with a maximum seiche value of 52cm (see Fig.3) and corresponding to this process is the large-scale weak (force 3, 4m/s) southerly (see Fig.4 for the corresponding weather map) which is caused by the weather system of being high in the east and low in the west. (2) In spring (April), there are two significant processes of seiche, one occurring on April 2 with a maximum seiche value of 22cm, which corresponds to the cold air in the north and the low pressure in the south; the other occurring on April 29 with a maximum seiche value of 20cm, which is related to the weak low pressuredisturbance moving eastwards near Lianyungang. (3) In autumn (November), there are two significant processes of seiche, one occurring on November 28 with a maximum seiche value of 20cm, which corresponds to the match of the cold air and the cyclone putting out to sea; the other occurring on November 21, with a maximum seiche value of 10cm and corresponding to a weak cyclone putting out to sea. (4) In winter (January), there is a significant process of seiche occurring on January 4, with a maximum seiche value of 10cm and corresponding to the match of a weak cyclone putting out to sea and the cold air. (5) None of the maximum seiche values in other processes exceeds 5cm.

d) The results of spectral analysis of the more significant processes of seiche in the four months are: The process of August 3: the period corresponding to the maximum spectral value is 130min (see Fig.5). The process of August 19: the period corresponding to the maximum spectral value is 122min. The

process of April 29: the period corresponding to the maximum spectral value is 106min. The process of November 28: the period corresponding to the maximum spectral value is 97min. The process of January 4: the period corresponding to the maximum spectral value is 111min.

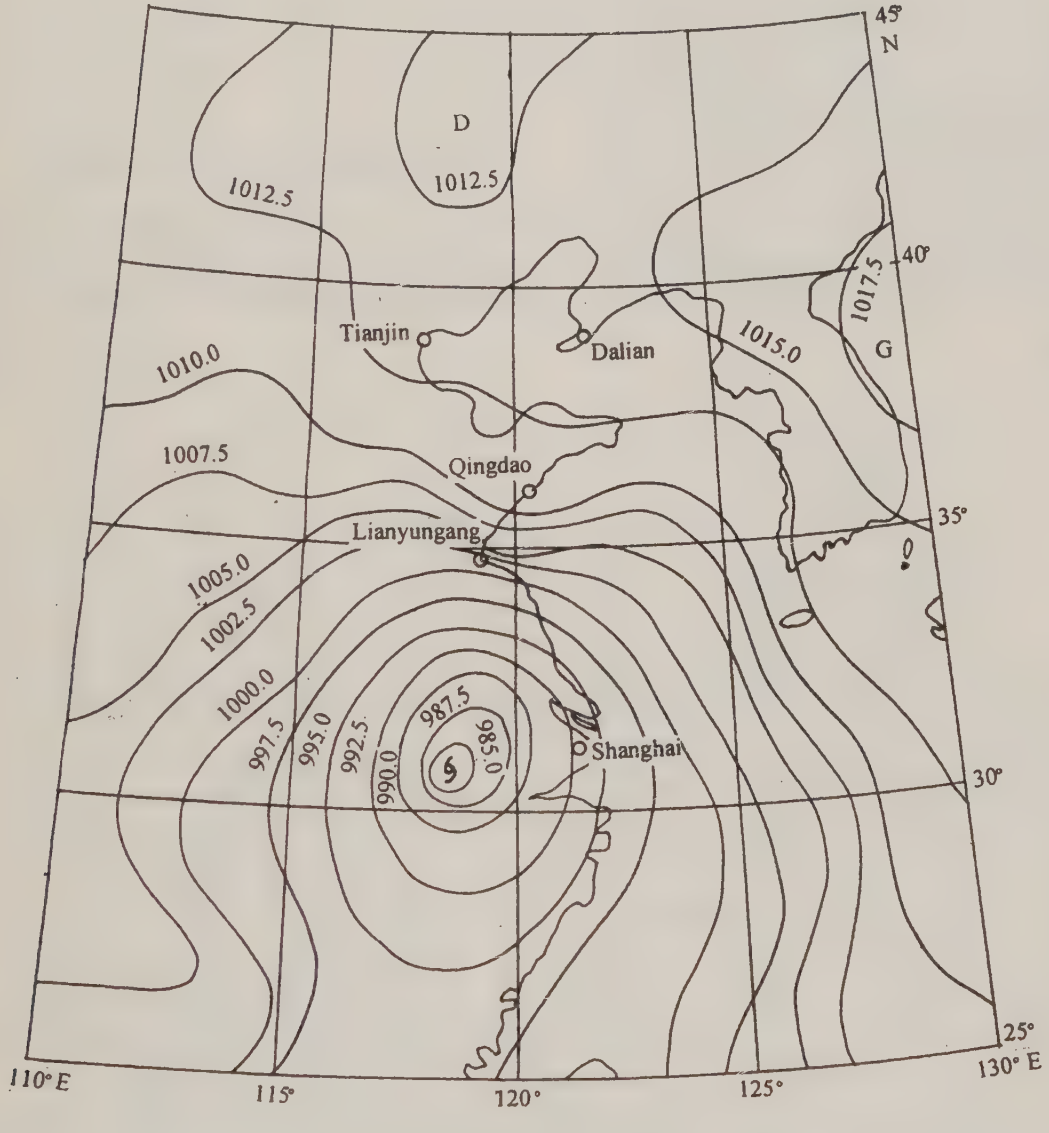

Fig.2 Surface weather chart at 14:00 on Aug.19, 1997

4.2 Daya Bay

The following results have been obtained from the statistical analysis of the data in 12 months of 1986:

a) Throughout 1986, there occurred processes of seiche in 84d which exceed 5cm height and their monthly distribution can be seen from Fig.6. Seiches occurred most frequently in August and rarely in

January, October, November and December. The mean value of the periods of all processes of seiche is 72min.

b) The maximum seiche magnitude is 45cm (see Fig.7), which occurred on July 12 and was caused by the typhoon No.8607. The magnitude of the seiche on August 10 was 35cm, which was caused by the typhoon No.8613, and the magnitude of the sieche on September 5 was 25cm, which was caused by the typhoon 8616. During April 21~22 there occurred a significant seiche (see Fig.8) with a magnitude of 28cm, which was caused by the cold air going down south.

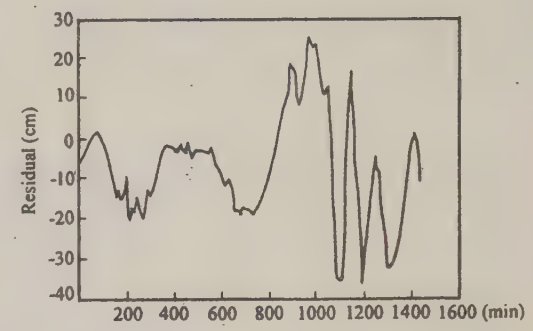

Fig.3 Curve of the residuals (observed tided level minus the forecast of astronomical tide) at the tidal station of Lianyuangang(1997-08-03, 00:00~24:00)

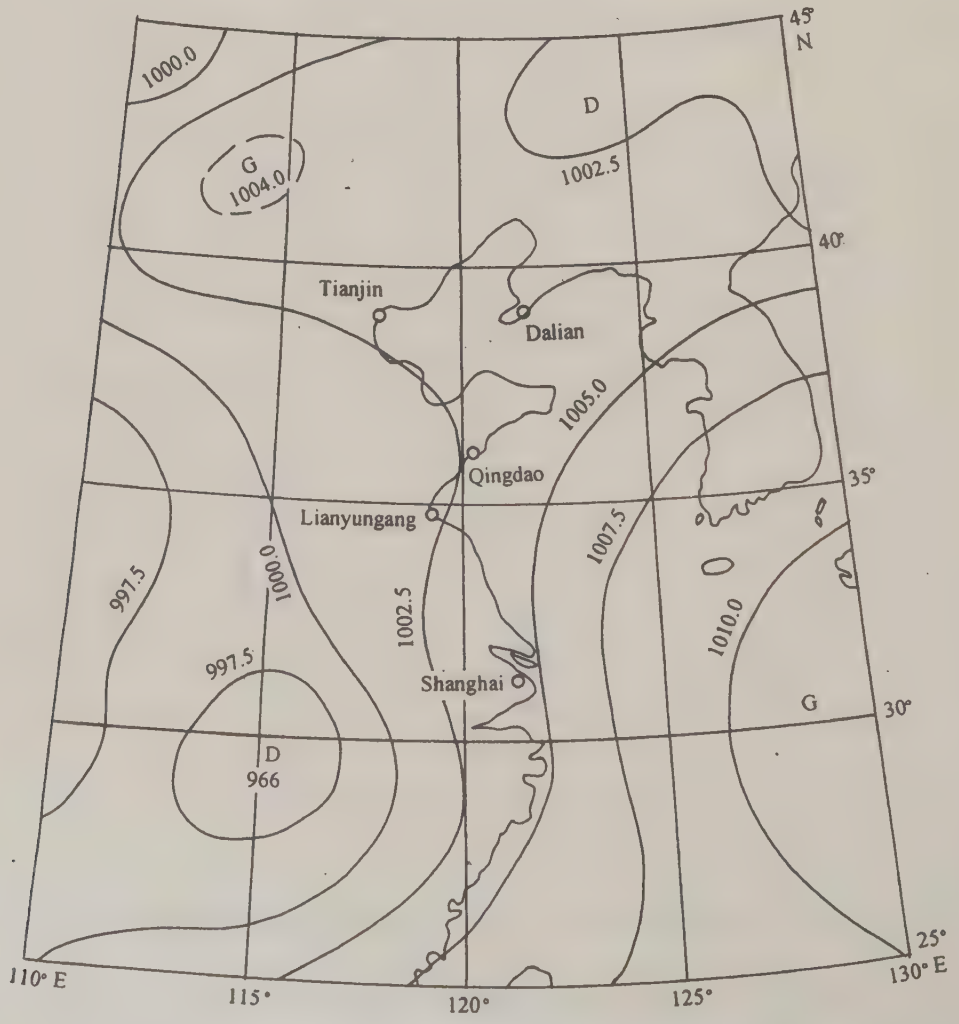

Fig.4 Surface weather chart at 20:00 on Aug.3, 1997

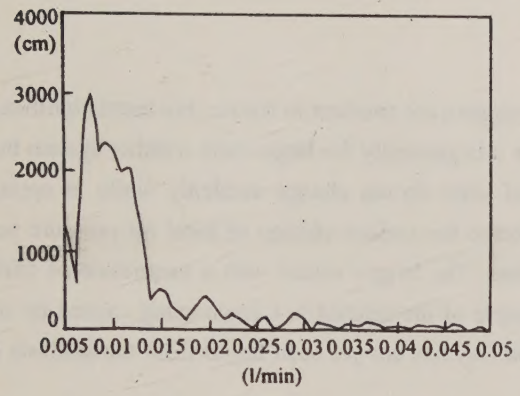

Fig.5 Spectral analysis of the residuals at the tidal station of Lianuyungang (1997-08-03)

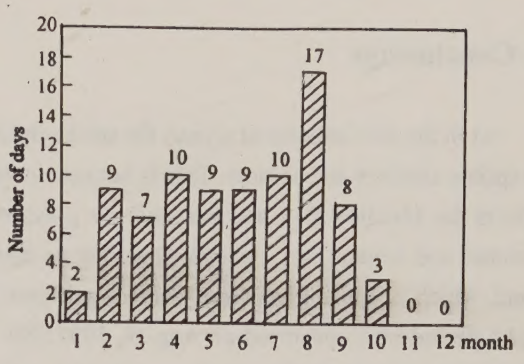

Fig.6 Number of seiche occurrence days in each month of 1986 in the Daya Bay

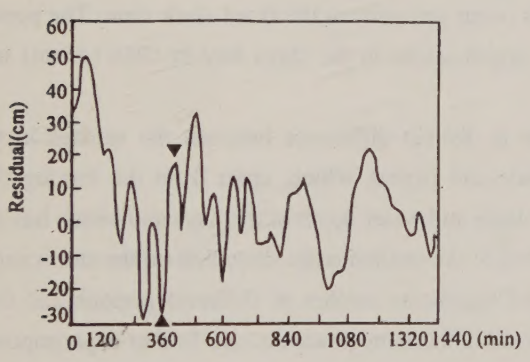

Fig.7 Curve of the residuals (observed tided level minus the forecast of astronomical tide) at the tidal station of Daya Bay (1986-07-12, 08:00~1986-07-13, 08:00)

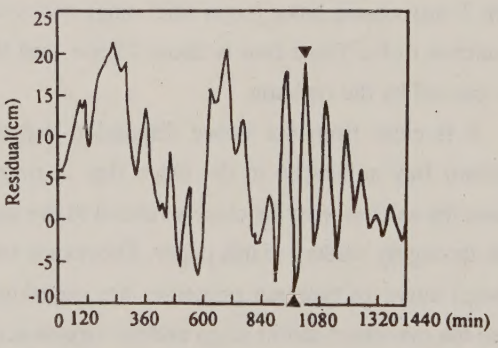

Fig.8 Curve of the residuals (observed tided level minus the forecast of astronomical tide) at the tidal station of Daya Bay (1986-04-21, 08:00~1986-04-22, 08:00)

c) The main weather systems giving rise to the seiches in the Daya Bay are the typhoon and the cold air system intruding southwards.

d) The seiches in the Daya Bay occur at flood, ebb or flood slack time, which may be related to the smaller tidal range in the Daya Bay (about 1m).

e) Spectral analysis of the significant seiches caused by the typhoons 8607, 8613 and 8616 and the seiche during April 21~22 shows that in the frequency band with frequencies of 0.013~0.014 (period is 71~72min) there occur significant peak values (see Fig.9).

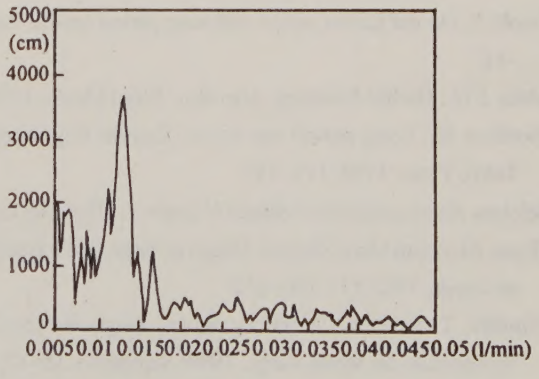

Fig.9 Residuals at the tidal station of the Daya Bay (1986-07-12, 08:00~1986-07-13, 08:00)

5. Conclusions

a) In the four seasons of a year, the seiche in Lianyungang are smallest in winter, but more significant in spring, summer and autumn. This is because in winter it is generally the large-scale weather system that affects the Haizhou Bay and the local air pressure and wind do not change suddenly while in spring, summer and autumn, the Haizhou Bay may be subjected to the sudden change of local air pressure and wind, which is opt to give rise to more significant seiches. The largest seiche with a magnitude of 58cm and a period of 2h occurred on Aug.19, 1997. No example of the seiches in Lianyungang caused by the oscillation propagated through the mouth of the Haizhou Bay has not yet been found from the analysis of the data of observed tidal level in 1997.

b) Seiches in the Daya Bay occur mainly in spring, summer and autumn, but rarely in winter. This is very similar to the seasonal distribution of seiches in Lianyungang and out of basically the same reason. However, the Daya Bay has a smaller tidal range and seiches occur at the flood, ebb and flood slack time while Lianyungang has a larger tidal range and seiches occur generally at the flood slack time. The period of seiches in the Daya Bay is about 72min; and the largest seiche in the Daya Bay in 1986 (45cm) was also caused by the typhoon.

It is clear from the above discussion that there is distinct difference between the seiches in the Haizhou Bay and those in the Daya Bay in magnitude and period, which, apart from the forcing that causes the seiches, may be closely related to the size, shape and water depth of the bays and which has not been throughly studied in this paper. The results for both of the studied areas show that on the storm surge (set-up) curve of typhoon processes are superimposed significant seiches of different periods and that when the maximum storm surge and the largest seiche are in the same phase and are further superimposed on by the astronomical high water, the actual tidal level would much higher. Therefore, it is of important significance for raising the accuracy of storm surge forecast to make a through study of seiches.

Reference

1 Unoki S. On the harbor seiche and long period waves. Proc. Sixth Conf. On Coastal Engineering in Japan, 1959, 1~11

2 Miles J.W., Harbor Seiching, Ann. Rev. Fluid Mech., 1974, 6, 17~35

3 Horikow K., Long period sea waves. Coastal Engineering, An Intrduction to Ocean Engineering. University of Tokyo Press, 1978, 119~183

4 Seiches. Shore protection Manual Volume 1, US Army Corps of Engineers. 1984, 1-96~3-99.

5 Hitani Kino and Oura Kinjiro, Origin of large-Scale Oscillation of Water Level (a Seiche) in the Nagasaki Bay, *Storm Surge*, 1983, (1): 100~110

6 Konishi T. Seiches Caused by Storm Surge in Tokyo Bay,*Storm Surge*, Proceedings of the International Symposium on Storm Surge, 1990, September 15~17, Beijing, China, China Ocean Press, 1987, 83~93

7 Qu Weizheng and Li Ruochun, Forecast of Marine Hazardous Phenomena,*Marine Forecast*, 1992, 9(3): 38~44

8 Wang Xingzhu, Li Kunping, Yu Zhouwen et al. Statistical Characteristics of Seiches in Longkou Harbor, J.P.O., 1987, 117(7): 1063~1065

Marine Science Bulletin

Marine Science Bulletin publishes papers on marine science and technology including physical oceanography, chemical oceanography, marine biology, marine geology, environmental oceanography, estuarine & coastal sciences, marine technology, digital ocean, coastal zone management, ocean engineering, marine economics, etc., and aims to promote international academic exchange.

Editor-in-Chief: Hou Wenfeng (侯文峰)
Deputy Editor-in-Chief: Lin Baofa (林宝法) Yang Ying (杨 鹰)
Executive Editor: Lu Mingsheng (卢明生)

Marine Science Bulletin (Vol.2 No.1 May 2000)

Responsible Institution:
State Oceanic Administration of China
Edited and Published Semi-annually by:
National Marine Data and Information Service
Address: 93 Liuwei Road, Hedong District, Tianjin 300171, China
E-mail: msb@mail.nmdis.gov.cn

ISSN1000-9620
CN12-1271/N

Price: $30.00 per year